NASA TECHNICAL MEMORANDUM NASA TM-75239

THEORETICAL INVESTIGATION OF MAINTAINING THE BOUNDARY LAYER OF REVOLUTION LAMINAR USING SUCTION SLITS IN INCOMPRESSIBLE FLOW

Peter Thiede

Translation of: "Theoretische Untersuchungen zur Laminarhaltung der Grenzschicht an Rotationskörpern durch Absaugeschlitze bei inkompressibler Strömung," VDI-Z Fortschrift-Berichte, Reihe 7, Stromungstechnik, No. 27, Nov. 1970, 115 pages

NATIONAL AERONAUTICS AND SPACE ADMINISTRATION
WASHINGTON, D. C. 20546 JUNE 1978

STANDARD TITLE PAGE

1. Report No. NASA-TM-75239	2. Government Accession No.	3. Recipient's Catalog No.
4. Title and Subtitle THEORETICAL INVESTIGATION OF MAINTAINING THE BOUNDARY LAYER OF REVOLUTION LAMINAR USING SUCTION SLITS IN INCOMPRESSIBLE FLOW		5. Report Date 6. Performing Organization Code
7. Author(s) Peter Thiede		8. Performing Organization Report No. 10. Work Unit No.
9. Performing Organization Name and Address SCITRAN Box 5456 Santa Barbara, CA 93108		11. Contract or Grant No. NASw-2791 13. Type of Report and Period Covered Translation
12. Sponsoring Agency Name and Address National Aeronautics and Space Administration Washington, D.C. 20546		14. Sponsoring Agency Code

15. Supplementary Notes

Translation of: "Theoretische Untersuchungen zur Laminarhaltung der Grenzschicht an Rotationskörpern durch Absaugeschlitze bei inkompressibler Strömung," VDI-Z Fortschrift-Berichte, Reihe 7, Stromungstechnik, No. 27, Nov. 1970, 115 pages.

16. Abstract

The transition of the laminar boundary layer into the turbulent state, which results in an increased drag, can be avoided by sucking off the boundary layer particles near the wall. The technically-interesting case of sucking the particles using individual slits is investigated for bodies of revolution in incompressible flow.

The results of the variational calculations show that there is an optimum suction height, where the slot separations are maximum. Combined with favorable shaping of the body, it is possible to keep the boundary layer over bodies of revolution laminar at high Reynolds numbers using relatively few suction slits and small amounts of suction flow.

17. Key Words (Selected by Author(s))	18. Distribution Statement
	Unclassified - Unlimited

19. Security Classif. (of this report)	20. Security Classif. (of this page)	21. No. of Pages	22.
Unclassified	Unclassified	107	

THEORETICAL INVESTIGATION OF MAINTAINING THE BOUNDARY LAYER OF REVOLUTION LAMINAR USING SUCTION SLITS IN INCOMPRESSIBLE FLOW

Peter Thiede*

The transition of the laminar boundary layer into the turbulent state, which results in an increased drag, can be avoided by sucking off the boundary layer particles near the wall. The technically-interesting case of sucking the particles using individual slits is investigated for bodies of revolution in incompressible flow.

The boundary layer calculation is done using the integral conditions for momentum and energy. In order to determine the laminar-turbulent transition point, a new semi-empirical criterion is introduced. The changed boundary layer quantities behind a suction slit are approximately determined using the remaining profile after the suction process. In order to evaluate the slit suction, we carry out a drag calculation with consideration of the suction power.

The calculation method uses a ALGOL program. The reliability of the method is confirmed by comparison calculations.

The results of the variational calculations show that there is an optimum suction height, where the slot separations are maximum. Combined with favorable shaping of the body, it is possible to keep the boundary layer over bodies of revolution laminar at high Reynolds numbers using relatively few suction slits and small amounts of suction flow.

This paper was done during the tenure of Prof. H. Hertel, the Institute Director.

/1†

†Numbers in margin indicate pagination in foreign text.

*From the Institute for Aircraft Design of the Technical University, Berlin, West Germany.

1. Notation

a_ν, b_ν, c_ν / a_ν, b_ν, c_ν	coefficients
A_Z, A_H / B_Z, B_H	coefficients
a	amplification ratio
b	slot length
c	exponent
c_D	dissipation coefficient
c_f	friction coefficient
c_p	pressure coefficient
c_Q	suction amount coefficient
c_w	drag coefficient
c_{w_Q}	equivalent suction drag coefficient
d	maximum thickness
F	area
F_1, F_2, F_3, F_4	universal functions
H_{12}, H_{32}	shape parameter
l	length
L	Mangler-constant
m	Hartree parameter
m_E	Hartree parameter of plane replacement flow
n, N	boundary layer variables
n_Q	number of suction points
N_Q	suction power
O	surface area
p	static pressure
q	stagnation pressure
q_Q	suction yield /6
Q	suction amount
r	body radius
Re	Reynolds number
s	slot width
t	time

u_{q_x}, u_{q_r}	induced velocity components
u_{q_t}	induced tangential velocity
u, v	velocity components
v_Q	average velocity in suction slot
V	volume
W	drag
W_Q	equivalent suction drag
x, r, φ	cylinder coordinates
x, y, z	cartesian coordinates
x'	coordinate along body contour
y_Q	suction height
Z	thickness parameter
α, β	boundary layer variables
β_i	buildup variable
$\pi \cdot \hat{\beta}$	cone angle, wedge angle
$\pi \cdot \hat{\beta}_E$	wedge angle of plane replacement flow
δ	boundary layer thickness
δ_1	displacement thickness
δ_2	momentum loss thickness
δ_3	energy loss thickness
δ_Q	suction loss thickness
δ_{1Q}	suction displacement thickness
δ_{2Q}	suction momentum loss thickness
δ_{3Q}	suction energy loss thickness
ε	boundary layer variable
η	relative wall separation, radius coordinate /7
η_Q	relative suction height
ϑ	tail point angle
Θ	momentum loss area
κ Λ	Pohlhausen-shape parameter
μ	dynamic viscosity
ν	kinematic viscosity
ξ	length coordinate
ϱ	density
ϱ_o	nose radius

ϑ_d	apex radius
τ	shear stress.

SUBSCRIPTS

A	referred to separation point
Abs	referred to suction region
B	nose part
E	end of rotationally-symmetric boundary layer calculation
F	referred to the area
G	referred to the velocity trial solution
H	tail part
h	referred to tail part
I	referred to the instability point
L	referred to length
la	laminar
M	middle part
O	referred to the surface
p	referred to potential flow
Q	referred to suction point
s	referred to support point
tu	turbulent
U	referred to transition point
V	referred to the volume
w	referred to the wall
δ	referred to edge of boundary layer
δ_2	referred to momentum loss thickness
∞	referred to incident flow
I	ahead of suction slit
II	behind suction slit
-	average value
$\sim$	transformed variable
*	nondimensional quantity.

/8

2. Introduction /9

Bodies of revolution are primarily used in aerodynamics and hydrodynamics in order to support useful loads (for example, aircraft bodies, underwater vehicles). Therefore, optimum bodies of revolution from the flow point of view are those whose flow resistance with respect to the useful volume is a minimum. Minimum specific drag is achieved by the following:

- by means of a large volume related to the surface in the flow,
- by a small drag coefficient referred to the surface area.

Whereas the volume-to-surface area is increased with increasing thickness ratio, the drag coefficient referred to the surface can be reduced by keeping the boundary layer laminar in the flow.

In contrast to conventional shapes with a long cylindrical central part and a small thickness ratio, Hertel [1 to 3] suggested spindle-shapes for aircraft bodies, which are characterized by a large thickness ratio and a pointed nose part, where the laminar boundary layer is stabilized. At high Reynolds numbers ($Re_1 > 10^8$), such as occur in aviation and underwater technology, the laminar effect which can be reached by shaping alone is not important. Already by sucking off small amounts of flow, the laminar boundary layer can be additionally stabilized, so that the boundary layer transition into the turbulent state is delayed, and the drag is reduced with consideration of the suction power. The amounts sucked off required to influence the boundary layer are smallest for a continuous distribution over the surface. This optimum case is the simplest to analyze theoretically, but cannot be realized in practice because of the technical effort for suction.

In technical applications, one can only consider sucking off the flow through slits arranged perpendicular to the flow direction, or using gaps or perforated strips. The effectiveness of such suction slits and slots was demonstrated by Pfenninger [4] to [6] and Lachmann [7] for airfoils. Based on the large number of suction points, the men- /10
tioned suction configurations are not completly satisfactory for technical applications.

In the case of spindle-shaped bodies of revolution, it seems promising to expand the laminar flow range even at high Reynolds numbers, using a relatively low number of suction points, so that the drag reductions considering the suction power will be worthwhile.

3. Problem Formulation and Assumptions

In the present paper, we will theoretically investigate the technically interesting case of maintaining a boundary layer laminar using suction slits on bodies of revolution. In particular, as a function of the body shape and the incident Reynolds number, we will determine the following:

- optimum position of suction slits for minimum number of slits,
- the flow drag with consideration of suction power.

The investigations are restricted to the following:

- bodies of revolution with flow in the axial direction,
- incompressible flow
- flow without any disturbances,
- hydraulically-smooth surface

The calculation method to be designed includes the following factors:

- calculation of the laminar and turbulent boundary layer over bodies of revolution with consideration of influencing the laminar boundary layer.
- determination of laminar-turbulent boundary layer transition for bodies of revolution.
- influencing of laminar boundary layer using suction slits. /11

As will be shown later on, we can neglect the following:

- pressure losses by suction slits, throttling points and lines when estimating the suction power,
- the sink effect of the suction slits.

The computer program to be established will allow the following systematic variations:

- variations in body shape
- variations in suction conditions
- variations in incident Reynolds number.

In addition, the program is to include the case without suction and the calculation of flat contours.

Based on available measurement results and theoretical solutions, we will demonstrate the reliability of the calculation method. In addition, we will carry out several characteristic variational calculations.

4. Contour and Pressure Distribution of Bodies of Revolution

4.1 Description of Body Contour

One can only vary the body shape in a systematic way if the body outline can be described mathematically.

A body of revolution consists of a nose part, a central part, and a tail part, as shown in Figure 1. In most cases the central part is cylindrical. In the case of the spindle shapes described in [2] and [3], the lengths of the central part and the nose radius are zero.

The mathematical description of the body contours is the simplest /12 if separate trail solutions are assumed for the nose, central, and tail parts. In this case, the thickness and length ratios do not occur in the contour functions, but only determine their coordinate system. For the other dimensions shown in Figure 1, shaped parameters are introduced which are independent of the thickness and length ratios.

If the coordinates for the nose, central, and tail contours are specified as shown in Figure 1, then the following relationships exist beteen the body of revolution outlined r(x) and the contour functions $\eta_B(\xi_B)$, $\eta_M(\xi_M)$, $\eta_H(\xi_H)$.

Nose	Central Part	Tail
$\xi_B = \dfrac{l_B/l - x/l}{l_B/l}$	$\xi_M = \dfrac{x/l - l_B/l}{l_M/l}$	$\xi_H = \dfrac{x/l - (1-l_H/l)}{l_H/l}$
$\eta_B = \dfrac{r_B/l}{d/2l}$	$\eta_M = \dfrac{r_M/l}{d/2l}$	$\eta_H = \dfrac{r_H/l}{d/2l}$

(4.1)

The requirements for the contour functions

- consideration of the most important body shape parameters
- and large shape selection

for the most part satisfy the polynomial trial solutions of Koschmieder and Walz [8]. In addition, if there is no central part, there can be a transition between the nose part and the tail part without any jump in curvature.

For body shapes with inflection points, the basis functions of Oehler [9] are especially suitable. By superimposing these basis functions, a large selection of shapes results.

4.2 Remarks Regarding the Pressure Distribution

In the case of a body with boundary layer suction, the pressure distribution caused by the body shape is superimposed with a sink action of the suction slits.

Except for the immediate vicinity of the tail tip, it is possible /13 to determine the pressure distribution of a body of revolution caused by the shape

$$c_p = 1 - \left(\frac{u_\sigma}{u_\infty}\right)^2 = f\left(\frac{x}{l}\right) \qquad (4.2)$$

using potential theory.

In this investigation, we will not discuss the calculation of the potential theory pressure distribution caused by the shape. Instead, we will indicate the calculation procedure of Oehler [9], which is especially suited for thick spindle shapes with high underpressure peaks.

The sink action of ring-shaped suction slots will be discussed in Chapter 7.4.

5. Boundary Layer Calculation and Drag Layer Calculation of Bodies of Revolution

5.1 Preliminary Remarks

In the case of calculation of the boundary layer over bodies of revolution with ring-shaped suction slits, one must distinguish the following:

- boundary layer development along the impermeable wall,
- influencing the boundary layer at the suction slits.

In Chapter 7 we will discuss influencing the laminar boundary layer using suction slits.

Schlichting [10] gave a summary about boundary layer theory. The Prandtl boundary layer equation is the point of departure for the boundary layer calculation. One must distinguish between the following:

- the exact solutions which satisfy the boundary layer equation at any point, and
- the approximate solutions which on the average satisfy the boundary layer equation over the boundary layer thickness.

It is only possible to exactly calculate the boundary layer equa- /14 tion for laminar boundary layers. In this case, there are substantial

difficulties for arbitrary body shapes and pressure distributions. The approximation theory can be used successfully in most practical problems, as Walz [11] showed, especially.

In the case of rotationally symmetric flow, the calculation of the boundary layer is more difficult than for plane flow. This is because the pressure distribution and the body shape appear in the boundary layer equation. The relationship between the plane boundary layer and the rotationally symmetric boundary layer was analyzed by Mangler [12].

The similar solutions of the Hartree [13] boundary layer equation determined by Hartree [13] are the basis for developing the approximate solutions. The most recent trial solutions for the laminar boundary velocity profile of Walz, [14], Magnler [15], Geropp [16], attempt to give the best possible approximation to the Hartree profile. The trial solutions for the turbulent velocity profile are empirical.

The approximate solution principle consists of satisfying the integral and boundary conditions for a velocity profile which is assumed to be known. These are derived from the boundary layer equation. The accuracy of the approximate method increases with the number of simultaneously satisfied boundary layer equations.

A quadrature method can be used to exactly calculate the laminar boundary layer for a pressure drop, which is based on the integral condition for momentum and the wall adhesion.

As Walz [17] showed later on, by using a single parameter method (with a shape parameter of the velocity profile), it is possible to obtain results which are more reliable, if instead of the wall condition, one introduces the energy integral condition.

In place of turbulent boundary layers, the accuracy which can be /15
achieved depends on the empirical law for wall shear stress and dissipation. A corresponding comparison can be found in Fernholz [18].

Just behind a suction point there are laminar velocity points, which differ substantially from the Hartree profiles. The authors Iglisch [19] and Schlichting, Bussmann [20] found similar solutions for the suction profiles of the plane plate, which were used to approximately calculate the suction boundary layers by Schlichting [21], Head [22], Eppler [23]. etc.

5.2 Integral Conditions for Momentum and Energy

In this discussion, the rotationally-symmetric laminar and turbulent boundary layers along the impermeable wall are calculated on the basis of the integral conditions for momentum and energy, with single parameter velocity profiles. The approximate theory for plane flows is discussed in detail in [11], and therefore we will only give the most important relationships here.

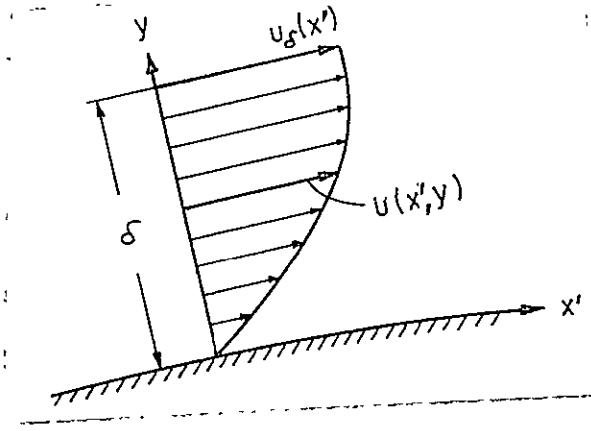

Velocity profile of boundary layer

Using the boundary layer variables

Displacement thickness $$\delta_1 = \int_0^\delta \left(1 - \frac{u}{u_\delta}\right) dy$$

momentum loss thickness $$\delta_2 = \int_0^\delta \frac{u}{u_\delta}\left(1 - \frac{u}{u_\delta}\right) dy$$

Energy loss thickness $$\delta_3 = \int_0^\delta \frac{u}{u_\delta}\left[1 - \left(\frac{u}{u_\delta}\right)^2\right] dy$$

Shape parameter $$H_{12} = \frac{\delta_1}{\delta_2}$$ (5.1)

the Prandtl boundary layer equation is the following for stationary, incompressible, and rotationally-symmetric flow

$$\varrho u \frac{\partial u}{\partial x'} + \varrho v \frac{\partial u}{\partial y} = -\frac{dp}{dx'} + \frac{\partial \tau}{\partial y} \; ; \quad \tau = \mu_e \frac{\partial u}{\partial y} \tag{5.2}$$

and the continuity equation is

$$\frac{\partial (ur)}{\partial x'} + \frac{\partial (vr)}{\partial y} = 0, \tag{5.3}$$

with the boundary conditions

$$\begin{aligned} y = 0 &: \quad u = v = 0 \\ y = \delta &: \quad u = u_\delta(x') \end{aligned}$$

The derived integral conditions for the momentum are

$$\frac{d\delta_2}{dx'} + \delta_2 (2+H_{12}) \frac{1}{u_\delta} \frac{du_\delta}{dx'} + \delta_2 \frac{1}{r} \frac{dr}{dx'} - c_f = 0 \tag{5.4}$$

and for the energy

$$\frac{d\delta_3}{dx'} + 3\delta_3 \frac{1}{u_\delta} \frac{du_\delta}{dx'} + \delta_3 \frac{1}{r} \frac{dr}{dx'} - 2c_D = 0 \tag{5.5}$$

where

$$\left.\begin{aligned} &\text{local friction coefficient} && c_f = \frac{\tau_w}{\frac{\rho}{2} u_\delta} \\ &\text{dissipation coefficient} && c_D = \frac{\int_0^{u_\delta} \tau \, du}{\frac{\rho}{3} u_\delta} \end{aligned}\right\} \tag{5.6}$$

It is assumed here that $\delta_1/r << 1$, that is, at the nose tip and /17 in the immediate vicinity of the rear tip, the boundary layer conditions are violated.

By introducing the new variables, we have

Thickness parameter

$$\left.\begin{aligned} Z &= \delta_2 \, Re_{\delta_2}^n; \quad Re_{\delta_2} = \frac{u_\delta \delta_2}{\nu} \\ H_{32} &= \frac{\delta_3}{\delta_2} \end{aligned}\right\} \tag{5.7}$$

: shape parameter

Then instead of δ_2 and δ_3 the integral conditions can be converted as follows:

Momentum theorem:

$$\frac{dZ}{dx'} + \left(F_1 \frac{1}{u_\delta} \frac{du_\delta}{dx'} + (n+1) \frac{1}{r} \frac{dr}{dx'}\right) Z - F_2 = 0 \qquad (5.8)$$

Energy Theorem

$$\frac{d H_{32}}{dx'} + F_3 \frac{1}{u_\delta} \frac{du_\delta}{dx'} H_{32} - \frac{F_4}{Z} = 0 \qquad (5.9)$$

with the abbreviations

$$\left.\begin{aligned} F_1 &= 2 + n + (n+1) H_{12} \\ F_2 &= (1+n) c_f Re_{\delta 2}^n \\ F_3 &= 1 - H_{12} \\ F_4 &= (2 c_D - c_f H_{32}) Re_{\delta 2}^n \end{aligned}\right\} \qquad (5.10)$$

If a single parameter velocity profile is used, the expressions (5.6) can be written as follows:

$$\left.\begin{aligned} c_f &= \frac{\alpha}{Re_{\delta 2}^n} \\ c_D &= \frac{\beta}{Re_{\delta 2}^N} \end{aligned}\right\} \qquad (5.11)$$

where the quantities α and β only depend on H_{32}, which can be seen /18 for a laminar boundary layer from the conversion

$$\alpha = \frac{\delta_2}{\delta} \left[\frac{\partial (u/u_\delta)}{\partial \eta}\right]_w$$

$$\beta = \frac{\delta_2}{\delta} \int_0^1 \left[\frac{\partial (u/u_\delta)}{\partial \eta}\right]^2 d\eta$$

and for turbulent boundary layers, this is confirmed by measurements.

In this way, we obtain

$$\left.\begin{aligned} F_1 &= 2 + n + (n+1) H_{12} & F_3 &= 1 - H_{12} \\ F_2 &= (1+n) \alpha & F_4 &= 2 \beta Re_{\delta 2}^{n-N} - \alpha H_{32} \end{aligned}\right\} \qquad (5.12)$$

Since for a single parameter velocity profile, H_{12} can also be represented as a function of H_{32}, the abbreviations (5.12) can be considered as universal functions of H_{32} with the coefficients

$$\begin{array}{lll} \text{laminar:} & n = 1 & \text{turbulent:} \quad n = 0.268 \\ & N = 1 & \qquad\quad N = N(H_{32}) \end{array} \tag{5.13}$$

In order to solve the boundary layer equations, (5.8) and (5.9), we therefore also need the relationships for the velocity profile

$$\left.\begin{array}{l} \alpha \\ \beta \\ H_{12} \end{array}\right\} = f(H_{32})$$

/19

5.3 Relationships for the Velocity Profile

5.3.1 Laminar Boundary Layers

No Suction.

In the case of a laminar boundary layer without suction action, the velocity profiles are approximated by the similar Hartree solutions of the type $u_\delta(x') \sim x'^m$ for the arbitrary external flow, and we set $m = m(x')$.

The Hartree profiles are defined in the range

$H_{32} = 1.515$ according to $\alpha = 0$, $m = -0.0904$ (laminar separation)

and

$H_{32} = 1.638$, according to $m \to \infty$

For the profile relationships required, we have the Walz [11] approximations:

$$\left.\begin{array}{l} \alpha = 1{,}441\ (H_{32} - 1{,}515)^{0{,}660} \\ \beta = 0{,}1573 + 1{,}691\ (H_{32} - 1{,}515)^{1{,}637} \\ H_{12} = 4{,}030 - 4{,}183\ (H_{32} - 1{,}515)^{0{,}3945} \end{array}\right\} \tag{5.14}$$

which are shown in Figure 2 for the entire Hartree range.

The more accurate relationships can be determined from the single parameter formula of Geropp [16] for the laminar velocity range, as shown in Figure 2.

With suction

When the laminar boundary layer is influenced by suction, the similar solutions for the plane plate with homogeneous suction are used for the velocity profiles, which differ substantially from the Hartree solutions. In order to have a good approximation in the entire H_{32} range, Epper [23] approximated the Hartree profiles with a pressure increase, and the sunction profiles of Iglisch [19] in the case of a pressure drop, by using the limiting case of asymptotic suction profiles $H_{32} = 5/3$, as shown in Figure 2.

$$
\left.
\begin{aligned}
\alpha &= 2{,}512589 - 1{,}686095\ H_{12} + 0{,}391541\ H_{12}^2 - 0{,}031729\ H_{12}^3 \\
&\quad \text{for } 1{,}51509 \leq H_{32} \leq 1{,}57258 \\
\alpha &= 1{,}372391 - 4{,}226253\ H_{32} + 2{,}221687\ H_{32}^2 \\
&\quad \text{for } 1{,}57258 < H_{32} \leq 1{,}66667 \\
\beta &= 7{,}853976 - 10{,}260551\ H_{32} + 3{,}418898\ H_{32}^2 \\
&\quad \text{for } 1{,}51509 \leq H_{32} \leq 1{,}66667 \\
H_{12} &= 4{,}02922 - (583{,}60182 - 724{,}55916\ H_{32} \\
&\quad + 227{,}18220\ H_{32}^2)\ \sqrt{H_{32} - 1{,}51509} \\
&\quad \text{for } 1{,}51509 \leq H_{32} \leq 1{,}57258 \\
H_{12} &= 79{,}870845 - 89{,}582142\ H_{32} + 25{,}715786\ H_{32}^2 \\
&\quad \text{for } 1{,}57258 < H_{32} \leq 1{,}66667
\end{aligned}
\right\} \qquad (5.15)
$$

The separation profile ($\alpha = 0$) is specified by $H_{32_{Ab}} = 1{,}51509$.

Using the approximations (5.15), very reliable results are achieved, even for a pressure increase. If one calculates the delay stagnation point flow

$$\frac{u_\delta}{u_\infty} = 1 - \frac{x}{l}$$

for which there is an exact solution of Howarth [24] available, the parameter separation point to an accuracy of 0.2%, as shown in Figure 3.

In the case of continuous suction with arbitrary suction intensity, no completely-laminar velocity profile can be obtained as $H_{32} = 5/3$, behind a suction slot there are velocity profiles with $H_{32} > 5/3$ as well, which violates the Prandtl boundary layer assumption $v/u << 1$. With the exception of the H_{12} approximation, these relationships (5.15) can also be used for $H_{32} > 5/3$. The approximation /21

$$H_{12} = 3,738 - \sqrt{13,43 \quad (H_{32}-1,4418)} \quad \text{for } H_{32} > 1,6667 \tag{5.16}$$

contains the rectangular profile with $H_{32} = 2$, $H_{12} = 1$ as the limiting case.

5.3.2 Turbulent Boundary Layer

According to Fernholz [18], in the case of a turbulent boundary layer, the following semi-empirical laws can be used with success for the velocity profile over the Reynolds number range of interest:

Wall shear stress law according to Walz [11],

$$\alpha = 0,0566 \; H_{32} - 0,0842 \tag{5.17}$$

Dissipation law of Rotta [25] and Truckenbrodt [26]

$$\left.\begin{aligned} \beta &= 0,0056 \\ N &= 0,168 \end{aligned}\right\} \tag{5.18}$$

Shape parameter relationship of Fernholz [18]

$$H_{12} = 1 + 1,48 \; (2-H_{32}) + 104 \; (2-H_{32})^{6,7} \tag{5.19}$$

Separation occurs for $H_{32_{A_{tu}}} \doteq 1.50 - 1.57$.

5.4 Stepwise Solution of Integral Conditions

Using the relationships given in the previous chapter for the velocity profile, the boundary layer calculation is reduced to the solution of the equation system (5.8) and (5.9), which applies both for the laminar and turbulent boundary layer. and the two unknowns are $Z(x')$ and $H_{32}(x')$.

Assuming that in a small interval we have

$$\Delta x'_{i,\,i-1} = x'_i - x'_{i-1}$$

and that the body contour and the velocity profile can be approxi- /22
mated by a linear law

$$\left.\begin{aligned} r(x') &= r_{i-1} + \frac{r_i - r_{i-1}}{\Delta x'_{i,\,i-1}}\,(x' - x'_{i-1}) \\ u_\delta(x') &= u_{\delta i-1} + \frac{u_{\delta i} - u_{\delta i-1}}{\Delta x'_{i,\,i-1}}\,(x' - x'_{i-1}) \end{aligned}\right\} \qquad (5.20)$$

and if we introduce average values for the variables $Z(x')$ and $H_{32}(x')$ and for the universal function $F_\nu(x')$,

$$\left.\begin{aligned} \bar{Z}_{i,\,i-1} &= \frac{1}{2}(Z_i + Z_{i-1}) \\ \bar{H}_{32i,\,i-1} &= \frac{1}{2}(H_{32i} + H_{32i-1}) \\ \bar{F}_{\nu\,i,\,i-1} &= F_\nu(\bar{H}_{32i,\,i-1}),\ \nu = 1, 2, 3, 4 \end{aligned}\right\} \qquad (5.21)$$

the momentum and energy theorems can be solved in closed form. The step formulas are the following in dimensionless notation, in the rotationally symmetric case

$$\left.\begin{aligned} \frac{Z_i}{l} &= A_Z \left[\frac{r_{i-1}/l}{r_i/l}\right]^{n+1} \frac{Z_{i-1}}{l} + B_Z \frac{\Delta x'_{i,i-1}}{l} \left[\frac{1 + \dfrac{r_{i-1}/l}{r_i/l}}{2}\right]^{n+1} \\ H_{32i} &= A_H\, H_{32i-1} + B_H \frac{\Delta x'_{i,i-1}/l}{Z_{i,i-1}/l} \end{aligned}\right\} \qquad (5.22)$$

with the coefficients

$$
\left.
\begin{aligned}
A_Z &= \left[\frac{u_{\delta i-1}/u_\infty}{u_{\delta i}/u_\infty} \right]^{\bar{F}_1} \\
A_H &= \left[\frac{u_{\delta i-1}/u_\infty}{u_{\delta i}/u_\infty} \right]^{\bar{F}_3} \\
B_Z &= \frac{\bar{F}_2}{1+\bar{F}_1} \; \frac{1-A_Z \dfrac{u_{\delta i-1}/u_\infty}{u_{\delta i}/u_\infty}}{1-\dfrac{u_{\delta i-1}/u_\infty}{u_{\delta i}/u_\infty}} \\
B_H &= \frac{\bar{F}_4}{1+\bar{F}_3} \; \frac{1-A_H \dfrac{u_{\delta i-1}/u_\infty}{u_{\delta i}/u_\infty}}{1-\dfrac{u_{\delta i-1}/u_\infty}{u_{\delta i}/u_\infty}}
\end{aligned}
\right\} \qquad (5.23)
$$

and the step along the contour is

$$
\frac{\Delta x'_{i,i-1}}{l} = \sqrt{\left(\frac{x_i}{l} - \frac{x_{i-1}}{l}\right)^2 + \left(\frac{r_i}{l} - \frac{r_{i-1}}{l}\right)^2} \qquad (5.24)
$$

In the plane case, in (5.22) we have $\dfrac{r_{i-1}/l}{r_i/l} = 1$, and in (5.20) and (5.24), y_i is replaced by r_i.

The stepwise determination of the boundary layer parameters Z and H_{32} at the end of the interval (i) is done by an iteration from the values at the beginning of the interval (i-1). Details are given in Chapter 8.2.2.

The boundary layer calculation for a laminar boundary layer is started at the following points:

- nose tip of body of revolution
- suction slit

and for a turbulent boundary layer,

- the laminar-turbulent transition point

The end of the boundary layer calculation occurs at the following points for the laminar boundary layer

- one suction slit
- the laminar-turbulent transition point

- or the laminar separation point.

and for turbulent boundary layer,

- the end of the range of validity of the integral conditions in the area near the tail tip of the body of revolution
- or the turbulent separation point.

5.5 Initial Calculation

At the nose tip ($x = 0$), the step formulas (5.22) fail because the thickness parameter is $Z_0/l = 0$.

Therefore, in the first step $\Delta x'_{1,0}/l$ the step formulas (5.22) at the nose tip are replaced by relationships which are derived from conical flow:

$$\left.\begin{aligned} H_{32_1} &= H_{32_o} = H_{32}\,(\hat{\beta}_E) = \text{const.} \\ \frac{Z_1}{l} &= \frac{1}{3}\,\frac{F_2}{1+m_E\cdot F_1}\,\frac{x'_1}{l} \end{aligned}\right\} \tag{5.25}$$

and the cone angle and the Hartree parameter of the plane replacement flow

$$\left.\begin{aligned} \hat{\beta}_E &= \frac{\hat{\beta}}{3-\hat{\beta}} \\ m_E &= \frac{\hat{\beta}_E}{2-\hat{\beta}_E} \end{aligned}\right\} \tag{5.26}$$

are specified by the cone angle

$$\hat{\beta} = \frac{2}{\pi}\,\arctan\,\frac{r_1/l}{x_1/l}. \tag{5.27}$$

In the plane case, the relationships for the first step are:

$$\left.\begin{aligned} H_{32_1} &= H_{32_o} = H_{32}\,(\hat{\beta}) \\ \frac{Z_1}{l} &= \frac{F_2}{1+mF_1}\,\frac{x'_1}{l} \end{aligned}\right\} \tag{5.28}$$

where

$$\hat{\beta} = \frac{2}{\pi}\,\arctan\,\frac{y_1/l}{x_1/l} \tag{5.29}$$

With the assumption that Hartree velocity profiles occur at the nose /25
tip, the relationship $H_{32}(\hat{\beta}_E$ and $\hat{\beta})$ can be approximated by

$$\left.\begin{aligned} H_{32} &= 1{,}5720 + 0{,}1561\ \hat{\beta}_E - 0{,}2470\ \hat{\beta}_E^2 + 0{,}2244\ \hat{\beta}_E^3 - 0{,}0804\ \hat{\beta}_E^4 \\ &\text{for } 0 \leq \hat{\beta}_E \leq 1 \\ H_{32} &= 1{,}5720 + 0{,}2258\ \hat{\beta}_E + 0{,}7663\ \hat{\beta}_E^2 + 5{,}3850\ \hat{\beta}_E^3 \\ &\text{for } -0{,}1988 < \hat{\beta}_E < 0 \end{aligned}\right\} \qquad (5.30)$$

The stagnation point flow

rotationally symmetric $(\hat{\beta} = 1;\ \hat{\beta}_E = 0{,}5)$: $H_{32_1} = 1{,}6113$

plane $(\hat{\beta} = 1)$ $H_{32_1} = 1{,}6250$

and the plane plate flow

$$\hat{\beta} = 0 : H_{32_1} = 1{,}5720$$

are contained as special cases.

5.6 Determination of Friction Drag and Pressure Drag

Because there is no boundary layer separation along the tail part, the external drag that is the sum of the friction drag and pressure drag of a body of revolution can be determined from the momentum loss in the wake. According to Young [27] and Pretsch [28], the drag coefficient of a body of revolution is the following with respect to surface area

$$c_{W_N} = \frac{W_N}{q_\infty O} = 2\,\frac{\Theta_\infty}{O} \qquad (5.31)$$

with the following definition of momentum loss area

$$\Theta = 2\pi \int_r^{r+\delta} \frac{u}{u_\delta}\left(1 - \frac{u}{u_\delta}\right) r\,dr \qquad (5.32)$$

By using the integral conditions for the momentum (5.4) on the wake ($\tau_W = 0$), the momentum loss area Θ_∞ at a large distance behind the body/26

$(p = p_\infty)$ can be reduced approximately to the boundary layer variables to the tail tip

$$\Theta_\infty = \Theta_h \left(\frac{u_{\delta h}}{u_\infty}\right) \frac{5+H_{12h}}{2} \tag{5.33}$$

In the immediate vicinity of the tail tip, however, the boundary layer calculation fails because of the integral conditions (5.8) and (5.9). This is because the condition $\delta/r \ll 1$ is not satisfied. It is found that the boundary layer calculation must be terminated $(x = x_E)$ in the case where $\delta_2/r \geq 1/15$.

In this investigation,

- laminar boundary layer suction
- high Reynolds numbers
- thick bodies

however, we have $1 - x_E/l \ll 1$ so that the friction drag component of this region

$$\Delta c_{w_R} = \frac{\Delta W_R}{q_\infty O} = \frac{4\pi r}{O l^2} \int_{x_E/l}^{1} \left(\frac{u_\delta}{u_\infty}\right)^2 \frac{r}{l} c_f \, d\left(\frac{x}{l}\right)$$

can be ignored, compared with the total drag coefficient $c_{w_{[N]}}$, due to the small local wall friction and the small body radii in the vicinity of the tail tip. In addition, in the case of bodies with sharp tail tips, the shape parameter in the tail tip region is almost constant

$$H_{12}\left(\frac{x'}{l}\right) = H_{12h} = H_{12E} = \text{const. for } \frac{x_E}{l} < \frac{x}{l} \leq 1,$$

then according to (5.33), we have

$$\Theta_h = \Theta_E \left(\frac{u_{\delta E}}{u_{\delta h}}\right) \frac{5+H_{12E}}{2} \tag{5.34}$$

and consequently,

$$\Theta_\infty = \Theta_h \left(\frac{u_{\delta E}}{u_\infty}\right) \frac{5+H_{12E}}{2} \tag{5.35}$$

so that the external drag coefficient is /27

$$c_{w_N} = 2 \frac{\Theta_E}{O} \left(\frac{u_{\delta_E}}{u_\infty}\right) \frac{5+H_{12E}}{2} \tag{5.36}$$

According to Scholz, [29], we have the following relationship for the momentum loss area

$$\frac{\Theta_E}{l^2} = 2\pi \frac{r_E}{l} \frac{\delta_{2E}}{l} \left(1+\frac{1}{2} \frac{\delta_{2E}/l}{r_E/l}\right) \tag{5.37}$$

so that the drag coefficient can be expressed by the boundary layer variable at the position x_E/l

$$c_{w_N} = \frac{4\pi}{O/l^2} \frac{r_E}{l} \frac{\delta_{2E}}{l} \left(1+\frac{1}{2} \frac{\delta_{2E}/l}{r_E/l}\right) \left(\frac{u_{\delta_E}}{u_\infty}\right) \frac{5+H_{12E}}{2} \tag{5.38}$$

where

$$\frac{\delta_{2E}}{l} = \left[\frac{Z_E/l}{\left(\frac{u_{\delta_E}}{u_\infty} Re_l\right)^n}\right]^{\frac{1}{n+1}}$$

$H_{12_E} = f(H_{32_E})$ according to (5.19).

In the plane case, the boundary layer is calculated to the trailing edge. The drag coefficient expressed by the trailing edge variables is then given by

$$c_{w_N} = \frac{W_N}{q_\infty F} = 2 \frac{\delta_{2h}}{l} \left(\frac{u_{\delta h}}{u_\infty}\right) \frac{5+H_{12h}}{2} \tag{5.39}$$

where

$$\frac{\delta_{2h}}{l} = \left[\frac{Z_h/l}{\left(\frac{u_{\delta h}}{u_\infty} Re_l\right)^n}\right]^{\frac{1}{n+1}}$$

$H_{12h} = f(H_{32h})$ according to (5.19)

The wake behind a flow body is turbulent at high Reynolds numbers. Even for laminar boundary layer suction to the end of the body, one must establish the latest boundary layer transition for the drag calculation.

Body of revolution: $\frac{x_U}{l} < \frac{x_E}{l}$

plane contour: $\frac{x_U}{l} < 1$

Comparison calculations for the drag determination are given in Chapter 6.5.

6. Determination of Instability Point and Transition Point Over Bodies of Revolution.

6.1 Preliminary Remarks

The laminar-turbulent transition point over a body in the flow could not be exactly calculated up to now, because the way in which turbulence is produced is not clarified.

In experiments, Schubauer and Skramstad [30] showed that boundary layer transition must be attributed to an instability in the laminar boundary layer.

If the disturbances in the laminar boundary layer caused by incident flow turbulence sound, vibration, or surface roughness are small, then the transition process can be divided into three regions:

I. stable laminar boundary layer
All perturbations are small in amplitude, and affect the laminar boundary layer and decay in time.

II. Unstable laminar boundary layer.
At least a few partial oscillations of the perturbation motion are built up. In the terminal phase, secondary and high frequency perturbations are superimposed, which forms a three-dimensional vortex system.

III. Laminar-turbulent transition range
Due to an instability in the secondary flow, turbulent spots are produced in the laminar flow, which propagate during the downstream motion until the completely turbulent state is reached. /29

The determination of the instability point after which there is a buildup of the disturbance motion is discussed in stability theory. Mathematically the problem consists of solving the Orr-Sommerfeld perturbation differential equation, which was successfully done, first by Tollmein [31] and later on by Lin [32] for the Blasius profile of the plane boundary layer. When there is a changing pressure gradient, the instability of the laminar boundary layer was calculated by Schlichting and Ulrich [33] for the Pohlhausen P6-profile. This was done by Pretsch [34] and Tetervin [35] for Hartree profiles.

The stability of the laminar boundary layer with suction was investigated by Bussmann and Muenz [36] for the asymptotic suction profile. It was calculated by Ulrich [37, 38] for the similar suction profiles given by Iglisch and by Schlichting and Bussmann. As long as the transition process is not completely clarified, only empirical relationships can be given for the length of the buildup length. The transition region, however, is so short according to experience that in the first approximation it can be ignored, and can be replaced by the transition point which refers to the beginning of transition.

Since in the case of small perturbations, the transition point lies between the instability point and the laminar separation point, these two limiting positions are often used as the transition conditions. In the case of high Reynolds numbers, the distance in the instability point and separation point is very large.

More recent transition criteria are based on stability theory. Michael [39] gave an empirical transition criterion for plane boundary layers which later on was analyzed theoretically by Smith and Gamberoni [40] using the build-up diagrams of Pretsch [41]. The criterion of Granville [42] also considers the influence of the pressure gradient on the length of the buildup path. In the case of plane flow, it is /30 possible to predict with some success the transition point using these criteria, but information for bodies of revolution is not reliable.

6.2 Stability Criteria

Pretsch [43] showed that the results of the stability theory can be transferred from the plane case to the rotationally-symmetric case, as long as $\delta/r << 1$.

Figure 4 shows the calculated instabilities

- for the Blasius profile of the plane boundary layer of Tollmien [31] and Lin [32],
- for the profiles of a boundary layer with a pressure gradient of
  * Schlichting, Ulrich [33] for Pohlhausen-P6 profiles
  * Pretsch [34] and Te tervin [35] for Hartree-profiles

in the form

$$\mathrm{Re}_{\delta_2} = f(H_{32})$$

The various stability calculations agree well. The pressure drop ($H_{32} > 1.5726$) has a stabilizing effect on the laminar boundary layer, whereas a pressure increase ($H_{32} < 1.5726$) has a deep stabilizing effect.

With suction there is an even greater stabilization of the laminar boundary layer.

The results of the stability calculations of
- Bussmann, Muenz [36] of the asymptotic suction profile
- Ulrich [37], for the Iglisch suction profiles,
- Ulrich [38], for Schlichting-Bussmann suction profiles,

are also shown in Figure 4.

One sees that the influence of a pressure gradient and suction on the stability of the laminar boundary layer can be approximately re- /31
placed by a single criterion. The following are used for approximating the stability criterion:

- in the case of a pressure increase, the results of Pretsch [34] for Hartree-profiles,
- for a pressure drop, the results of Ulrich [37] for Iglisch suction profiles with a limiting case of asymptotic suction profiles.

Approximately, one obtains the following for the position of the instability point as a function of the shaped parameter

$$\log \mathrm{Re}_{\delta_2} = 4{,}556 - 76{,}87\ (1{,}670 - H_{32})^{1{,}542} \qquad (6.1)$$

in the range $1{,}5150 \leq H_{32} \leq 1{,}6667.$

Using the approximation (6.1), in the case of a pressure drop, the influence of a pressure gradient is very accurately represented up to the rotationally-symmetric stagnation point ($H_{32} = 1.6113$).

6.3 Transition Criteria for Plane Flow

6.3.1 Discussion of the Known Criteria

By evaluating the transition measurements which have become known, empirical transition criteria have been found which are similar to the parameters of stability theory. It is assumed that turbulence is produced by the fact that the perturbation amplitude reaches a certain level. The buildup of the perturbations depends considerably on the pressure gradient of the flow.

Granville [42] assumes that for plane flow, the length of the buildup path characterized by the Reynolds number difference

$$\Delta \mathrm{Re}_{\delta_2} = \mathrm{Re}_{\delta_{2U}} - \mathrm{Re}_{\delta_{2J}} ,$$

only depends on the average pressure gradient between the instability point and the pressure point, with the assumptions made. It is given /32 by the following expressed in terms of the average value of the Pohlhausen shape-parameters,

$$\bar{\kappa}(x'_U) = \frac{1}{x'_U - x'_J} \int_{x'_J}^{x'_U} \kappa(x')\, dx' , \qquad (6.2)$$

where

$$\kappa = - \left[\frac{\partial^2 (u/u_\delta)}{\partial (y/\delta_2)^2} \right]_w .$$

From the corresponding evaluated transition measurements, the empirical law

$$\mathrm{Re}_{\delta_{2U}} - \mathrm{Re}_{\delta_{2J}} = f(\bar{\kappa}), \qquad (6.3)$$

has been derived.

Smith and Gamberoni [40] assume that the self-excitation of the Tollmien-Schlichting-Wellen waves represents the dominant process between the instability point and the transition point, even though the assumption of small perturbations is no longer satisfied in the vicinity of the transition point. They introduce an apparent amplification ratio, at the beginning of transition, to which the amplitudes of the Tollmien-Schlichting waves are to be subjected with the prevailing critical frequency. Using the built-up diagrams established by Pretsch

[41] for Hartree profiles in [40], numerous transition measurements have been evaluated. It has been found that the apparent amplification ratio

$$a = e^{\int_{t_s}^{t_u} \beta_i dt} = e^{9} = 8103 \tag{6.4}$$

can be used as the transition parameter, where

the damping buildup is $\beta_i \begin{cases} < 0 \text{ damping} \\ > 0 \text{ buildup} \end{cases}$

This finding was also confirmed by Ingen [44].

With this convention, it was possible to subsequently correct /33 the purely empirical transition criterion of Michel [39] in [40]

$$Re_{\delta_{2u}} = f(Re_{x_u})$$

The criterion was approximated as follows in [40]

$$Re_{\delta_{2u}} = 1{,}174 \; Re_{x_u}^{0{,}46} \tag{6.5}$$

$$\text{for } 3 \cdot 10^5 < Re_{x_u} < 2 \cdot 10^7$$

The bodies of revolution, the transition criteria (6.3) and (6.5), are not suitable, because the buildup ratio is expressed by boundary layer variables which are different in the plane and rotationally-symmetric cases. The suggestion of Granville [42] to use the criterion (6.3) for plane boundary layers in an unchanged form for rotationally-symmetric boundary layers must of necessity lead to inaccurate results. However, Smith and Gamberoni [40] point out that in the case of bodies of revolution, the criterion (6.5) must be applied to the plane replacement boundary layer. However, this does not consider the fact that the boundary layer transformation can only be performed along the buildup path.

6.3.2 Suggestion for a new Criterion

Because of the deficiencies of the transition conditions mentioned above, we suggested a semi-empirical criterion which can be transferred from the plane case to the rotationally-symmetric case. Since the transition points will be less reliable, the more single processes of the transition process are considered, and the instability point can be determined very accurately, we will consider the buildup path separately. Therefore, in the following, instead of considering the transition criterion, we will give for the length of the buildup path.

Using the transition condition (6.4) we can derive a criterion for the length of the buildup path in the case of similar velocity profiles ($\hat{\beta}$ or H_{32} = const.) between the instability and the transition point /34 using the buildup curves of Pretsch [41]. In this, the influence of the pressure gradient and the suction is included.

According to [41], Figure 5 shows the following buildup curves

$$\int \beta_i \, dt \begin{cases} = 0: & \text{stability condition according to [34]; see Figure 4} \\ = 9: & \text{transition condition according to [40] and [44].} \end{cases}$$

For a constant-shaped parameter, the distance between both curves expressed by the boundary layer variables given in Chapter 5, where

$$\overline{Re_{\delta_{2U}} - Re_{\delta_{2J}} = f(H_{32})} \tag{6.6}$$

where $\overline{H_{32} = f(\hat{\beta})}$ = const. according to (5.30)

is a measure for the length of the buildup path.

The evaluation of the transition measurement for wing profiles with low turbulence initial flow [30, 46-54] done by Moeller [45] shows that the relationship (6.6) is a more reliable criterion for the length of the buildup path for constant shape parameter than the one discussed in 6.3.1, if we introduce the following average value for the shape parameter for instability and transition

$$\left.\begin{aligned} Re_{\delta_{2U}} - Re_{\delta_{2J}} &= f(\overline{H}_{32}) \\ \overline{H}_{32} &= \frac{1}{x'_U/l - x'_J/l} \int_{x'_J/l}^{x'_U/l} H_{32}\left(\frac{x'}{l}\right) d\left(\frac{x'}{l}\right) \end{aligned}\right\} \tag{6.7}$$

This is shown in Figure 6. The criterion has been confirmed by measurements if one ignores certain scatter, which is due to the differences in test conditions of the individual authors.

With special consideration of the transition measurements [30], criterion (6.7) is approximated by the following expressions: /35

$$\left.\begin{aligned} \log\left(Re_{\delta_{2U}} - Re_{\delta_{2J}}\right) &= 1{,}6435 - 24{,}20\ (1{,}5150 - \overline{H}_{32}) \\ &\text{for}\quad 1{,}5150 \leq \overline{H}_{32} \leq 1{,}5600 \\ \log\left(Re_{\delta_{2U}} - Re_{\delta_{2J}}\right) &= 3{,}312 - 967{,}5\ (1{,}6250 - \overline{H}_{32})^{2{,}715} \\ &\text{for}\quad 1{,}5600 < \overline{H}_{32} \leq 1{,}6250 \end{aligned}\right\} \qquad (6.8)$$

This is shown in Figure 6, so that the transition point of a plane laminar boundary layer can be determined directly.

The criterion of Granville [42] shown for comparison in Figure 6 only gives approximately the same values in the central shape parameter range.

6.4 Transfer of the Transition Criterion to Bodies of Revolution

Smith and Gamberoni [40] determined the the transition conditon (6.4) also applies for rotationally-symmetric boundary layers. This means that criterion (6.7) or its approximation (6.8) can be transferred to the plane replacement boundary layer of a body of revolution using the Mangler transformation [12].

$$\widetilde{Re}_{\delta_{2U}} - \widetilde{Re}_{\delta_{2J}} = f\left(\overline{H}_{32}\right) \qquad (6.9)$$

Using the assumption

$$\widetilde{u}_{\delta}(x') = u_{\delta}(x') \qquad (6.10)$$

the coordinates of the plane replacement flow are the following for a body of revolution with the contour r(x'),

$$\left.\begin{aligned} \widetilde{x}' &= \frac{1}{L^2}\int_0^{x'} r^2(x')\,dx' \\ \widetilde{y} &= \frac{r(x')}{L}\,y \end{aligned}\right\} \qquad (6.11)$$

where the constant L is a characteristic length. However, if we introduce L = L(x') in such a way that everywhere /36

$$\tilde{x}' = x' \quad , \tag{6.12}$$

then we obtain

$$L(x') = \sqrt{\frac{\int_0^{x'} r^2(x')\, dx'}{x'}} \tag{6.13}$$

The boundary layer transformation starts at the instability points, so that

$$\tilde{Re}_{\delta_{2_J}} = Re_{\delta_{2_J}}$$

and because of (6.11)

$$\left(\frac{r}{L}\right)_J = 1$$

Consequently, the Mangler constant is calculated from the following using a dimensionless notation

$$\frac{L}{l} = \sqrt{\frac{1}{x'/l - x'_J/l} \int_{x'_J/l}^{x'/l} \left[\frac{r(x')}{l}\right]^2 d\left(\frac{x'}{l}\right)} \tag{6.14}$$

in the range $\frac{x'_J}{l} \leq \frac{x'}{l} \leq \frac{x'_U}{l}$

Using the assumption (6.10) and the relationships

$$\tilde{\delta}_2 = \frac{r/l}{L/l}\, \delta_2$$

$$\tilde{\delta}_3 = \frac{r/l}{L/l}\, \delta_3$$

according to (6.11), the transformed thickness parameters are

$$\tilde{Re}_{\delta_2} = \frac{r/l}{L/l}\, Re_{\delta_2} \; ; \quad Re_{\delta_2} = \sqrt{\frac{u\delta}{u_\infty} \frac{Z}{l}\, Re_l} \tag{6.15}$$

and the transformed shape parameters are

$$\left.\begin{aligned} \tilde{H}_{32} &= H_{32} \\ \tilde{\bar{H}}_{32} &= \bar{H}_{32} = \frac{1}{x'/l - x'_J/l} \int_{x'_J/l}^{x'/l} H_{32}\left(\frac{x'}{l}\right) d\left(\frac{x'}{l}\right) \end{aligned}\right\} \tag{6.16}$$

The expressions $(L/I)^2$ according to (6.14) and $\bar{H}_{32}$ according to (6.16) are formally the same, and are calculated in steps according to the boundary layer parameters (5.7). This means we have the following step formulas in dimensionless form for the Mangler constant /37

$$\left(\frac{L}{I}\right)^2_i = \left(\frac{L}{I}\right)^2_{i-1} - \frac{\frac{\Delta x'_{i,i-1}}{I}}{\sum_{\nu=1}^{i} \frac{\Delta x'_{i,i-1}}{I}} \left[\left(\frac{L}{I}\right)^2_{i-1} - \frac{\left(\frac{r}{I}\right)_{i-1} + \left(\frac{r}{I}\right)_i}{2}\right], \qquad (6.17)$$

and the average shape parameter is

$$\bar{H}_{32_i} = \bar{H}_{32_{i-1}} - \frac{\frac{\Delta x'_{i,i-1}}{I}}{\sum_{\nu=1}^{i} \frac{\Delta x'_{i,i-1}}{I}} \left[\bar{H}_{32_{i-1}} - \frac{H_{32_{i-1}} + H_{32_i}}{2}\right] \qquad (6.18)$$

The step along the contour $\Delta x'_{i,i-1}/l$ is specified by (5.24). The instability point is the initial point.

The transition measurements for two bodies of revolution with a low turbulence incident flow [54 and 55] have been evaluated using the above method, and this is shown in Figure 6. Because of the fact that the measured points of the bodies of revolution do not have a greater scatter than those of the profiles, we therefore have found an experimental verification of the transfer rule for the criterion (6.7) of two bodies of revolution.

6.5 Comparison Calculations

The comparison calculations were performed using the computer program discussed in Chapter 8.

The criterion for the instability point and the transition point can most easily be tested using a plate in longitudinal flow, as shown in Figure 7. The stability criterion (6.1) contains the exact solutions for the Blasius profile of Tollmien [31] and Lin [32] in a satisfactory /38 way. The measurements of Schubauer and Skramstad [30] are well-represented by the transition criteria (6.8). The calculation drag coefficients for natural transition and completely turbulent states agree well with the laws given in [10].

The transition measurements and the drag measurements of Boltz,

Kenyon, and Allen [54, 55] are good test examples for the rotationally-symmetric case. As Figure 8 shows, there is good agreement between the calculated results and the measurements. The theory predicts somewhat longer buildup laminar paths at high Reynolds numbers, and accordingly at lower drag coefficients. A calculation using the calculated transition point positions showed that there was no difference to be detected between the calculated and measured drag coefficients.

7. Influencing the Laminar Boundary Area by means of Suction Slits

7.1 Preliminary Remarks

Suction of the boundary layer particles near the wall causes the following:

- reduction of the boundary layer thickness
- the velocity profile becomes fuller, and
- the potential flow is influenced by a sink effect.

By changing the boundary layer variables, a stabilization of the laminar boundary layer is brought about, as can be seen from the stability diagram in Figure 4.

Even though a continuous distribution of suction over the surface would be optimum from a suction power point of view, only a local suction through slits arranged perpendicularly to the flow direction is possible in technical applications. Also gaps or perforated strips could be used, as shown in Figure 9. Since the influence on the laminar boundary layer is very similar in all three cases, we will only discuss suction slits in the following. /39

In the boundary layer calculation, the suction slits represent discontinuity points, because the assumption of the Prandtl boundary layer equation at the wall $v_w/u_\delta \leq 1/\sqrt{Re_l}$ is violated because of the considerably increased suction velocities. Influencing of the boundary layer at the suction points must therefore be treated separately. Two approaches are possible:

a) the suction points are considered as strips with a finite width, with an intensive area of suction.

For this case, exact solutions have been given by Rheinboldt

[56], Smith and Clutter [57] and Krause [58], as well as the approximate solutions of Bethel [59] and Wuest [60] for specific applications.

b) the suction points are considered as slits with a negligible width. In this case, Walz [61] and Wuest [62] suggest to approximately determine the boundary layer parameters behind the suction point from the started residual profile (amputation principle).

The solutions of a continuous suction over a path are complicated. They are also restricted to a small suction velocity range which is not of practical interest. The amputation principle can be used for an arbitrary suction velocity, body shape, and pressure distribution.

In the following we will give the general approximate relationships for influencing the boundary layer by means of suction slits according to the amputation principle. These are valid both for the laminar and the turbulent boundary layers. After this, we will apply this principle to the laminar boundary layer and will investigate the effects of suction slits on the laminar boundary layer.

We will show that the sink effect of the suction slits is in general negligible because of the low sucked-away amount, when the boundary layer is influenced. /40

7.2 Approximate Solution According to Amputation Principle

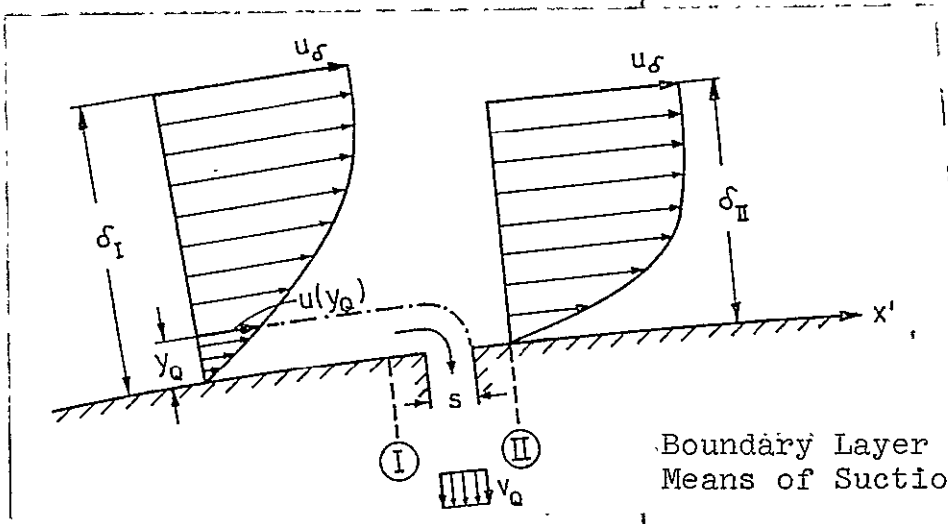

Boundary Layer Influencing by Means of Suction Slit

The amputation principle of Walz [61] is based on the following idea: we will assume that a velocity profile I exists ahead of the suction slit, which is divided up into the following:

- a region near the wall of height y_Q, which is sucked into the slit;

- an external region (residual profile) which goes along the stagnation line, which goes on through the slit. It is deformed without losses in such a way that the incident velocity $u(y_Q)$ decreases at the rear slit edge to $u = 0$ (wall condition). It forms the initial profile II for the boundary layer development behind the slit.

7.2.1 Changed Boundary Layer Variables Behind the Suction Slit

The changed boundary layer variables II behind the slit can be determined from the residual profile with the assumption that the mass, momentum, and energy of the initiated residual profile do not change during the motion over the slit.

If we select a single parameter velocity profile /41

$$\left(\frac{u}{u_\delta}\right)_I = f(\eta, H_{32_I})$$

with the profiles according to (5.1)

$$\frac{\delta 1_I}{\delta_I} = \int_0^1 \left[1-\left(\frac{u}{u_\delta}\right)_I\right] d\eta$$

$$\frac{\delta 2_I}{\delta_I} = \int_0^1 \left(\frac{u}{u_\delta}\right)_I \left[1-\left(\frac{u}{u_\delta}\right)_I\right] d\eta$$

$$\frac{\delta 3_I}{\delta_I} = \int_0^1 \left(\frac{u}{u_\delta}\right)_I \left[1-\left(\frac{u}{u_\delta}\right)_I^2\right] d\eta$$

and the initiation point is at the relative height $\eta_Q = y_Q / \delta_I$, then the boundary layer variables of the residual profile are

$$\left.\begin{aligned}
\frac{\delta 1_{II}}{\delta_I} &= \int_{\eta_Q}^1 \left[1-\left(\frac{u}{u_\delta}\right)_I\right] d\eta \\
\frac{\delta 2_{II}}{\delta_I} &= \int_{\eta_Q}^1 \left(\frac{u}{u_\delta}\right)_I \left[1-\left(\frac{u}{u_\delta}\right)_I\right] d\eta \\
\frac{\delta 3_{II}}{\delta_I} &= \int_{\eta_Q}^1 \left(\frac{u}{u_\delta}\right)_I \left[1-\left(\frac{u}{u_\delta}\right)_I^2\right] d\eta
\end{aligned}\right\} \qquad (7.1)$$

In this way we obtain the changed variables for the boundary layer calculation behind the suction slit

$$\left.\begin{aligned} \frac{Z_{II}}{Z_I} &= \left[\frac{\delta_{2_{II}}/\delta_I}{\delta_{2_I}/\delta_I}\right]^2 \\ H'_{32_{II}} &= \frac{\delta_{3_{II}}/\delta_I}{\delta_{2_{II}}/\delta_I} \end{aligned}\right\} \qquad (7.2)$$

In order to again order the velocity profile II into the family of the single-parameter velocity profiles, instead of the shape parameter H'_{32II} we will introduce the averaged value /42

$$H_{32_{II}} = \frac{1}{2}\left(H'_{32_{II}} + H''_{32_{II}}\right), \qquad (7.3)$$

where

$$H''_{32_{II}} = f\left(H_{12_{II}}\right) = f\left(\frac{\delta_{1_{II}}/\delta_I}{\delta_{2_{II}}/\delta_I}\right), \qquad (7.4)$$

The functional relationship in (7.4) is unique for single-parameter velocity profiles. The shape parameters $H'_{32_{II}}$ and $H''_{32_{II}}$ deviate only slightly from one another.

In the case of single parameter velocity profiles ahead of the suction slit, the boundary layer variables behind the slit only depend onthe shape parameter H_{32_I} and the relative suction height η_Q.

7.2.2 Suction Variables

By using the following definition of the relative suction thickness

$$\frac{\delta_Q}{\delta_I} = \int_0^{\eta_Q} \left(\frac{u}{u_\delta}\right)_I d\eta = \eta_Q - \frac{\delta_{1_Q}}{\delta_I}, \qquad (7.5)$$

we can calculate the amount of air sucked away by a slit corresponding to the suction height η_Q, referred to the slit length b (body of revolution: $b = 2\pi r$).

$$\frac{Q}{b} = u_\delta \delta_Q$$

or the local suction coefficient amount

$$c_Q = \frac{Q}{u_\infty b l} = \frac{u_\delta}{u_\infty} \frac{\delta_Q}{l} \tag{7.6}$$

In addition, we define the nondimensional suction amount coefficient

$$c_Q^* = c_Q \frac{Re_l}{Re_{\delta 2}} = \frac{\delta_Q / \delta_I}{\delta_{2I} / \delta_I} \tag{7.7}$$

where /43

$$\frac{Re_l}{Re_{\delta 2I}} = \sqrt{\frac{Re_l}{\overline{Z}_I / l \; u_\delta / u_\infty}}$$

which only depends on H_{32_I} and η_Q for a single parameter velocity profile ahead of the slit.

According to Gregory [63], the disturbance of the boundary layer due to the slits is minimal if the slit s is equal to the suction height η_Q. Accordingly, the optimum slit width is

$$\frac{s}{l} \equiv \frac{y_Q}{l} = \eta_Q \frac{\delta_I}{l} \tag{7.8}$$

The nondimensional slit width

$$s^* = \frac{s}{l} \frac{Re_l}{Re_{\delta 2I}} \frac{u_\delta}{u_\infty} = \frac{\eta_Q}{\delta_{2I} / \delta_I} \tag{7.9}$$

only depends on H_{32_I} and η_Q for single parameter velocity profiles.

Using the continuity law, we obtain the average suction velocity in the slit as follows:

$$\frac{v_Q}{u_\infty} = \frac{c_Q}{s/l} = \frac{c_Q^*}{s^*} \frac{u_\delta}{u_\infty} \tag{7.10}$$

7.3 The Amputation Principle to the Laminar Boundary Layer

7.3.1 Suction Relationships

The relationships in Chapter 7.2 apply for any boundary layer state. Here, we will derive relationships for influencing the laminar boundary layer by suction slits. We will assume the laminar velo- /44
city profile ahead of the suction slit can be approximated by the single parameter model of Geropp [16] [1]

$$\frac{u}{u_\delta} = 1-(1-\eta)^c \ (1+a_1\eta + a_2\eta^2 + a_3\eta^3) \tag{7.11}$$

with the coefficients

$$\left.\begin{aligned} a_1 &= c - \varepsilon \\ a_2 &= \frac{\Lambda}{2} - c\,\varepsilon + \frac{c\ (c+1)}{2} \\ a_3 &= \frac{\Lambda}{2}\,c - \varepsilon\ \frac{c\ (c+1)}{2} + \frac{c\ (c+1)\ (c+2)}{6} \end{aligned}\right\} \tag{7.12}$$

and the following analytic expressions for

$$\left.\begin{aligned} \varepsilon &= \left[\frac{\partial (u/u_\delta)}{\partial \eta}\right]_{\eta=0} = -0{,}89855 + \sqrt{1{,}60901\,\Lambda + 13{,}6795} \\ c &= 5{,}22550 + \sqrt{1{,}30839\,\Lambda + 10{,}85171} \end{aligned}\right\} \tag{7.13}$$

The Pohlhausen-shape parameter which occurs in these relationships is related to the shape parameter

$$\Lambda = \left[\frac{\partial^2 (u/u_\delta)}{\partial \eta^2}\right]_{\eta=0}$$

by means of the following approximations

$$\Lambda = 38{,}745\ \hat{ß} - 7{,}1178\ \hat{ß}^2 + 6{,}3726\ \hat{ß}^3 \tag{7.14}$$

and

$$\left.\begin{aligned} \hat{ß} &= -2788{,}62 + 5439{,}97\ H_{32} - 3539{,}62\ H_{32}^2 + 768{,}15\ H_{32}^3 \\ &\quad \text{for } 1{,}5237 \leq H_{32} \leq 1{,}5729 \\ \hat{ß} &= -35461{,}01 + 67123{,}15\ H_{32} - 42356{,}63\ H_{32}^2 + 8910{,}45\ H_{32}^3 \\ &\quad \text{for } 1{,}5729 < H_{32} \leq 1{,}6239 \end{aligned}\right\} \tag{7.15}$$

The Geropp model is valid in the following range: /45

Separation profile $\left\{ \begin{array}{l} -0.1988 \leq \hat{\beta} \leq 1.0 \\ 1.5237 \leq H_{32} \leq 1.6239 \end{array} \right\}$ plane stagnation point profile

The boundary layer thickness used as the reference variable for the suction height is defined in many ways*:

- in the boundary layer theory of Prandtl $\delta = y(u/u_{\delta_p} = 0{,}99)$
- in the approximate model of Geropp $\delta^G = y(u/u_{\delta_p} = 1{,}0)$.

One must distinguish between the following relative suction height

$$\eta_Q = \frac{y_Q}{\delta}$$

of practical interest, and the theoretical quantity

$$\eta_Q^G = \frac{y_Q}{\delta^G}$$

which occurs in the suction relationships.

The relationship

$$\frac{\delta}{\delta^G} = \frac{\eta_Q^G}{\eta_Q} = f(H_{32})$$

is shown in Figure 10 and can be approximated by the following polynomial

$$\frac{\delta}{\delta^G} = 5378{,}67 - 12707{,}78\ H_{32} + 11189{,}97\ H_{32}^2 - 4346{,}14\ H_{32}^3 + 627{,}10\ H_{32}^4 \qquad (7.16)$$

$$\text{for } 1{,}5237 \leq H_{32} \leq 1{,}6239 \ .$$

The boundary layer variables ahead of the suction slit are written using the velocity model of Geropp

*The quantity δ_2 is introduced as a reference quantity for the suction relationships independent of the selected velocity model, but the evaluation of the following integral expressions would become much more difficult.

$$\left.\begin{aligned}
\frac{\delta 1_I}{\delta_I} &= \int_0^1 \left(1-\frac{u}{u_\delta}\right) d\eta = I_{1_I} \\
\frac{\delta 2_I}{\delta_I} &= \int_0^1 \frac{u}{u_\delta}\left(1-\frac{u}{u_\delta}\right) d\eta = I_{1_I} - I_{2_I} \\
\frac{\delta 3_I}{\delta_I} &= \int_0^1 \frac{u}{u_\delta}\left[1-\left(\frac{u}{u_\delta}\right)^2\right] d\eta = 2I_{1_I} - 3I_{2_I} + I_{3_I}
\end{aligned}\right\} \qquad (7.17)$$

The integral expressions

$$\left.\begin{aligned}
I_{1_I} &= \int_0^1 (1-\eta)^c (1+a_1\eta + a_2\eta^2 + a_3\eta^3)\, d\eta \\
I_{2_I} &= \int_0^1 (1-\eta)^{2c} (1+a_1\eta + a_2\eta^2 + a_3\eta^3)^2\, d\eta \\
I_{3_I} &= \int_0^1 (1-\eta)^{3c} (1+a_1\eta + a_2\eta^2 + a_3\eta^3)^3\, d\eta
\end{aligned}\right\} = f(H_{32_I}) \qquad (7.18)$$

are evaluated in the appendix.

Accordingly, we convert the boundary layer variables of the remaining profiles

$$\left.\begin{aligned}
\frac{\delta 1_{II}}{\delta_I} &= \int_{\eta_Q^G}^1 \left(1-\frac{u}{u_\delta}\right) d\eta = I_{1_{II}} \\
\frac{\delta 2_{II}}{\delta_I} &= \int_{\eta_Q^G}^1 \frac{u}{u_\delta}\left(1-\frac{u}{u_\delta}\right) d\eta = I_{1_{II}} - I_{2_{II}} \\
\frac{\delta 3_{II}}{\delta_I} &= \int_{\eta_Q^G}^1 \frac{u}{u_\delta}\left[1-\left(\frac{u}{u_\delta}\right)^2\right] d\eta = 2I_{1_{II}} - 3I_{2_{II}} + I_{3_{II}} \\
\frac{\delta_Q}{\delta_I} &= \int_0^{\eta_Q^G} \frac{u}{u_\delta}\, d\eta = \eta_Q^G - (I_{1_I} - I_{1_{II}})
\end{aligned}\right\} \qquad (7.19)$$

the boundary layer parameters of the remaining profile

$$\frac{Z_{II}}{Z_I} = \left[\frac{\delta_{2_{II}}/\delta_I}{\delta_{2_I}/\delta_I}\right]^2 = \left[\frac{I_{1_{II}} - I_{2_{II}}}{I_{1_I} - I_{2_I}}\right]^2 \qquad (7.20)$$

$$H'_{32_{II}} = \frac{\delta_{3_{II}}/\delta_I}{\delta_{2_{II}}/\delta_I} = 2 - \frac{I_{2_{II}} - I_{3_{II}}}{I_{1_{II}} - I_{2_{II}}}$$

$$H''_{32_{II}} = f\left(H_{12_{II}} = \frac{\delta_{1_{II}}/\delta_I}{\delta_{2_{II}}/\delta_I} = \frac{I_{1_{II}}}{I_{1_{II}} - I_{2_{II}}}\right) \qquad (7.20)$$

(continued)

and the nondimensional suction variables

$$c^*_Q = \frac{\delta_Q/\delta_I}{\delta_{2_I}/\delta_I} = \frac{\eta^G_Q + I_{1_{II}} - I_{1_I}}{I_{1_I} - I_{2_I}}$$

$$s^* = \frac{\eta^G_Q}{\delta_{2_I}/\delta_I} = \frac{\eta^G_Q}{I_{1_I} - I_{2_I}} \qquad (7.21)$$

The relationship $H''_{32_{II}} = f(H_{12_{II}})$ in (7.20) is approximated by

$$H''_{32_{II}} = 2{,}660594 - 0{,}922220\ H_{12_{II}} + 0{,}276058\ H^2_{12_{II}} - 0{,}036478\ H^3_{12_{II}} + 0{,}001836\ H^4_{12_{II}}$$
$$\text{for } 1{,}5237 \leq H''_{32_{II}} \leq 1{,}5726$$

$$H''_{32_{II}} = 1{,}741773 - \sqrt{0{,}038887\ H_{12_{II}} - 0{,}072234}$$
$$\text{for } 1{,}5726 < H''_{32_{II}} \leq 1{,}6667 \quad \text{analog (5.15)}$$

$$H''_{32_{II}} = 1{,}4418 + 0{,}07444\ (3{,}738 - H_{12_{II}})^2$$
$$\text{for } H''_{32_{II}} > 1{,}6667 \quad \text{analog (5.16)} \qquad (7.22)$$

The integral expressions

$$I_{1_{II}} = \int_{\eta^G_Q}^{1} (1-\eta)^c\ (1+a_1\eta + a_2\eta^2 + a_3\eta^3)\ d\eta$$

$$I_{2_{II}} = \int_{\eta^G_Q}^{1} (1-\eta)^{2c}\ (1+a_1\eta + a_2\eta^2 + a_3\eta^3)^2\ d\eta$$

$$I_{3_{II}} = \int_{\eta^G_Q}^{1} (1-\eta)^{3c}\ (1+a_1\eta + a_2\eta^2 + a_3\eta^3)^3\ d\eta \qquad = f(H_{32_I}, \eta^G_Q) \qquad (7.23)$$

are evaluated in the appendix.

/48

7.3.2 Results for Arbitrary Pressure Gradients

Figure 11 shows the velocity profiles behind a suction slit which was produced for different relative suction heights from the Blasius profile ahead of the suction slit. Much more full velocity profiles occur already for small suction heights.

For arbitrary pressure gradients, we have plotted the following:

- Figure 12, the shape parameter behind the suction slit $H_{32_{II}}$
- Figure 13, the ratio of the thickness parameter before the suction slit, Z_{II}/Z_I
- Figure 14, the nondimensional suction amount coefficient c_Q^*
- Figure 15, the optimum nondimensional suction width, s*.

As a function of the shape parameter ahead of the suction slit H_{32_I} and the relative suction height η_Q^G, the shape parameter H_{32_I} can vary in the limits

$$1{,}5237 \leq H_{32_I} \leq 1{,}6239 \ ,$$

for which Geropp velocity model is valid. For complete boundary layer suction removal $\eta_Q^G = 1$, one obtains a rectangular profile ($H_{32_{II}} = 2$) with $Z_{II}/Z_I = 0$ as a limiting value behind the suction slit. In addition, Figures 12 to 15 show the asymptotic suction profile as a limiting case for continuous suction.

In the case of the plate boundary layer ($H_{32_I} = 1.5726$), there is a relationship between the suction amount coefficient c_Q^* and the suction height η_Q^G which is shown in Figure 16. Since in this case there is only one free parameter, the shape parameter behind the suction slit, the thickness parameter ratio Z_{II}/Z_I and the slit width s* can be represented as functions of the suction amount coefficient c_Q^* as shown in Figure 17.

In order to evaluate the slit suction, it is important how fast /49 the suction effect drops off behind the slit. The variation of the boundary layer parameters H_{32} and Z/I behind a suction slit shown for a flat-plate as a function of the suction amount coefficient c_Q^* shows the following:

- The shape parameter increase decays behind the suction slit, as the thickness parameter reduction still has a large effect at a large distance behind the slit.

- as the suction amount increases, the shape parameter increase along the trailing slit edge increases, but it decays faster because of the related thickness reduction.

This is shown in Figure 18.

This means that for a certain suction amount, the influence range of a suction slit becomes a maximum. For large suction amount coefficients, the laminar boundary layer behind the slit becomes thinner, but not more stable.

Figure 19 shows the example of a plane boundary layer. The shape parameter influence behind the suction slit decays faster, the thinner the boundary layer ahead of the slit. Therefore, we can already draw the conclusion that as the boundary layer thickness increases, the slit separations increase in the flow direction.

7.3.3 Comparison Calculations

As in a test example for the approximate solution for determining the laminar boundary layer influence by suction slits, we can use a suction strip over a plane plate, which has been discussed by several authors.

Krause [64] calculated the influencing of the boundary layer by suction strips of various widths for a constant amount of sucked-off flow, as shown in Figure 20. If in the case of slit suction, the corresponding suction amount coefficient is

$$c_Q^* = \frac{s}{x_Q} \; v_w^* \; \frac{\sqrt{Re_l}}{Re_{\delta_2}} = \frac{s}{x_Q} \; \frac{v_w^*}{0{,}6641}$$

If the boundary layer influence plotted against the width of the suction strip is extrapolated to the width of the suction slit, then we find the following: /50

- The thickness parameter reduction Z_{II}/Z_I through a suction slit agrees well with the thickness parameter reduction through a suction strip.

- The shape parameter increase $(H_{32_{II}} - H_{32_I})$ through a suction slit can not be completely verified by the exact solution for a suction strip; for example, we have to consider the fact that at $Re_l = 10^8$, the narrowest investigated suction strip is about 220 times wider than the

corresponding suction slit.

The comparison calculation given in Figure 21 shows that for the same suction amount, the influence on the boundary layer behind a suction slit according to the amputation method and behind a suction strip according to the calculations of Rheinboldt [56], Smith and Clutter [57], Bethel [59], and Krause [64] are very similar if the slit is arranged in the middle of the strip. The relationship

$$c_Q^* = \frac{s/x_o}{\sqrt{1+s/2x_o}} \quad \frac{v_w^*}{0{,}6641}$$

exists.

The reliability of the amputation method has therefore been proven. Therefore, the results of the slit suction calculation apply approximately for narrow suction strips.

7.4 Sink Effect of Ring-Shaped Suction Slits

An additional velocity is induced through each suction slit, which is superimposed on the potential flow. /51

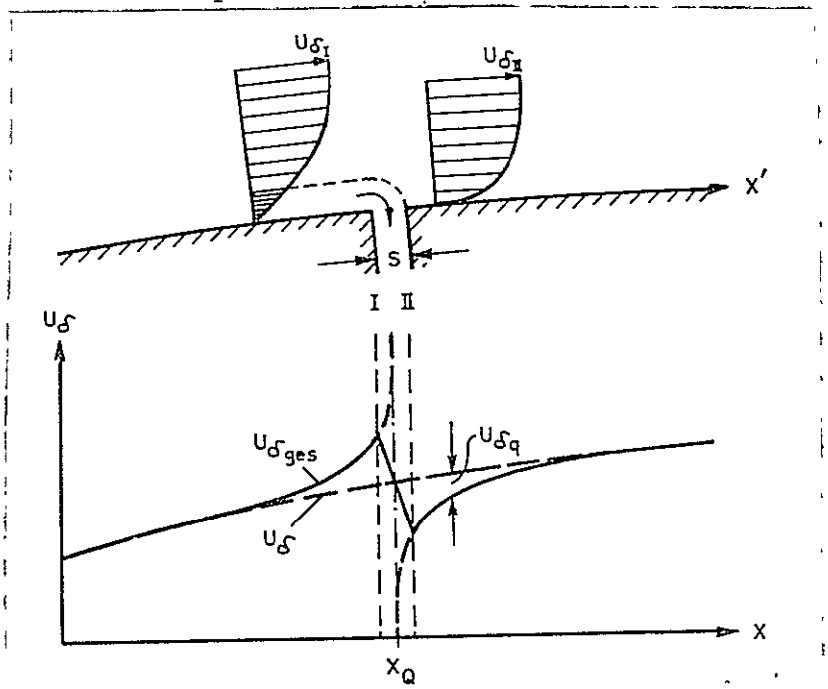

Influencing of the Velocity Distribution By Means of a Suction Slit.

In the case of a body of revolution, we have the problem of estimating the additional velocities induced by ring-shaped suction sinks.

We will assume that a source ring (x_Q, r_Q) with yield $q_Q(\varphi_Q) =$

q_Q = const., induces the following axial and radial velocity components at a point P(x, r, ϕ).

$$u_{q_x} = \frac{q_Q}{2\pi r_Q} u^*_{q_x}$$

$$u_{q_r} = \frac{q_Q}{2\pi r_Q} u^*_{q_r} \qquad (7.24)$$

The reduced, induced velocity components /52

$$\left.\begin{matrix} u^*_{q_x} \\ u^*_{q_r} \end{matrix}\right\} = f\left(\frac{x}{r_Q}, \frac{r}{r_Q}\right)$$

were tabulated by Kuechemann and Weber [65] as well as Dreger [66].

If we introduce for the yield q_o for the suction amount coefficient c_Q according to (7.6),

$$q_Q = -\frac{Q}{2\pi r_Q} = -\frac{c_Q u_\infty O}{2\pi r_Q} \qquad (7.25)$$

then it is possible to write the velocity components in a dimensionless form

$$\left.\begin{aligned} \frac{u_{q_x}}{u_\infty} &= -\frac{c_Q O/l^2}{4\pi^2 (r_Q/l)^2} u^*_{q_x} \\ \frac{u_{q_r}}{u_\infty} &= -\frac{c_Q O/l^2}{4\pi^2 (r_Q/l)^2} u^*_{q_r} \end{aligned}\right\} \qquad (7.26)$$

The tangential component

$$\frac{u_{q_t}}{u_\infty} = \frac{\frac{u_{q_x}}{u_\infty} + \frac{dr}{dx}\frac{u_{q_r}}{u_\infty}}{\sqrt{1 + \left(\frac{dr}{dx}\right)^2}} \equiv \frac{u_{\delta q}}{u_\infty} \qquad (7.27)$$

is the additional velocity induced on the body surface by a suction ring.

For small suction amount coefficients, the sink effect is restricted to the immediate vicinity of the suction sink, so that when there are several suction sinks, only the influence of the two adjacent sinks

$$\frac{u_{\delta_{ges}}}{u_\infty} = \frac{u_\delta}{u_\infty} + \frac{u_{\delta_{qi-1}}}{u_\infty} + \frac{u_{\delta_{qi}}}{u_\infty} \qquad (7.28)$$

has to be considered in the range $\frac{x_{i-1}}{T} \leq \frac{x}{T} \leq \frac{x_i}{T}$ /53

The additional velocity that is positive ahead of the suction sink is negative behind the sink. This means that there is a pressure drop due to the sink effect in the vicinity of the suction sink, which is superimposed on the shape-determined pressure distribution.

$$c_{p_{ges}} = 1 - \left(\frac{u_{\delta_{ges}}}{u_\infty}\right)^2 \qquad (7.29)$$

The sink influence is estimated for a circular cylinder in axial flow having a suction ring in the center, which is given in Figure 22. Because of $r = r_Q = \text{const.}$, and $dr/dx = 0$, we have the following for the circular cylinder

$$\frac{u_{\delta q}}{u_\infty} = \frac{u_{q_x}}{u_\infty}$$

Since the slit width in relationship to the boundary layer $s/\delta = \eta_Q \ll 1$, the additional velocity in the immediate vicinity of the suction slit depends substantially on the boundary layer thickness and increases with increasing incident Reynolds number.

As can be seen from Figure 22, the additional velocities induced by ring-shaped slits over a body of revolution in the case of laminar boundary layer suction are so small compared to the incident velocity over the Reynolds number range of interest that they can be ignored.

7.5 Optimum Suction

7.5.1 Optimum Position of Suction Slits

In technical applications we are interested in the configuration of the suction slits, so that a body surface can be made laminar using the minimum number of suction points.* /54

*Technically we are also interested in the question of how the body surface can be made laminar with the minimum amount of sucked-in flow for a specified position of the suction slits. The maximum possible slit separations are then taken from the present paper.

The suction relationships in Chapter 7.3 say nothing about the position of the suction slits, but instead contain the following free parameters:

- the boundary layer parameter ahead of the suction slits, Z_{I_i}, $H_{32_{I_i}}$
- and the relative suction heights η_{Q_i}.

A condition for avoiding boundary layer transition is that the laminar boundary layer remains stable in the entire suction region. If the state is partially unstable, the boundary layer perturbations would be built up in an uncontrollable manner in spite of suction, and this would lead to premature transition. The stability criterion (6.1) therefore is a boundary condition for optimum suction of the laminar boundary layer.

The first suction slit is an exception to this, ahead of which one can allow an unstable laminar boundary layer, as experiments bv Pfenninger have shown [6] - if there is a sufficiently long suction region behind it, which serves as a damping path. Therefore, we will introduce the transition criterion (6.8) as the boundary condition for the first suction slit. With this assumption we can bring about a substantial reduction in the number of slits, because as will be shown later on, the slit separation required for the stability criterion is small.

By introducing the stability condition or the transition condition into the suction relationships, we specify the boundary layer parameters ahead of the suction slits. The position of the suction slits depends only on the relative suction height η_{Qi} for a specified body shape and incident Reynolds number.

The region of influence of a suction slit can not be arbitrarily /55
extended by increasing the relative suction height, as we showed in Chapter 7.3.2. It becomes optimum at a relative optimum suction height η_{Qopt}.

When optimizing the relative suction height for maximum slit separation, we will assume the same relative suctionheight for all suction slits.

The end of the suction region is one of the free variables.

7.5.2 Total Sucked-In Flow

The total suction amount of a body in a flow with n_Q suction points is

$$Q = \sum_{i=1}^{n_Q} Q_i \quad .$$

The total suction amount coefficient of a body of revolution is calculated from

$$c_Q = \frac{Q}{u_\infty O} = \frac{2\pi}{O/l^2} \sum_{i=1}^{n_Q} \frac{r_i}{l} \, c_{Qi} \qquad (7.30)$$

where the local suction amount coefficient is defined by (7.6).

Accordingly, the total suction amount coefficient of a plane contour is

$$c_Q = \frac{Q}{u_\infty F} = \sum_{i=1}^{n_Q} c_{Qi} \qquad (7.31)$$

7.5.3 Consideration of Suction Power in the Drag Balance

When evaluating a body in a flow with boundary layer suction, it is necessary to consider the required suction power in the drag balance calculation. The references Edwards [67] and Torenbeek [68] contain approximate calculation methods for the suction power for special suction installations over wings.

Assuming that the suction amount does not contribute to the thrust, that is, it emerges with $u = u_\infty$ and $p = p_\infty$, at one point of the body again, the following pumping power is required for the suction slit (i) in the case of incompressible flow /56

$$\eta_P N_{Qi} = Q_i \frac{\varrho}{2} u_\infty^2 - Q_i (\Delta p_i + \Delta p_{V_i}) \qquad (7.32)$$

The pumping efficiency η_p and the pressure losses Δp_{V_i} on the suction points and throttling points, as well as in the lines, are only known after design of the suction installation has taken place. The publications of Pfenninger [69] and Gregory [63] state that the total pressure losses of a suction installation are rarely greater than $\Delta p_V = (0.1 \pm 0.2)\, q_\infty$. In order to estimate the suction power, it is therefore possible to ignore the pressure losses, and we can set the pumping efficiency $\eta_p = 1$ so that approximately we have the following for the suction point (i).

$$N_{Qi} = Q_i (q_\infty - \Delta p_i), \tag{7.33}$$

and for n_Q suction points,

$$N_Q = \sum_{i=1}^{n_Q} Q_i (q_\infty - \Delta p_i). \tag{7.34}$$

Instead of the suction power, we will define an internal or equivalent suction drag

$$W_Q = \frac{N_Q}{v_\infty} \tag{7.35}$$

Accordingly, using (7.6) we can calculate the equivalent suction drag coefficient of a body of revolution

$$c_{w_Q} = \frac{W_Q}{q_\infty O} = \frac{2\pi}{O/l^2} \sum_{i=1}^{n_Q} \frac{r_i}{l} c_{Qi} (1-c_{p_i}) \tag{7.36}$$

and of a plane contour

$$c_{w_Q} = \frac{W_Q}{q_\infty F} = \sum_{i=1}^{n_Q} c_{Qi} (1-c_{p_i}). \tag{7.37}$$

We then obtain the total drag of a body with consideration of the suction power from the sum of the external and internal drag values /57

$$W = W_N + W_Q. \tag{7.38}$$

Accordingly, the total drag coefficient of a body of revolution, with respect to the surface is

$$c_{w_O} = \frac{W}{q_\infty O} = c_{w_N} + c_{w_Q}, \tag{7.39}$$

and with respect to the volume, it is

$$c_{w_V} = \frac{W}{q_\infty V^{2/3}} = c_{w_O} \frac{O}{V^{2/3}}, \tag{7.40}$$

which is determined from (5.38) as c_{w_N}.

In the plane case, the total drag coefficient is

$$c_{w_F} = \frac{W}{q_\infty F} = c_{w_N} + c_{w_Q} \tag{7.41}$$

where c_{w_N} is given by (5.39).

7.5.4. Comparison Calculations

As a test example for a body in a flow with slit suction, we can use the suction experiments of the Pfenninger group [6] with the test aircraft F-94A. In the test experiments the boundary layer was held laminar along the top side of a wing without sweep back using 69 suction slits in the range $0.410 \leq x_{Abs}/l \leq 0.953$ up to the Reynolds number $Re_l = 3.6 \times 10^7$. It was kept laminar into the region of the trailing edge.

Figure 23 shows the contour and the pressure distribution of the profile topside for the lift coefficient $c_A = 0.15$. This lift coefficient corresponds to the incident Reynolds number $Re_l = 3 \times 10^7$, where the comparison calculations were made.

The position of the first suction slit in the experiments agrees very well with the calculated transition point positions for the case without suction, $x_{Abs}/l = 0.410$.

Using the computer program discussed in Chapter 8, however, we can not simultaneously maintain the suction conditions of Pfenninger

- slit number $n_Q = 69$
- total suction amount coefficient $c_Q = 3 \times 10^{-4}$

because they are not optimum with respect to minimum slit number. Therefore, in the comparison calculations we vary the parameter n_Q so that one suction condition of the experiments each was satisfied. The comparison calculations are given in Figures 23 and 24.

- if $n_Q = 69$ is specified, then the calculation gives about the same slit separations, a substantially reduced suction amount, and a somewhat reduced total drag compared with the suction experiment.
- if $c_Q = 3 \times 10^{-4}$ is specified, then the calculation gives substantially less suction points but about the same total drag.

We should consider that the suction experiments were performed at the Mach number $M = 0.6$, but that the calculation was restricted to incompressible flow.

The comparison calculations confirm that the equivalent suction drag can be approximated using the approximations agreed to in Chapter 7.5.3. Therefore, the drag coefficients calculated for slit suction are valid. If the relative suction height is suitably selected, it is possible to substantially reduce the number of slits and the suction amount compared with the suction configuration of Figure 9.

/59

8. Description of Computer Program

8.1 Preliminary Remarks

A computer program was developed for characterizing the boundary layer and drag of bodies in flows with laminar influencing suction slits. It allows the following systematic variations:

- rotationally-symmetric or plane contours.
  - *thickness ratio d/l
  - *length ratio of { Nose, l_B/l ; Middle part l_M/l ; Tail l_H/l }
  - *body function of { nose $\eta_B = f(\xi_B)$; tail $\eta_H = f(\xi_H)$ }
- the suction conditions for slit suction
  - * relative suction height η_Q
  - * suction region x_{Abs}/l { Beginning ; End }
  - * number of suction points n_Q
- transition point position x_u/l in the case without suction
  - * natural
  - * forced, especially { completely laminar / completely turbulent }

- and the incident Reynolds number Re_1.

Using the program, the following are calculated: /60

- the boundary-layer variables at the support points Z/l, H_{32}, $Re_2 = f(x_s/l)$.
- The boundary layer and suction variables at the suction points

$$\eta_a^G \;,\; Z_I/l,\; H_{32_I} \;,\; Z_{II}/l,\; H_{32_{II}} \;,\; c_{Q_i},\; s/l = f(x_Q/l)$$

-
- The boundary layer variables at the points

$$Z/l,\; H_{32} \;,\; Re_{\delta_2} = f(x_K/l)\,,$$

- The total suction removal coefficient c_Q
- And the drag coefficients c_{W_N}, c_{W_Q}, c_{W_O}, c_{W_V}.

8.2 Structure of Computer Program

8.2.1 Numerical Methods

Boundary Layer Calculation Using the Step Formulas (5.22).

The boundary layer variables Z, H_{32} at the end of interval (i) are determined by iteration from the values at the beginning of the interval (i-1). For the first interval iteration step $\nu = 0$, the variables at the previous interval (i-1) are used. The iteration accuracy is

$$\left| H_{32_i}^{(\nu)} - H_{32_i}^{(\nu-1)} \right| \leq 5 \cdot 10^{-5} \qquad (8.1)$$

The iteration converges rapidly

$$\left| \frac{u_{\delta_i}}{u_{\delta_{i-1}}} - 1 \right| \leq 0{,}03 \qquad (8.2)$$

and

$$\left| H_{32_i}^{(0)} - H_{32_{i-1}} \right| \leq 0{,}003 \qquad (8.3)$$

In the program, there is a step selection which is automatic, starting with the distance to the next support point /61

$$\frac{\Delta x_{i,i-1}^{(0)}}{l} = \frac{x_s}{T} - \frac{x_i}{T} \qquad (8.4)$$

The step is cut in half

$$\frac{\Delta x_{i,i-1}^{(\mu)}}{l} = \frac{1}{2}\,\frac{\Delta x_{i,i-1}^{(\mu-1)}}{l} \tag{8.5}$$

when the convergence conditions with the selected step are not satisfied, or if the accuracy cannot be reached in $\nu = 10$ iteration steps. A maximum of $\mu = 80$ step halving operations is allowed. Investigations of the time optimization of the boundary layer calculation were performed by Otte [70].

Determination of the Exceptional Points in a Boundary Layer Calculation

The following are exceptional points for the boundary layer variation (G):

- suction slits
- instability point
- transition point
- laminar separation point
- turbulent separation point
- end of the region where the rotationally-symmetric boundary layer calculation is valid

for which the criteria (K) are specified. The calculation of these points leads to determining the zeroes of the function

$$F_G\left(\frac{x}{l}\right) - F_K\left(\frac{x}{l}\right) = 0 \tag{8.6}$$

with the required accuracy

$$\left|\frac{x_K}{l} - \frac{x_i}{l}\right| \leq 10^{-4} \tag{8.7}$$

Since the function (8.6) is not available in analytic form, the /62 zeroes are calculated numerically by boxing in.

8.2.2 Program Structure

The computer program consists of the following:

- the main parts
  - * initial calculations
  - * boundary layer calculations

*Initial calculation

- and the routines

*suction slit

*Mangler transformation.

In the "suction slit" routine, the suction variables are shown in Figures 12 to 15.

In the "Mangler" transformation routine, the Mangler constant L/l and the average shape parameter, $\overline{H}_{32}$ which are requird for the transition point determination. Formulas (6.17) and (6.18) are used.

8.2.3 Special Conventions

The possibilities of the computer program can be found in Chapter 8.1. Additionally, the following conventions are agreed upon:

- there is boundary layer transition at the laminar separation point,
- there is no drag calculation for turbulent separation
- the drag calculation from the boundary layer variables is done as follows:

*At the point $\delta_2/r = 1/15$ for rotationally-symmetric contours,

*At the last support point for plane contours.

- the last boundary layer transition occurs as follows:

*at the boundary layer $\delta_2/r = 1/16$ for a rotationally-symmetric contour,

*at the next-to-last support point for a plane contour. /63

- the suction region ends prematurely,

*for a forced boundary layer transition

*as soon as $1.5237 > H_{32_I} > 1.6250$ applies ahead of the suction point.

If the laminar boundary layer is still unstable behind the first suction slit, then the suction height is increased until a stable state is reached.

8.3 ALGOL-Program

The computer program is written in ICL-ALGOL for the ICL 1900 computer installation of the Berlin Technical University[1]. Compared

[1]The computer program is available from the Institute For Aircraft Design for T.U., Berlin.

with ALGOL declarations, there are only slight modifications.

The program has a memory requirement of nominally 13,250 locations in this computer. For 100 support points and 100 suction points, this is expanded to about 17,500 locations. In calculations without suction, the memory requirement is substantially reduced, if the program variation is used without the suction slit "routine".

The calculation time primarily depends on the number of slits. Without suction, it is about 30 seconds and increases to about 7 minutes for about 100 suction slits.

Figures 3, 7, 8, 23, and 24 show test calculations with the program.

For systematic contour variations, the program can be coupled with a pressure distribution program, which contains a suitable shape systematic program and a support point interpolation. If the input and outputs of the programs are coordinated, then the input of the support point values is reduced to certain parameters which characterize the body shape. A program for pressure distribution has been given by Oehler for bodies of revolution [9].

9. Results of the Variation Calculation

The computer program discussed in Chapter 8 affords the possibility of extensive parameter studies. We will select a few to give an idea about technical applications.

9.1 Plane Plate: Variation of Suction Conditions

Already by using the example of a plane plate in longitudinal flow (pressure gradient $dp/dx = 0$), we can obtain basic information about the optimum configuration of the suction slits. In this case, the most important influences in the variables are the following:

- the incident Reynolds number Re_1
- the relative suction height η_Q
- and the suction region x_{Abs}/l.

The Reynolds number Re_1 is given by the problem formulation. The suction height η_Q should be optimized for a minimum number of slits, if we agree that the suction region is such that it starts in the transition point and ends for a relative plate length of $x/l = 0.95$.

Figure 25 shows the boundary layer variation for $Re_1 = 10^7$ and $\eta_Q = 0.1$. Figure 26 shows the suction variables plotted over the plate length. As already discussed in Chapters 7.3.2, the suction slits with small suction heights bring about a substantial shape parameter increase and a slight thickness parameter decrease. The boundary layer /65
thickness increases in the flow direction, nevertheless. However, the suction action behind a slit decreases more slowly the thicker the boundary layer is. At η_{Q_i} = const. the slit separations become greater with path length. Accordingly, the optimum slit widths and the local suction amount coefficients increase in the flow direction. In the literature, this basic fact has not yet been published.

Figure 27 shows that the slit separations, slit widths, and the local suction amount coefficients are reduced within increasing incident Reynolds number because of the decrease in the boundary layer thickness.

The increase in the number of slits with increasing incident Reynolds number shown in Figure 28 is caused by the earliest beginning of suction and the reduction of the slit separations. The reduction in drag due to suction is also considerable, if one considers the suction power. For $\eta_Q = 0.1$, the drag coefficient of the plate which has been made laminar by the suction slits is only slightly above the Blasius curve. The total suction amount coefficient first increases because of the increase in the number of slits with incident Reynolds number. It then reaches a maximum value, and then decreases again at high Reynolds numbers, because then the reduction in the suction amount coefficients has a greater effect than the increase in the number of slits. If the suction already starts at the instability point, then the slit number increases at all Reynolds numbers. The drag coefficients and the suction amount coefficients only increase in the lower Reynolds number range.

The results of the simultaneous variation of relative suction height and infinite Reynolds number are shown in Figures 29 and 30. The optimum relative suction height is almost independent of the Reynolds number, at which the number of slits becomes a minimum,

$$\eta_{Q\,opt} = \eta_Q (n_{min}) \approx 0,1$$

If less air is sucked away at these suction points, then the drag and the total suction amount decrease, but the required slit number

increases rapidly ($\eta_Q < 0.1$). At $\eta_Q = 0.02$, one comes very close to the case of continuous suction, see Figure 29. An increased suction $\eta_Q > 0.1$ is out of the question; then the slit number and the drag, as well as the total suction amount, increase considerably.

9.2 Bodies of Revolution

9.2.1 Variation of Suction Conditions

For a body of revolution we will investigate the ways in which the influence of the pressure gradient affects the optimum configuration of the suction slits, compared with the plane plate. For this purpose, we must vary the incident Reynolds number Re_1, the relative suction height η_Q, as well as the suction range x_{Abs}/l.

As far as selecting the body shape is concerned, it should be mentioned that without suction, spindle shapes with a pointed nose part have been suggested, see Hertel [1 to 3]. These satisfy the condition for minimum specific drag much better than conventional shapes with a long cylindrical central part and a small thickness ratio. It has been found that these spindle shapes are favorable in the case of suction, compared with conventional shapes.

Since the nose contour of low drag spindle bodies is approximately parabolic according to [2] and [3], as a basic shape we will select the following symmetrical paraboloid for the variation calculation, where

the length ratios are $\frac{l_B}{l} = \frac{l_H}{l} = 0{,}5; \quad \frac{l_M}{l} = 0$

the thickness ratio is $\frac{d}{l} = 0{,}2$

and the contour functions are $\begin{cases} \eta_B = 1 - \xi_B^2 \\ \eta_H = 1 - \xi_H^2 \end{cases}$

This basic shape can be matched to various problems by changing the thickness setback and the thickness ratios. From the transition and drag curve of the basic shape shown in Figure 31, we can see that the "laminar effect" is lost at high Reynolds numbers. As we will now show, making the flow laminar using slit suction in this area leads to substantial drag savings. /67

Figures 32 and 33 show the boundary layer variation and the suc-

tion variables of the paraboloid distributed over the body shape, for the incident Reynolds number $Re_1 = 5 \times 10^7$ and the suction conditions $\eta_Q = 0.1$ and $x_{Abs}/l = 0.5$. They are very similar to those of the plane plate shown in Figures 25 and 26. The length of the laminar buildup path behind the last suction slit is substantial.

Figure 34 shows that in spite of the reduction in the stabilizing pressure gradient, at η_Q = const., the slit separations of a spindle body are increased in the flow direction with the exception of the tail end, where there is a steep pressure increase. The relative slit width and the local suction amount coefficient depend on the Reynolds number and increase greatly because of the thickening of the boundary layer at the tail end. Increasing the slit separations in the tail area of the bodies of revolution comes about because in the case of bodies of revolution, the reducing pressure gradient is opposed by an increased boundary layer thickness, due to a decrease in the body radius. This effect does not occur in plane flow, as shown in Figure 23.

For applications, various suction regions are possible for bodies of revolution, for example,

- in the case of an aircraft body, it only seems that keeping the nose part of the aircraft laminar is promising because of the disturbing influence of the wings,

- it seems promising to make the entire body surface of an underwater vehicle laminar using suction slits.

Figures 35 and 36 show the results of a suction region variation and Reynolds number variation at $\eta_Q = 0.1$. Already a small suction region with a corresponding low suction amount is sufficient to keep the nose part laminar, and this is associated with a substantial savings in drag. The entire body surface can be kept laminar with a small /68 number of additional suction slits, but the total amount of sucked air increases drastically. The extremely low drag coefficients in the case of suction to the area of the tail tip are caused by the fact that when the body surface is made completely laminar, not only is the friction drag reduced, but the pressure drag is also greatly reduced. The jump in the displacement of the transition point, and the reduction in the drag coefficient due to a suction slit are covered by special conventions in the computer program, see chapter 8.2.3.

When there is a simultaneous variation of the relative suction

height and the incident Reynolds number, Figures 37 and 38 show that the slit number becomes a minimum for bodies of revolution, independent of the Reynolds number. If the suction height is

$$\eta_a = \eta_{a\,opt} \approx 0{,}1$$

Figure 39 shows that the optimum relative suction height is also approximately independent of the suction region. The variation of the suction conditions over a spindle body shows that $\eta_Q = 0.1$ is an optimum suction parameter for technical applications of slit suction.

9.2.2 Variation of Body Shape

In applications we are interested in the effect of the change in the body shape of a body of revolution on the configuration of the suction slits.

At $\eta_{Q\,opt} = 0.1$, we will investigate the influence of
- the thickness setback or the relative noselength l_B/l
- and the thickness ratio d/l

on the minimum slit number. We will start with the base shape discussed in the previous chapter.

Figure 40 shows the contour and the pressure distribution of spin- /69
dle bodies where the thickness setback was varied with the same thickness ratio d/l = 0.2, and shows that in the case without suction, the bodies with a large thickness setback have the lowest drag in the low Reynolds number range, because of the long laminar buildup paths. At the higher Reynolds numbers, this tendency is reversed. The influence of the thickness setback on the optimum suction configuration ($\eta_Q = 0.1$) is given in Figures 42 and 43. With the exception of small Reynolds numbers, the slit number is substantially reduced with decreasing thickness setback.

Figure 44 shows the contour and the pressure distribution of spindle bodies, in which the thickness ratio has been varied for the same thickness setback $l_B/l = 0.5$. Figure 45 shows that in the case without suction, the thicker bodies have a higher drag. One exception is the medium Reynolds number range, where the long or laminar buildup paths produce a smaller drag for the thicker shapes. It is remarkable that for a thickness ratio d/l = 0.3, there is still no turbulent boundary layer separation at the tail.

The effect of the thickness variation on the optimum suction configuration ($\eta_Q = 0.1$) is shown in Figures 46 and 47. As the body thickness increases, the slit number decreases in the entire Reynolds number range.

The thickness setback variation and the thickness variation of a spindle body clearly show that the pressure gradient over the nose part is most important for determining the minimum number of suction points, even if suction takes place near the tail tip.

10. Summary

In aviation and underwater theory, only slits, gaps, or perforated strips can be used for practical boundary layer suction applications. /70 Up to now, continuous suction has been almost the exclusive case which has been treated, since the investigations are usually restricted to plane contours.

In the present paper, we discuss the technically interesting case of keeping a boundary layer laminar using suction slits over bodies of revolution in incompressible flow.

The calculation of the rotationally-symmetric laminar and turbulent boundary layers is done by the integral conditions for momentum and energy, and assuming a single parameter velocity profile.

A new semi-empirical criterion is introduced for determining the laminar-turbulent transition point of bodies of revolution, and its reliability has been demonstrated from transition measurements.

The changed boundary layer variables behind the suction slit are determined approximately from the remaining profile which remains after suction. By comparison with exact solutions, which are available in the special case for a narrow suction strip, we confirm the reliability of this method. From these results we draw the conclusion that the effects which can be brought about by the suction slits can also be approximately reached by perforated suction strips.

In order to evaluate the slit configuration, we calculated the drag with consideration of the suction power. This calculation was confirmed by suction experiments.

The ALGOL program was developed for the systematic variation of body shape, incident Reynolds number, and suction conditions, which also

includes the case of no suction and the calculation of plane contours.

In addition to the stability and transition conditions, we also introduce the relative suction height and the suction region as parameters in the suction relationships. For constant relative suction height, the slit separations in the flow directions are increased, as long as there is no great pressure increase.

The local suction amount coefficients and relative slit widths increase greatly towards the tail tip.

The variational calculations show that, independent of the body shape, incident Reynolds number and suction region for the relative suction height, the slit separations are a maximum and consequently the number of slits are a minimum. Compared with the continuous suction ($\eta_Q \to 0$, $n_Q \to \infty$), the suction amount coefficient increases drastically at $\eta_Q = 0.1$. The drag coefficient only increases slightly with consideration of suction power.

Finally, we investigated the influence of the body of revolution shape on the optimum configuration of the suction slits. It is found that pointed spindle shapes with a large thickness ratio and a small thickness setback can be made laminar using a relatively small number of suction slits due to the large pressure drop over the nose, even at high Reynolds numbers.

The combination of favorable body shapes and optimum suction conditions leads to solutions, which satisfy the condition for a small flow resistance with a small number of suction points and a small suction amount, for the most part, at high Reynolds numbers.

11. REFERENCES

1a. Hertel, H.: Biological Technical Research on Structures, Shapes, Drives. VDI-Zeitschrift, Bd. 109, Nr. 18, 19, 22, 24, and 26, 1967.

1b. Hertel, H.: Biological-Technical Research on Structure, form, and movement in "Bioengineering, an Engineering View". Herausgeg von G. Bugliarello, San Francisco Press, Inc., 1968.

2a. Hertel, H.: Body Shape with Minimum Specific Drag for an Aircraft at a High Subsonic Velocity. German Patent Application P 1556934.4, 1965, USA-Patent 3,476,336, 1969.

2b. Hertel, H.: Measures for Reducing the Drag of Bodies of Revolution. German Patent Announcement, P 1531 422.4 – 22, 1967.

3 Hertel, H., Oehler, C., Thiede, P.: Studies for selecting a body of minimum specific drag for new aircraft projects in Incompressible flow. Report of the Inst. f. Luftfahrzeugbau TU Berlin, 1966.

4. Pfenninger, W.: Investigations about Friction Reduction over Wings, Especially using boundary layer suction. Inst. f. Aerodynamik, ETH Zurich, Nr. 13, 1946.

5. Pfenninger, W.: Experiments on a laminar suction aerofoil of 17% thickness. Journal Aero Sci., 16, 1949.

6. Pfenninger, W.; Groth, E.: Low drag boundary layer suction experiments in flight on a wing glove of an F-94A airplane with suction through a large number of fine slots. In "Boundary Layer and flow control", Vol. 2, Herausgeg. von G. V. Lachmann, Pergamon Press, Oxford, 1961.

7. Lachmann, G. V.: Aspects of Design, Engineering, and Operational Economy of Low Drag Aircraft. In "Boundary Layer and Flow Control, Vol. 2. Herausgeg. von G. V. Lachmann, Pergamon Press, Oxford, 1961.

8. Koschmeider, F. P., Walz, A.: Simple Shapes for Profiles of Low Mechanics. Unpublished new version of a 1943 restricted publication of the central for Scientific Reporting of the DVL, FB, 1961.

9. Oehler, C.: Subsonic Flow Around Bodies of Revolution in Axial Flow. Dissertation TU Berlin, 1969.

10. Schlichting, H.: Grenzschicht-Theory (Boundary Layer Theory, 5th Edition, Verlag G. Braun, Karlsruhe, 1965.

11. Walz, A.: Stromungs- und Temperaturgrenzschichten (Fluid and Temperature Boundary Layers), Verlag G. Braun, Karlsruhe, 1966.

12. Mangler, W.: Relationship between plane and rotationally-symmetric boundary layers in incompressible fluids. ZAMM Bd. 28, Heft 4, 1948.

13. Hartree, D. R.: On an Equation Occurring in Falkner and Skan's approximate treatment of the equations of the boundary layer. Proc. Cambr. Phil. Soc., Vol. 13, Part II, 1937.

14. Walz, A.: A new Trial Solution for the Velocity Profile of the Laminar Friction Layer, Lilienthal-Report, 141, 1941.

15. Mangler, W.: Momentum Method for Approximate Method of the Laminar Friction Layer. ZAMM Bd. 24, 1944.

16. Geropp, D.: Approximate theory for compressible and laminar boundary layer with two shape parameters for the velocity profile: Dissertation, TH Karlsruhe, 1963.

17. Walz, A.: Application of the Energy Theorem of Wieghardt to single parameter velocity profile in laminar boundary layers. Ing. Arch. 14, 1948.

18. Fernholz, H.: Semi-empirical laws for calculating turbulent boundary layers using the method of integral conditions. Ing. Arch. 33, Heft 6, 1964.

19. Iglisch, R.: Exact Calculations of the laminar friction layer in a Plane Plate in Longitudinal Flow with Homogeneous Suction. Publications of dtsch. Akad. d. Luftfahrtforschung 8b, 1944. No. 1.

20. Schlichting, H., Bussmann, K.: Exact solutions for laminar friction layer with suction and blowing. Literature of the dtsch. Akad. d. Luftfahrtforschung 7B, 1943.

21. Schlichting, H.: An Approximate Method for Calculating the Laminar Boundary Layer with Suction. Ing. Arch. 16, 1948.

22. Head, M. R.: Approximate Methods of Calculating the two-dimensional laminar boundary layer with suction. In "Boundary Layer and Flow Control", Vol. 2, Herausgeg. von G. V. Lachmann, Pergamon Press, Oxford, 1961.

23. Eppler, R.: Calculation of Laminar and Turbulent Suction Boundary Layers, Ing. Arch. 32, Heft 4, 1963.

24. Howarth, L.: On the Solution of the Laminar boundary layer equation. Proc. Roy. Soc., London A 164, 1938.

25. Rotta, J.: Shear Stress distribution and Energy Dissipation for turbulent boundary layers. Ing. Arch. 20, 1952.

26. Truckenbrodt, E.: A quadrature method for calculating the laminar and turbulent friction layer for plane and rotationally-symmetric flow. Ing. Arch 20, 1952.

27. Young, A. D.: The calculation of the total and skin friction drags of bodies of revolution at zero incidence.. R and M 1874, 1939.

28. Pretsch, J.: Theoretical Calculation of Profile Drag of Bodies of Revolution. Dtsch. Luftfahrtforschung UM 3185, 1944.

29. Scholz, N.: Rational Calculation of Flow Drag of Slender Bodies with Arbitrary Rough Surface. Schiffbautechn. Ges., Bd. 45, 1951.

30. Schubauer, G. B., Skramstad, H. K.: Laminar Boundary Layer Oscillations and Transitions on a flat plane. NACA Rep. 909, 1948.

31. Tollmien, W.; The Production of Turbulence. First communication, Nachr. Ges. Wiss, Goettingen, 1929.

32. Lin, C. C.: On the Stability of Two-Dimensional Parallel Flows, Quart. Appl. Math. 3, 1945.

33. Schlichting, H., Ulrich, A.: Calculation of Laminar-Turbulent Transition. Yearbook dtsch. Luftfahrtforschung, 1942.

34. Pretsch, J.: Stability of a Plane Laminar flow for a pressure drop and Pressure Increase. Yearbook. dtsch. Luftfahrtforschung, 1941.

35. Tetervin, N.: Charts and Tables for Estimating the Stability of the Compressible Laminar Boundary-layer with Heat Transfer and Arbitrary Pressure Gradient. NASA MEMO 5-4-59L, 1959.

36. Bussmann, K., Munz, H.: Stability of the Laminar Friction Layer with Suction. Yearbook dtsch. Luftfahrtforschung, 1942.

37. Ulrich, A.: Theoretical investigations about the drag savings by keeping the flow laminar with suction. Publication of dtsch. Akad. d. Luftfahrtforschung 8B, 1944.

38. Schlichting, H.: Influence in the Boundary Layer By Suction and Blowing. Yearbook Dtsch. Akad. d. Luftfahrtforschung, 1943/44.

39. Michel, R.: Study of the Transition over Wing Profiles. Establishment of a criterion for determining the transition point and calculation of the profile drag in incompressible flow. ONERA Rap. 1/1578, A, 1951. /77

40. Smith, A.M.O., Gamberoni, N.: Transition, pressure gradient, and stability theory. Douglas Aircraft Rep. ES 26388, 1956.

41. Pretsch, J.: Buildup of unstable perturbations in a laminar friction layer. Yearbook dtsch. Luftfahrtforschung, 1942.

42. Granville, P. S.: The calculation of viscous drag of bodies of revolution. Navy Department. The David Taylor Model Basin., Rep. 849, 1953.

43. Pretsch, J.: Stability of Laminar Flow Around a sphere. Luftfahrtforschung, 18, 1941.

44. v. Ingen, J. L.: A suggested semi-empirical method for the calculation of the boundary-layer transition region. Delft Rep. V.T.H., 74, 1956.

45. Moeller, R.: Evaluation of Laminar-Turbulent Measurements for an for an Empirical Transition Criterion. Diploma Thesis at Inst. f. Luftfahrzeugbau, TU Berlin, 1966.

46. v. Doenhoff, A. E.: Investigation of the boundary-layer about a symmetrical airfoil in a wind tunnel of low turbulence. NACA Wartime Rep. L-507, 1940.

47. Braslow, A. L., Visconti, F.: Investigation of boundary-layer Reynolds number for transition on a NACA 65(215)-114 airfoil in the Langley two-dimensional low-turbulence pressure tunnel. NACA TN 1704, 1948.

48. Jones, M. B.: Flight experiments on the boundary layer. JAS Vol. 5, Nr. 3, 1938.

49. Zalovčik, J. A., Skoog, R. B.: Flight Investigation of boundary layer transition and profile drag of an experimental low-drag wing installed on a fighter-type airplane. NACA Wartime Rep. L-94, 1945.

50. Wetmore, J. W., Zalovčik; J. A. Platt, R. C.; A flight investigation of the boundary layer characteristics and profile drag of the NACA 35-215 laminar flow airfoil at high Reynolds numbers. NACA Wartime Rep. L-532, 1941.

51. Smith, F., Higton, D. J.: Flight tests on "King Cobra FZ 440" to investigate the practical requirements for the achievement of low profile drag coefficients on a low drag airfoil. R and M 2375, 1945.

52. Davies, H.: Some Aspects of Flight Research. JAS 55, 1951.

53. Plascott, R. H.:, Higton, D. J., Smith, F., Bramwell, A. R.: Flight tests on "Hurricane II Z. 3687" fitted with special wings of low-drag design. R and M 2546, 1946.

54. Boltz, F. W., Kenyon, G. C., Allen, C. Q.: The boundary-layer transition characteristics of two bodies of revolution, a flat plate and an unswept wing in a low-turbulence wind tunnel. NASA-TN-D-309, 1960. /79

55. Boltz, F. W., Kenyon, G. C., Allen, C. Q.; Measurements of Boundary Layer Transition at low speed on two bodies of revolution in a low turbulence wind tunnel, NACA RM A 56 G17, 1956

56. Rheinboldt, W.; Calculation of steady boundary layer for continuous suction with discontinuous suction velocity. J. Rat. Mech. Anal., Vol. 5, No. 3, 1956.

57. Smith, A. M. O., Clutter, D. W.: Solution of the Incompressible laminar boundary layer equation. AIAA Journal, Vol. 1, No. 9, 1963.

58. Krause, E.: Numerical Solution of the boundary-layer equations. AIAA Journal, Vol. 5, No. 7, 1967.

59. Bethel, H. E.: Approximate solution of the laminar boundary-layer equations with mass transfer. AIAA Journal, Vol. 6, No. 2, 1968.

60. Wuest, W.: Approximate Calculation and Stability Behavior of Laminar Boundary Layer Suction with Suction by Single Slits. Ing. Arch. 21, 1953.

61a. Walz, A.: Theory of suction of the friction layer. ZWB-Report 1775, AVA Goettingen, 1943.

/80

61b. Walz, A.: Approximate Theory for Boundary Layer Suction Individual slits. DVL-Report 184, 1962.

62. Wuest, W.: Development of a Laminar Boundary Layer Behind a Suction point. Ing. Arch. 17, 1949.

63. Gregory, N.: Research on Suction surfaces for laminar flow. In "Boundary Layer and Flow Control," vol. 2. Published by von. G. V. Lachmann, Pergamon Press, Oxford, 1961.

64. Krause, E.: Shape Parameter of Incompressible Boundary layers for large suction rates. DVL-Report 889, 1969.

65. Kuechemann, D., Weber, J.: Aerodynamics of Propulsion. McGraw-Hill, New York, 1953.

66. Dreger, W.: A method for calculating the Potential suction. Schiff-technik Bd. 6, Heft 34, 1959.

67. Edwards, J. B.: Fundamental Aspects of Propulsion for Laminar Flow Aircraft. in "Boundary Layer and Flow Control, published by G. V. Lachmann, Pergamon Press, Oxford, 1961 (vol. 2.)

68. Torenbeek, I. E.: The Propulsion of Aircraft with Laminar Flow Control. Department of Aeronautical Engineering. Delft University of Technology. Rep. VTH-150, 1968.

69. Pfenninger, W.: Some General Considerations of losses in boundary layer suction ducting systems. Northrop Rep. BLC-29, 1954.

70. Otte, F.: Determination of the Drag Around Bodies for Optimum Suction of the Laminar Boundary Layer by Single Slits. Study Paper at the Inst. f. Luftfahrzeugbau, TU Berlin, 1968.

12. Figures

Body shape r(x)

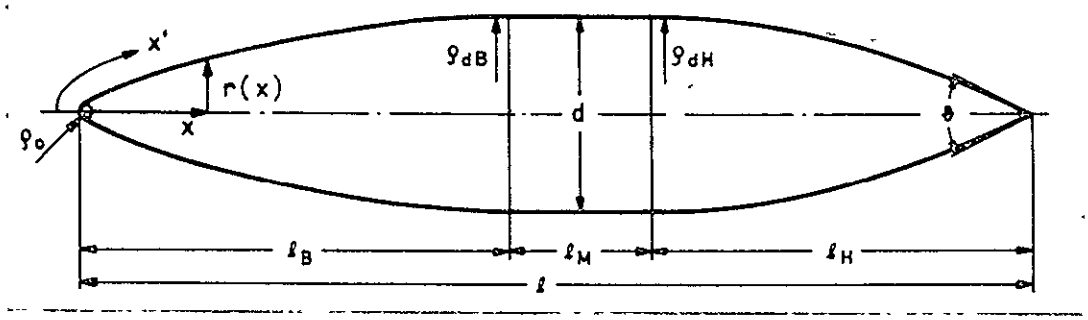

Body dimensions

Thickness ratio $\frac{d}{\ell}$

Length Ratios
Nose $\frac{\ell_B}{\ell}$
Middle Part $\frac{\ell_M}{\ell}$
Tail $\frac{\ell_H}{\ell}$

Relative nose radius $\frac{\varrho_o}{\ell}$

Tail tip angle ϑ

Relative apex radii
Nose $\frac{\varrho_{dB}}{\ell}$
Tail $\frac{\varrho_{dH}}{\ell}$

Contour Functions $\eta = f(\xi)$

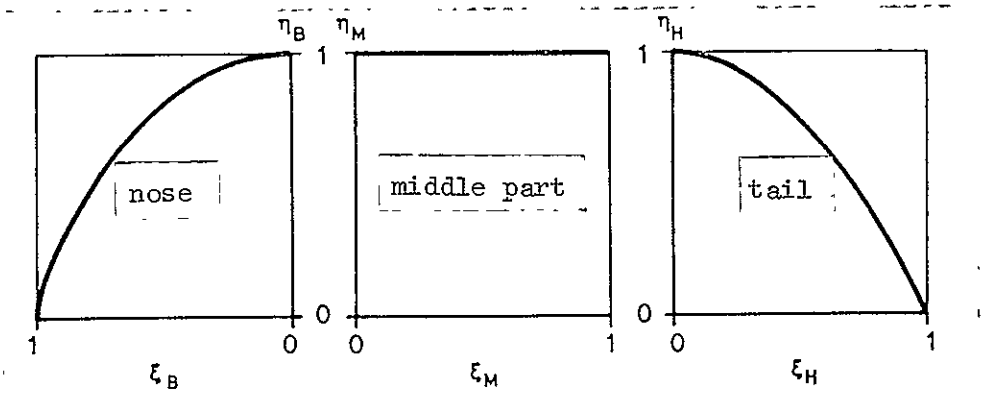

Figure 1: Contour of a Body of Revolution.

approximation: ——— according to Eppler [23]
- - - according to Walz [11]
-.-.-.- according to Geropp [16]

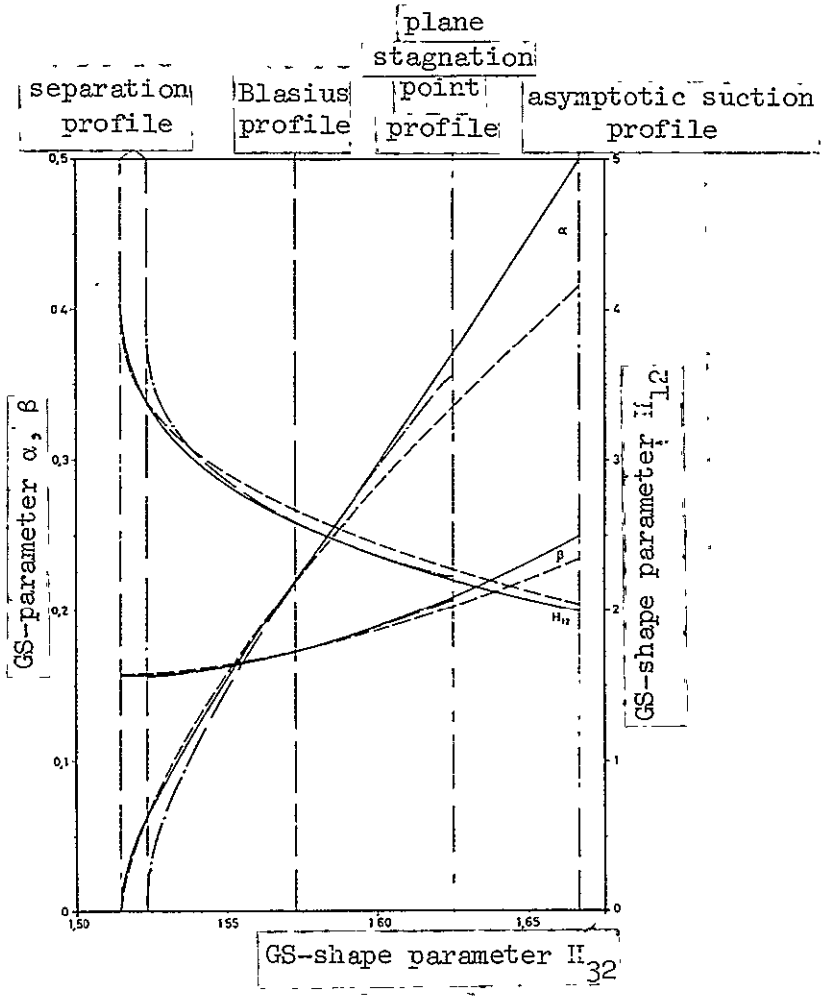

Figure 2: Relationships for laminar velocity profiles with suction influence.

Comparison: Delayed stagnation point flow $\frac{u_\delta}{U_\infty} = 1 - \frac{x}{l}$
Laminar separation point

– – – – – – Exact solution of Howarth [24] $x_{A_{1a}}/l = 0{,}1198$

———— Present calculation method with approximations of Eppler [23] $x_{A_{1a}}/l = 0{,}1196$

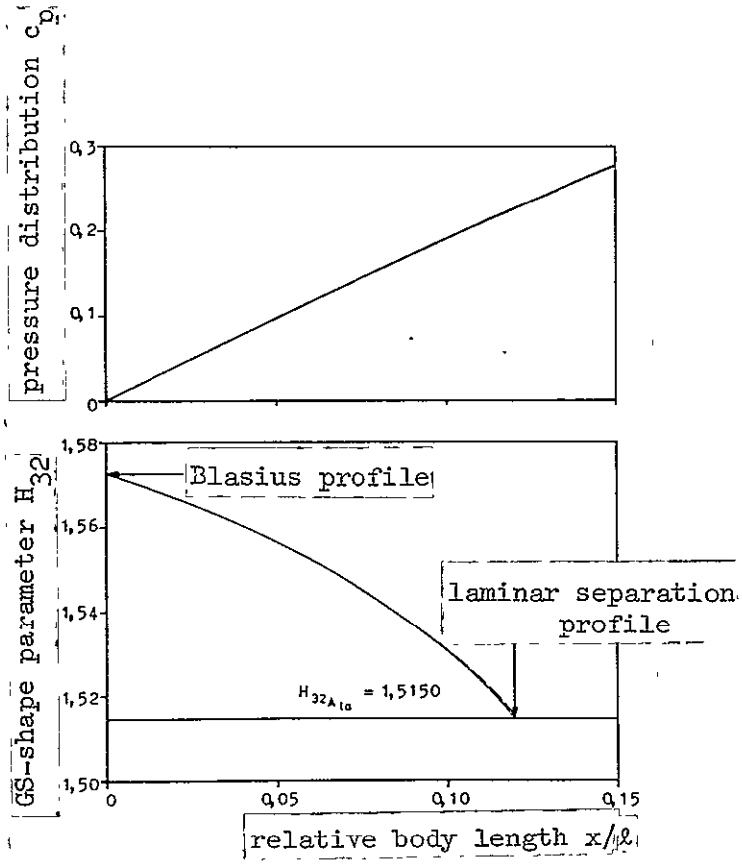

Figure 3: Delayed stagnation point flow. Laminar separation point. Calculation method – exact solution

Stability Calculations

without suction	with suction
▫ Tollmien, Lin (Blasius Profile) [31], [32]	▪ Bussmann, Muenz (asymptotic suction profile) [36]
○ Schlichting, Ulrich (Pohlhausen P6 Profile) [33]	● Ulrich (Iglisch Profile)[37]
◇ Pretsch (Hartree Profile) [34]	▲ Ulrich (Schlichting-Bussmann profile) [38]
▽ Tetervin (Hartree Profile) [35]	

Stability Criterion:

——— Approximation $\log Re_{\delta_1} = 4{,}556 - 76{,}87\,(1{,}670 - H_{32})^{1{,}942}$

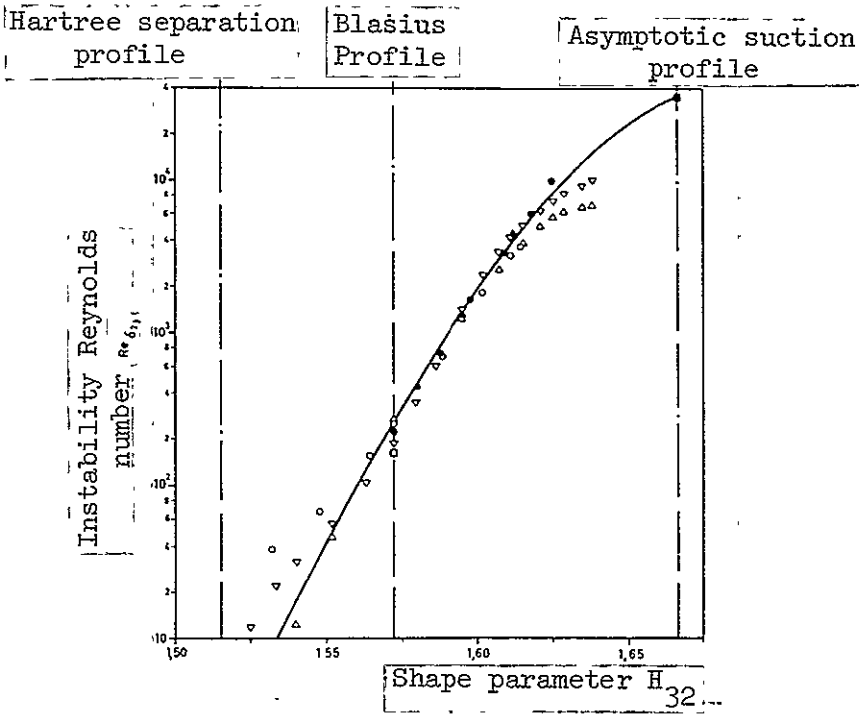

Figure 4: Stability of the laminar boundary layer with pressure gradients and suction.

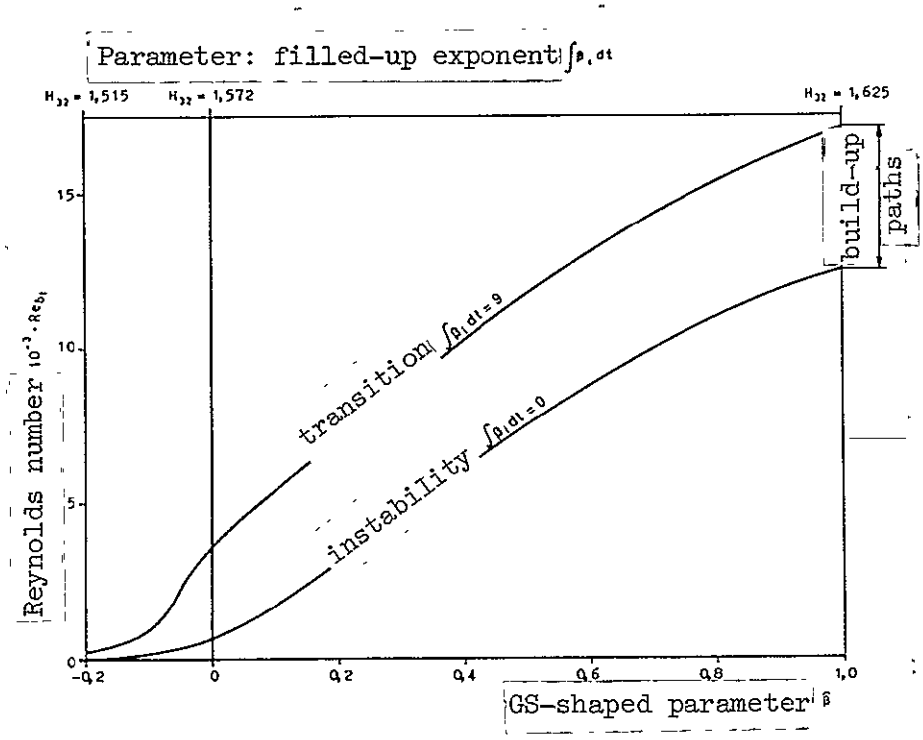

Figure 5: Build-up curves of the Hartree velocity profiles according to Pretsch [41].

Transition Measurement

	Wind Tunnel	Free Flight
Plane Flow	o Braslow, Visconti [47] □ v. Doenhoff [46] △ Schubauer, Skramstad [30] ▽ Boltz, Kenyon, Allen [54]	● Jones [48] ■ Zalovcik, Skook [49] ▲ Wetmore, Zalovcik, Platt [50] ▼ Davies, Smith, Higton [51] [52] ◆ Plascott, Higton, Smith, Bramwell [53]
Rotationally Symmetric Flow	⊙ Boltz, Kenyon, Allen [55]	

Transition Criteria

——— Approximation

$$1{,}515 \leq \bar{H}_{32} \leq 1{,}560 : \log\left(Re_{\delta_{2U}} - Re_{\delta_{2_3}}\right) = 1{,}6435 - 24{,}20\,(1{,}5150 - \bar{H}_{32})$$

$$1{,}560 < \bar{H}_{32} \leq 1{,}625 : \log\left(Re_{\delta_{2U}} - Re_{\delta_{2_3}}\right) = 3{,}312 - 967{,}5\,(1{,}6250 - \bar{H}_{32})^{2{,}715}$$

—·— Buildup $a = e^{3}$

- - - - Empirical, according to Granville [42]

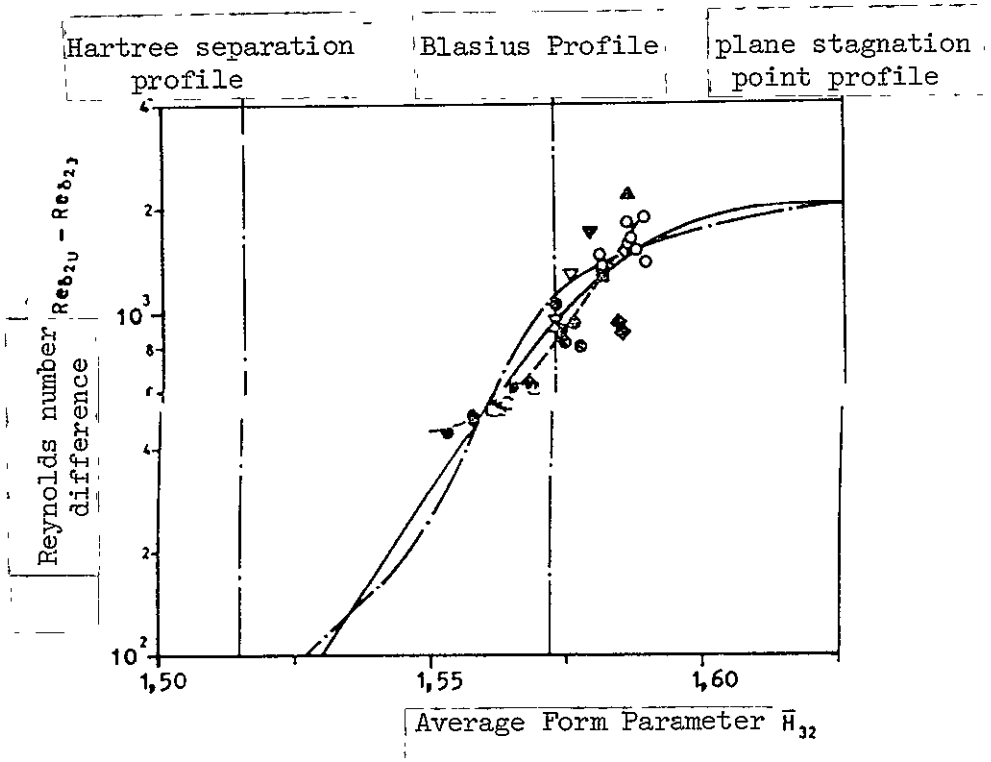

Figure 6: Length of the buildup paths for natural transition of the laminar boundary layer with pressure gradient.

Comparison: Flat Plate

- - - Known solutions

——— Present computation method

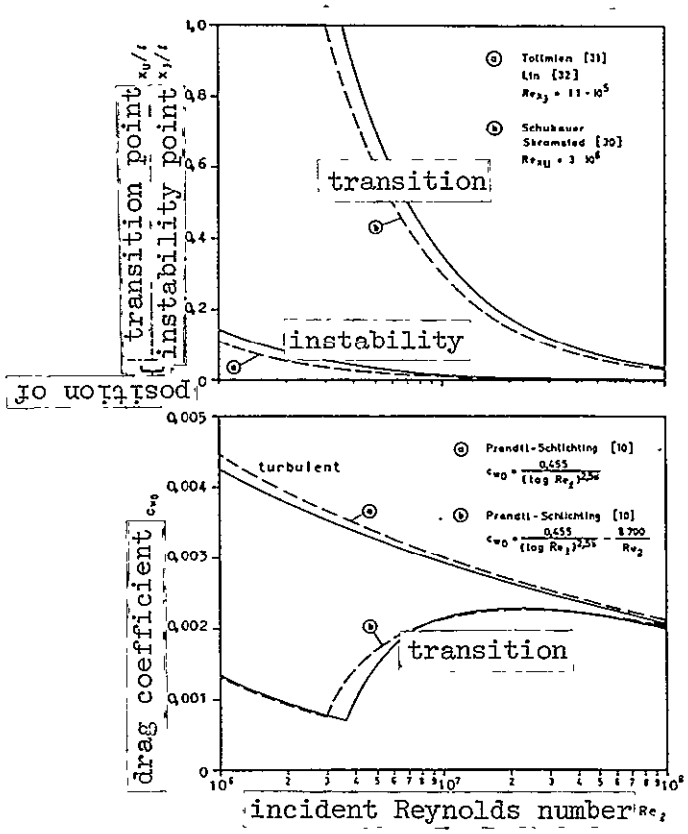

Figure 7: Flat plate in longitudinal flow. Instability and transition point positions. Drag coefficient. Computation method - known solutions.

Comparison:

○ } measurement of Boltz, Kenyon, Allen [54, 55]

——— present calculation method

- - - present calculation method

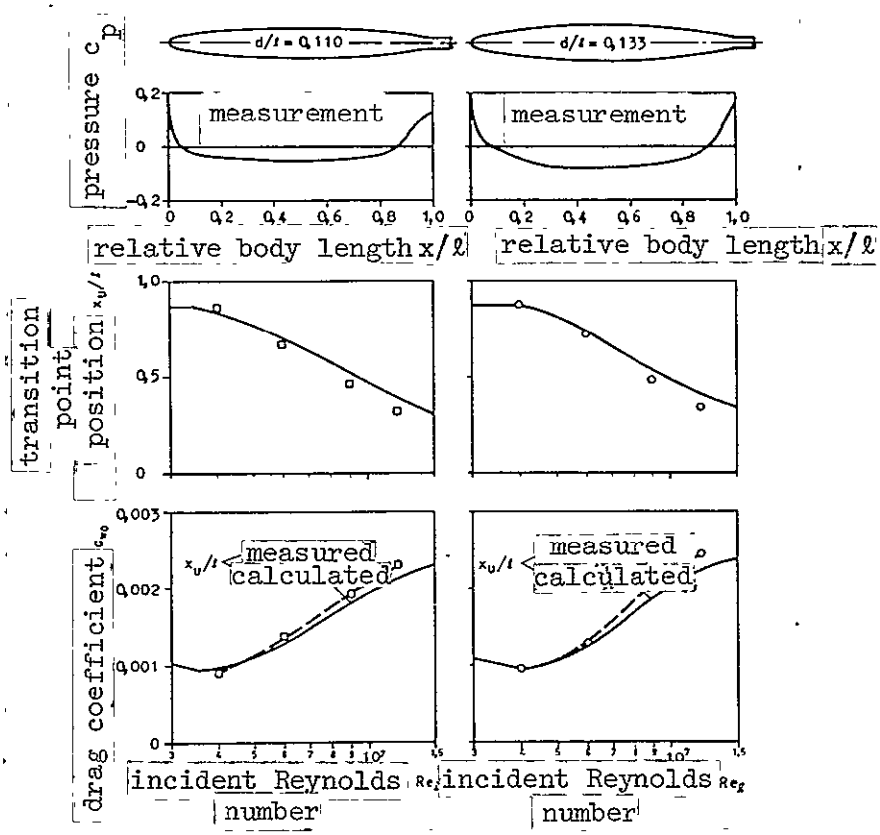

Figure 8: Body of revolution. Transition point position. Drag Coefficient. Calculation Method – Measurements.

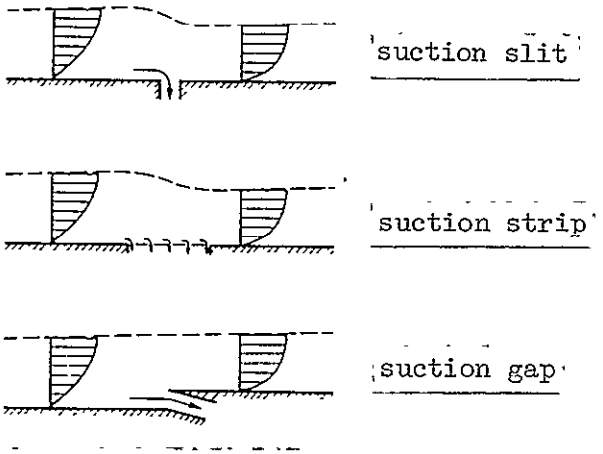

Figure 9: Possibilities of local boundary layer suction

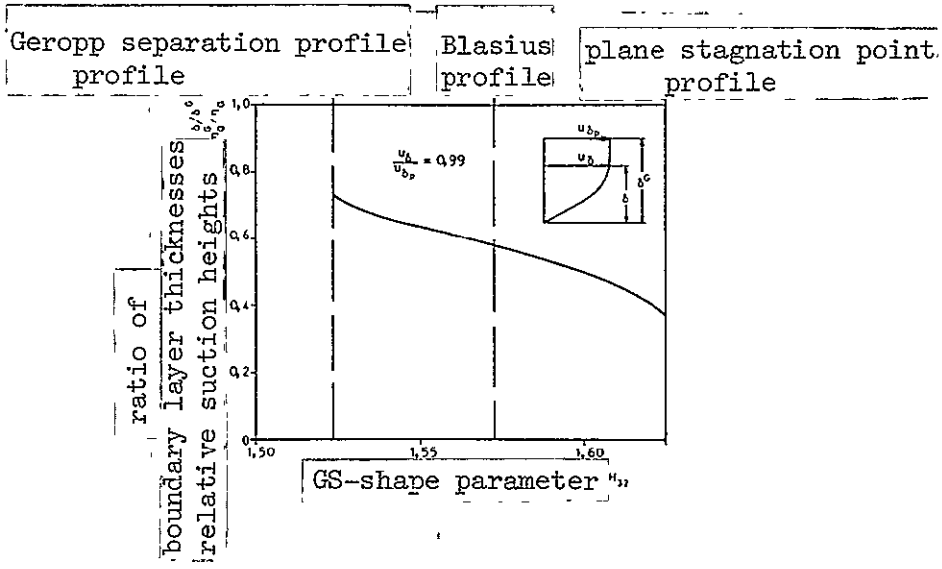

Figure 10: Ratio of Boundary Layer Thicknesses, Geropp [16] model.

Parameter: Relative suction height η_Q^G

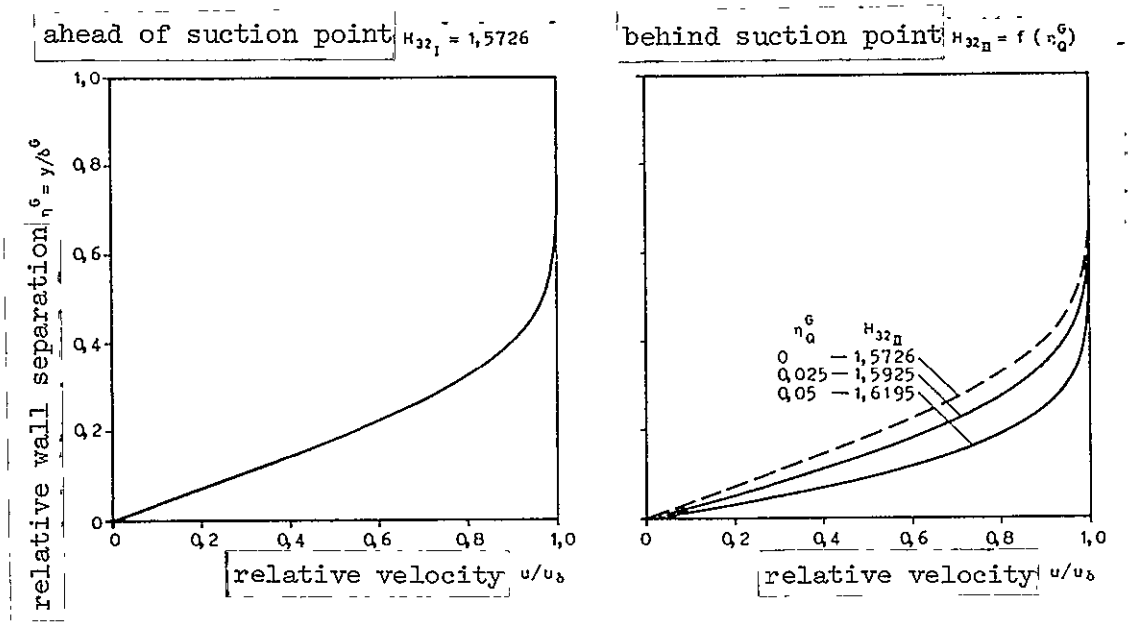

Figure 11: Laminar Velocity Profile ahead of/behind a suction slit. Single parameter model of Geropp [16].

Figures 12-15: Influencing of laminar boundary layer through a suction slit.

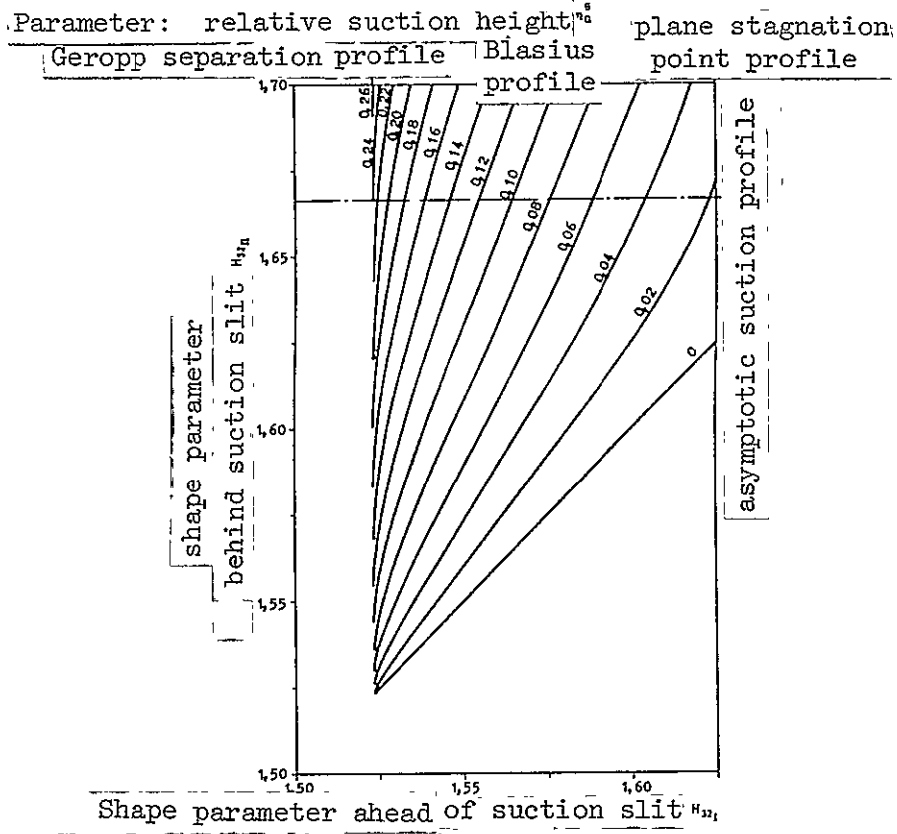

Figure 12: Changed shape parameter

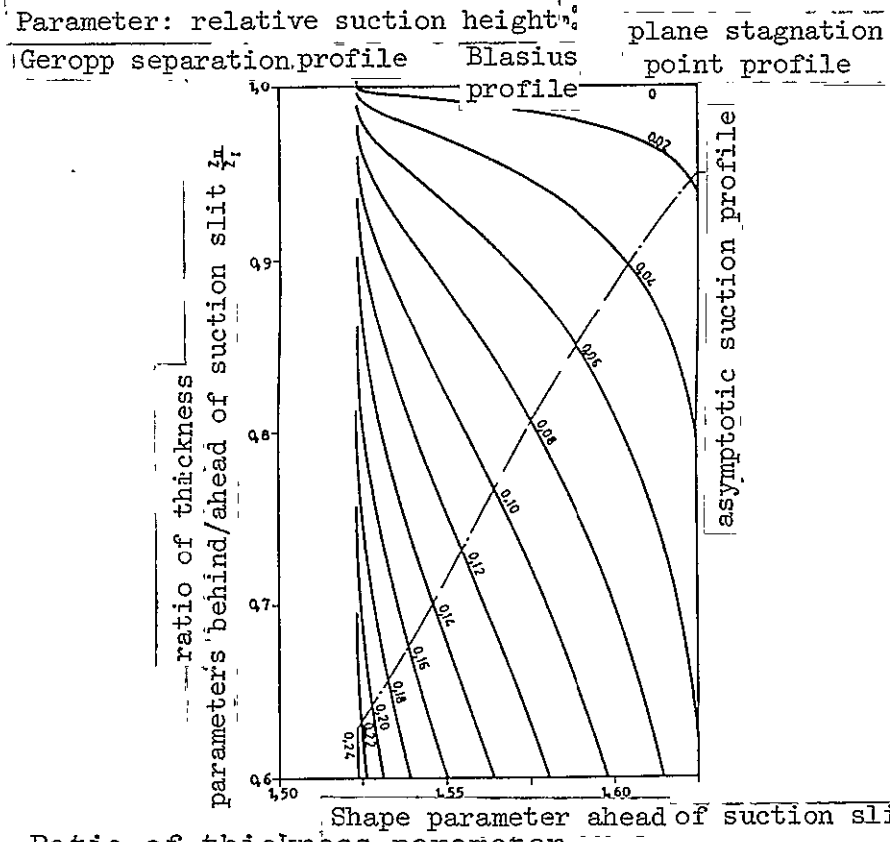

Figure 13: Ratio of thickness parameter

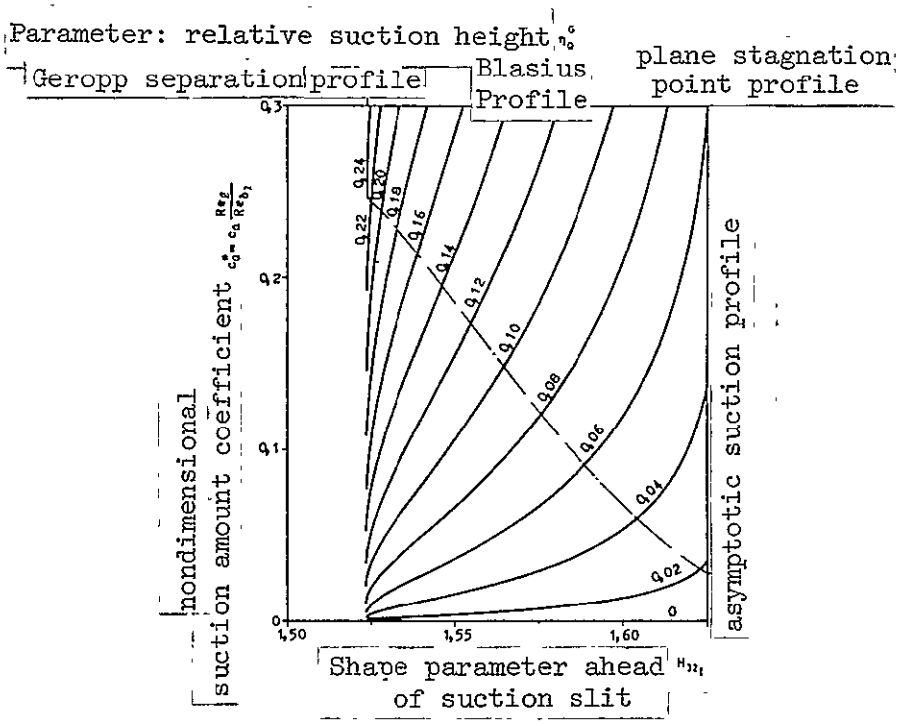

Figure 14: Nondimensional Suction Amount Coefficient

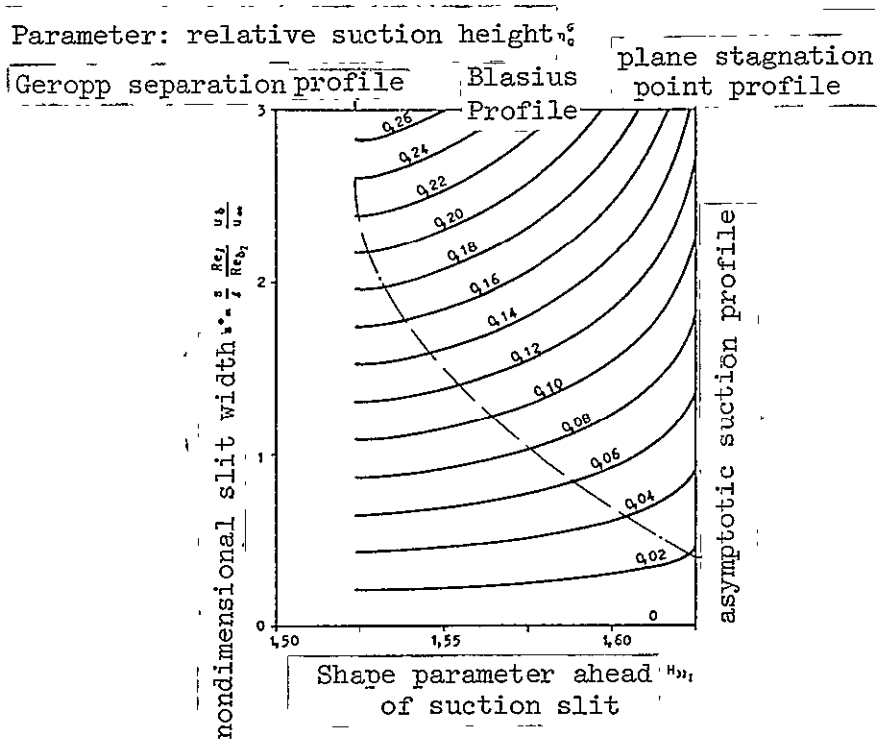

Figure 15: Nondimensional slit width

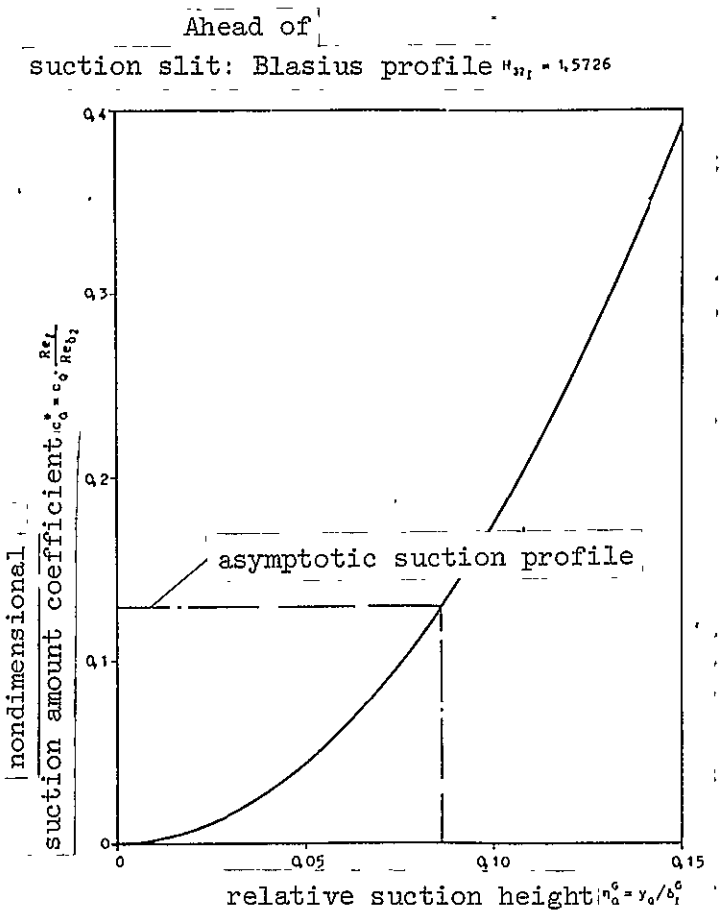

Figure 16: $c_Q^* = f(\eta_Q^G)$

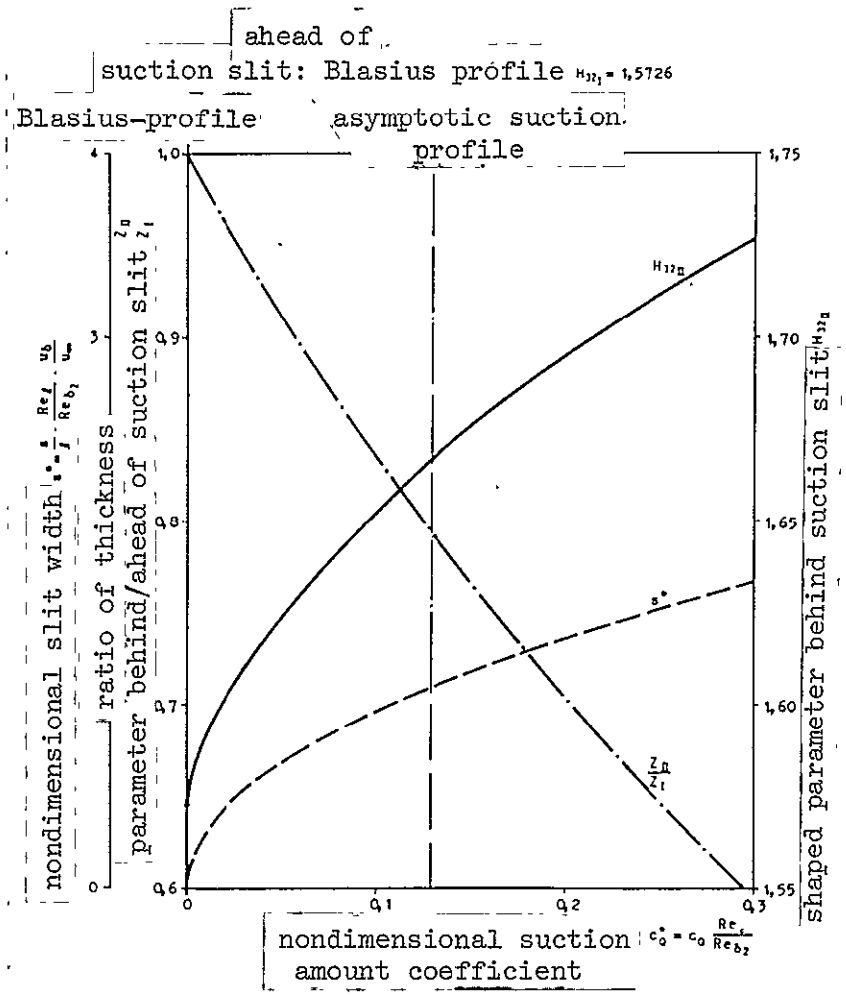

Figure 17: $H_{32_{II}}$, Z_{II}/Z_I, $s^* = f(c_Q^*)$

Figure 16-17: Influencing of the laminar plate boundary layer by means of a suction slit.

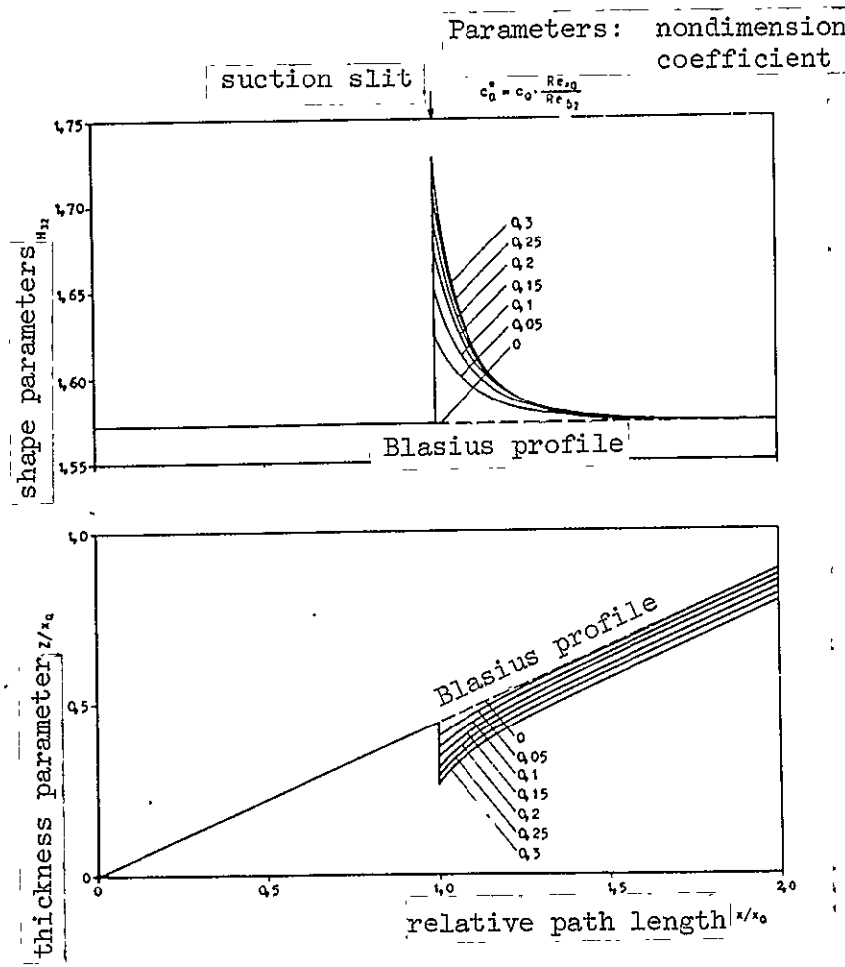

Figure 18: Influencing of Boundary Layer as a Function of Suction Amount Coefficient.

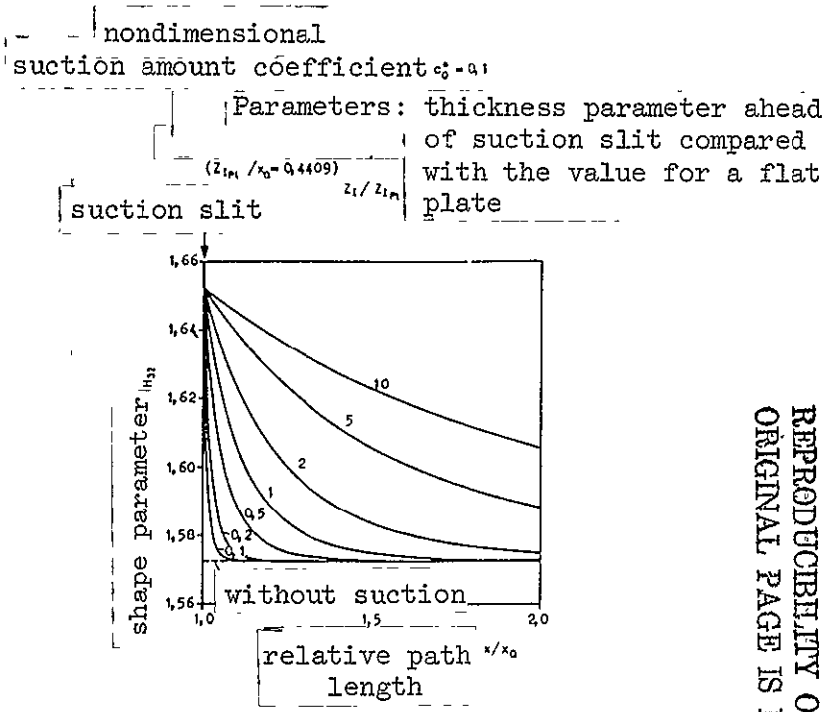

Figure 19: Influencing of Boundary Layer as a Function of Boundary Layer Thickness ahead of slit.

Figures 18-19: Influencing of laminar plate boundary layer by means of a suction slit.

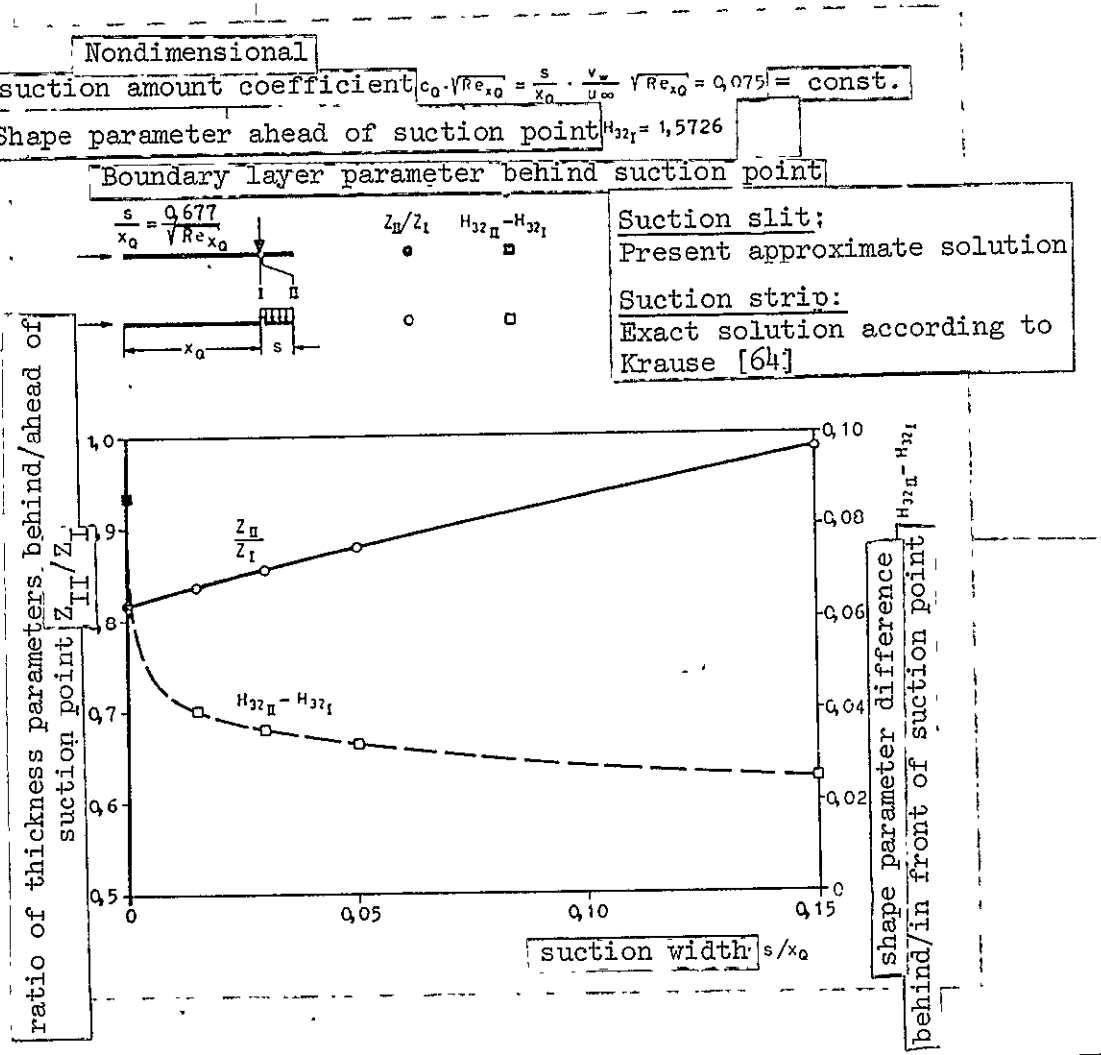

Figure 20: Suction slit-Suction strips of various widths for constant amounts of sucked-in flow

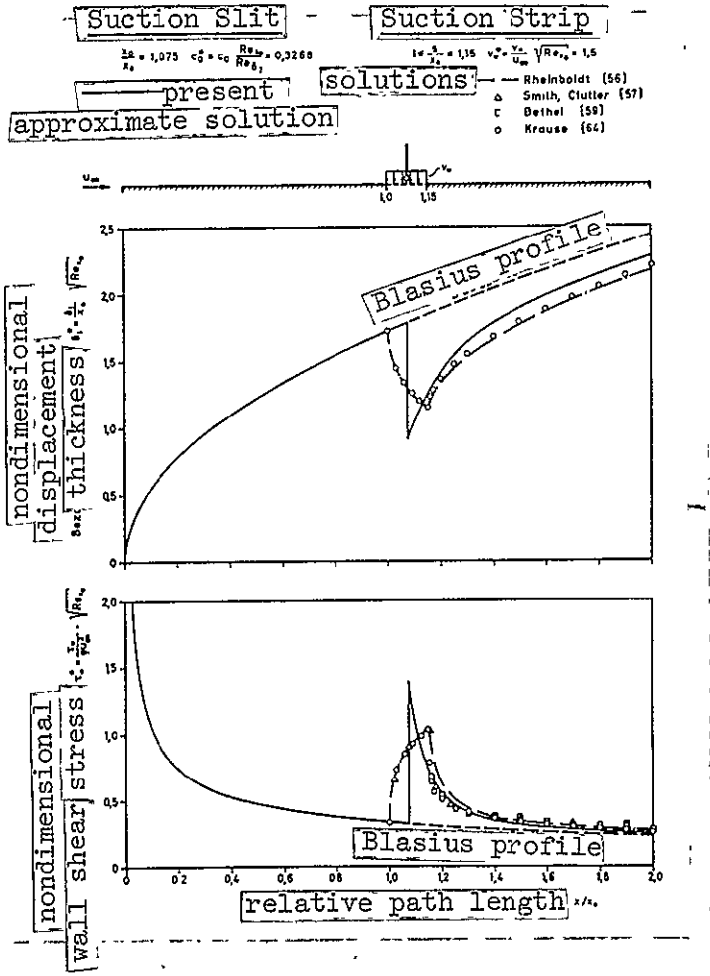

Figure 21: Suction slit-Suction strips for constant amounts of sucked-in air.

Figures 20-21: Influencing of laminar plate boundary layer through a suction point.

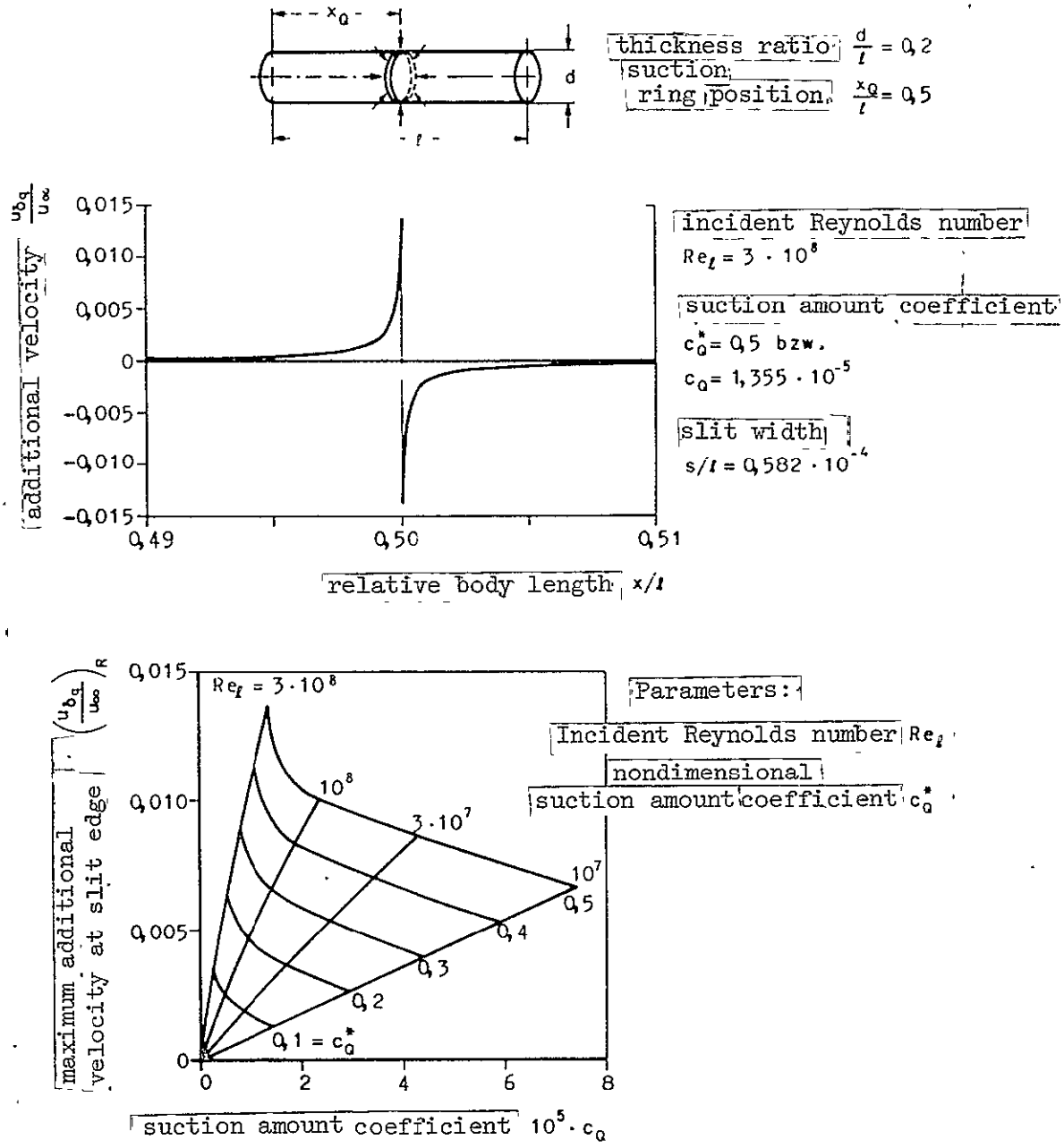

Figure 22: Sink effect of a ring-shaped suction slit over a body of revolution.

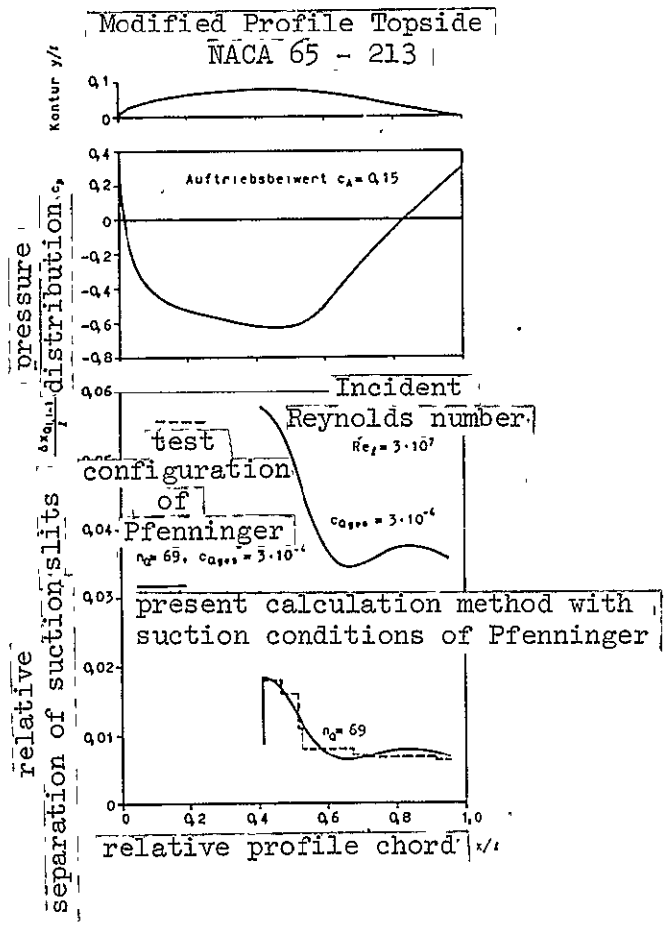

Figure 23: Position of suction slits.

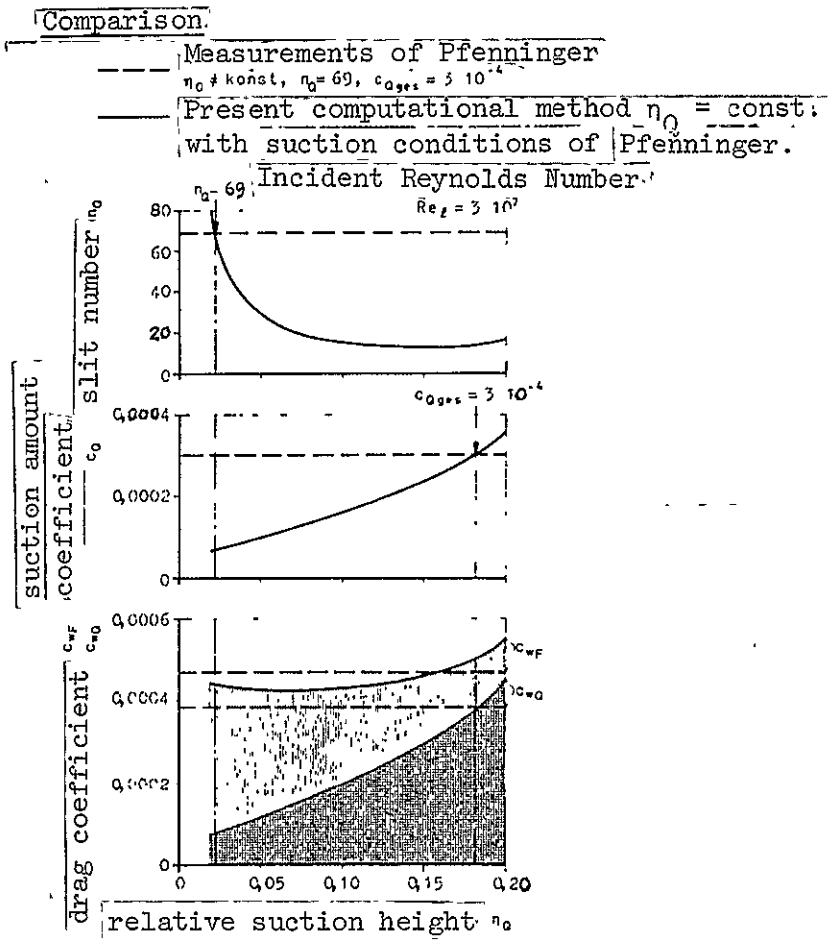

Figure 24: Equivalent suction resistance coefficient c_{wQ}. Drag coefficient with respect to the suction power c_{wF}

Figures 23–24: Wind profile with slit suction. Calculation method – measurements of Pfenninger [6].

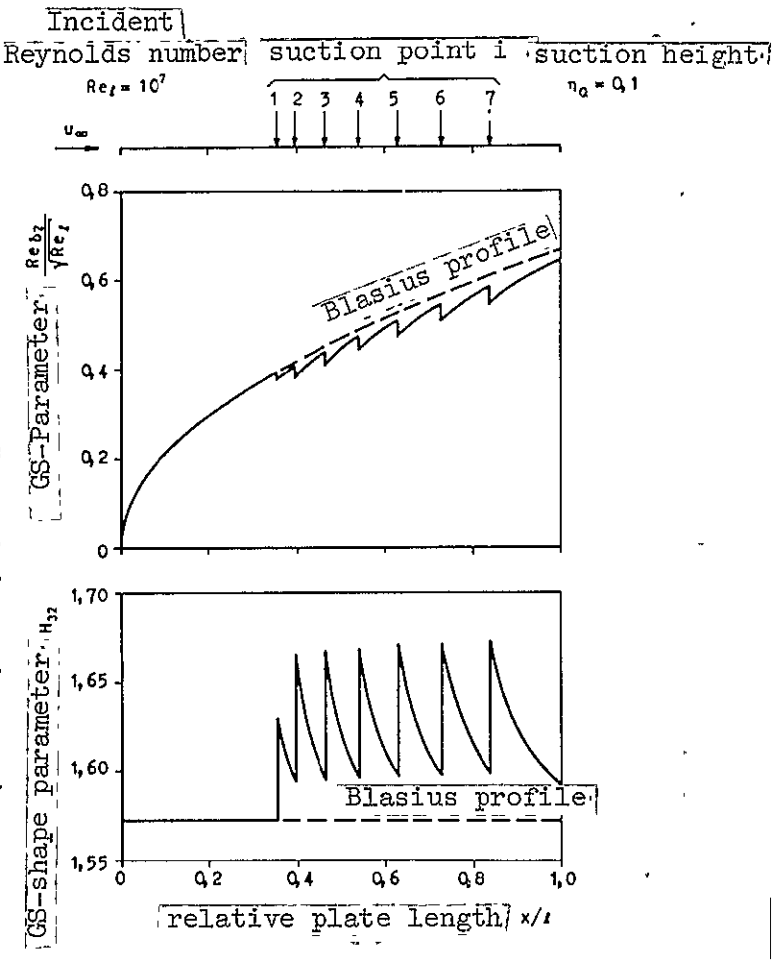

Figure 25: Boundary Layer Variation

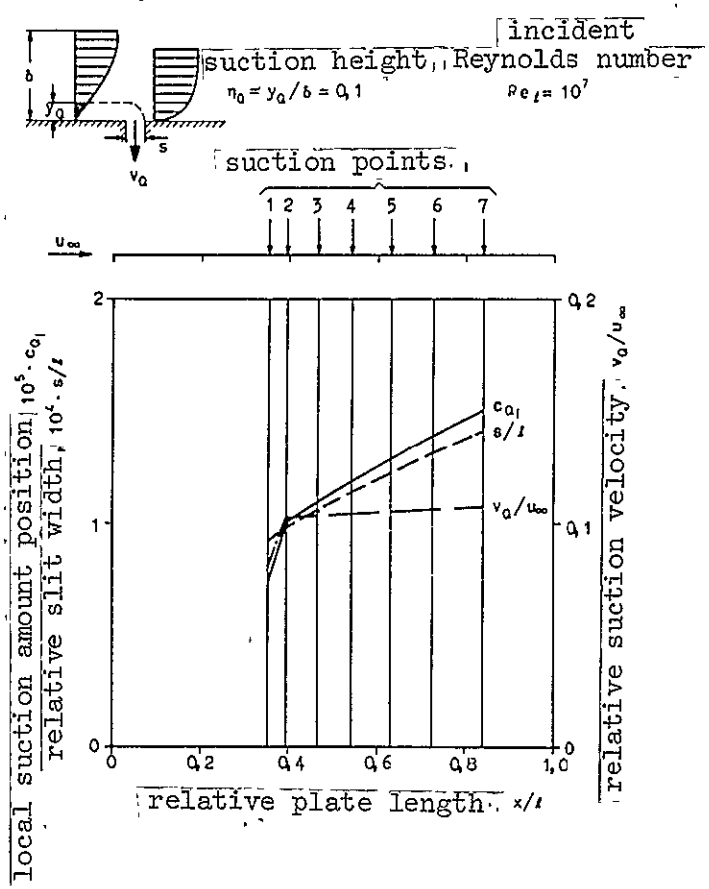

Figure 26: Local Suction Variables

Figures 25-26: Flat Plate with Slit Suction

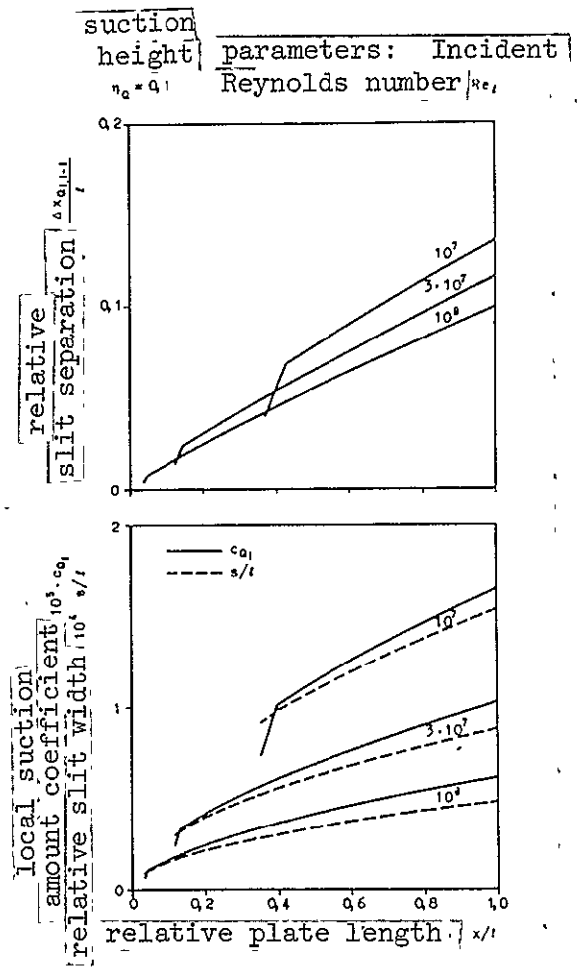

Figure 27: Slit separation, slit width. Local suction amount coefficient

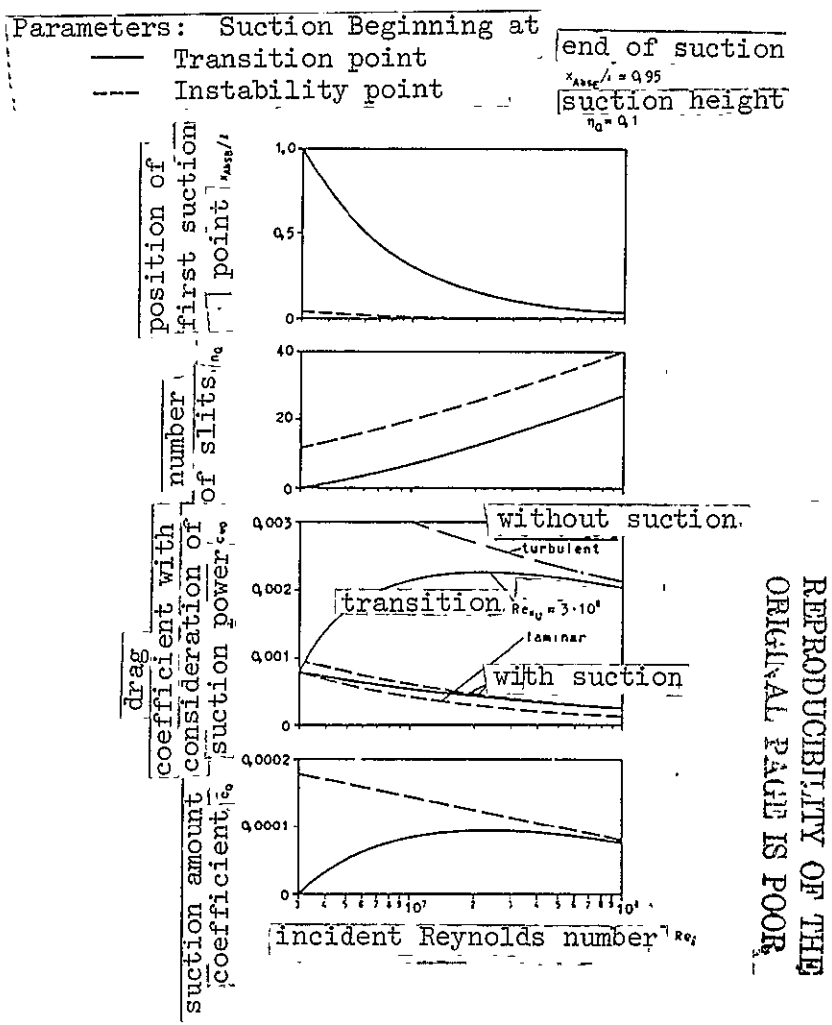

Figure 28: Slit number, drag coefficient, total suction amount coefficient for various suction beginnings.

Figures 27-28: Flat Plate with Slit Suction

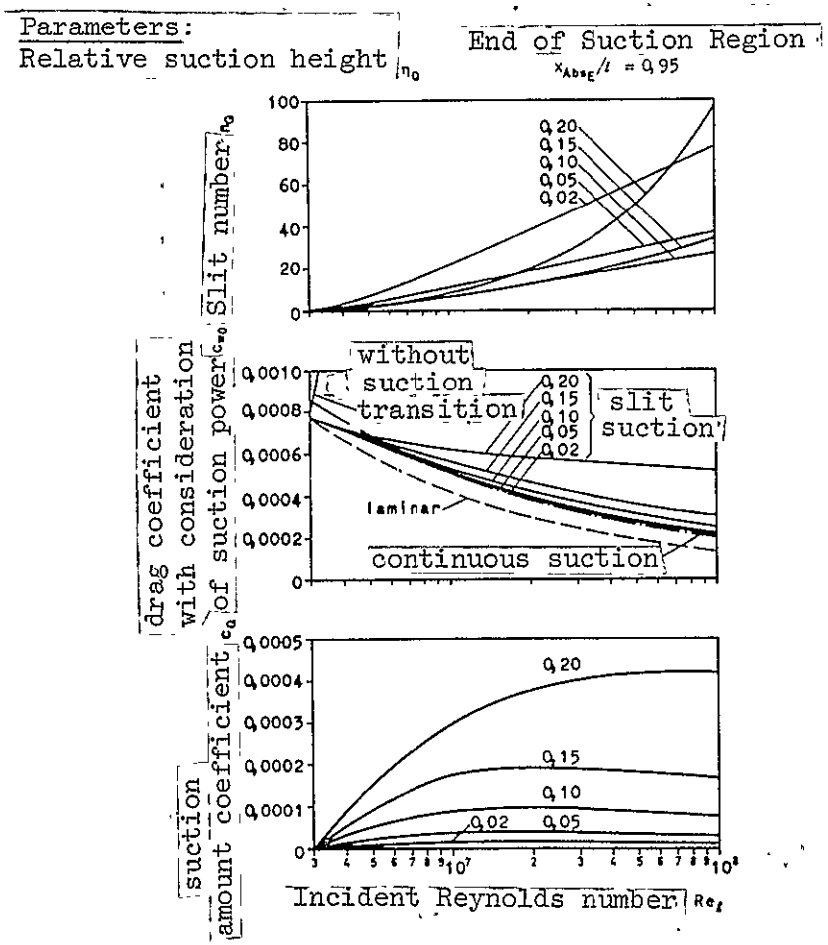

Figure 29: n_Q, c_{w0}, $c_Q = f(Re_1)$, Parameter η_Q

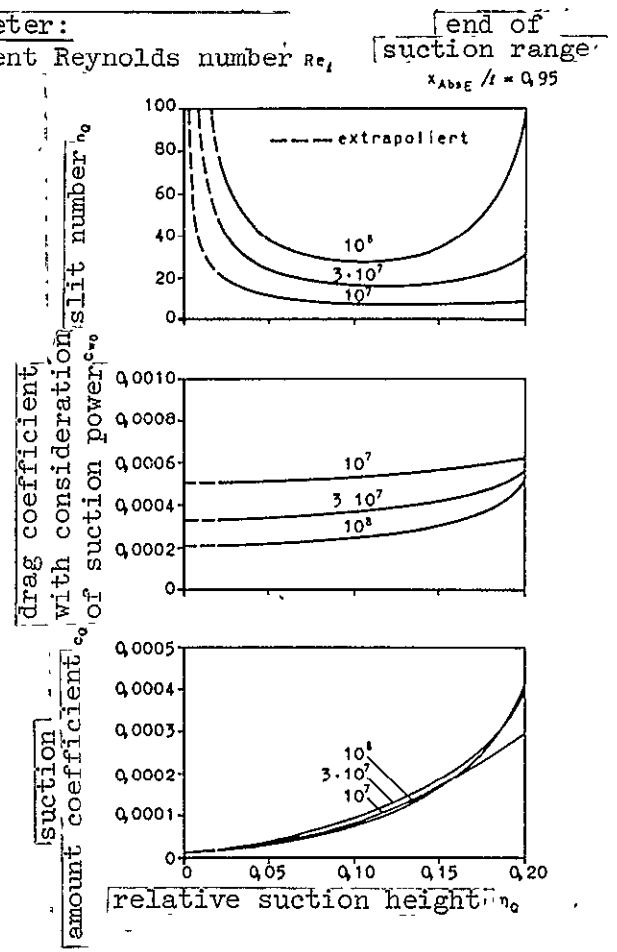

Figure 30: n_Q, c_{w0}, $c_Q = f(\eta_Q)$, Parameter Re_1

Figure 29-30: Flat plate with Slit Suction. Slit number, drag coefficient, suction amount coefficient.

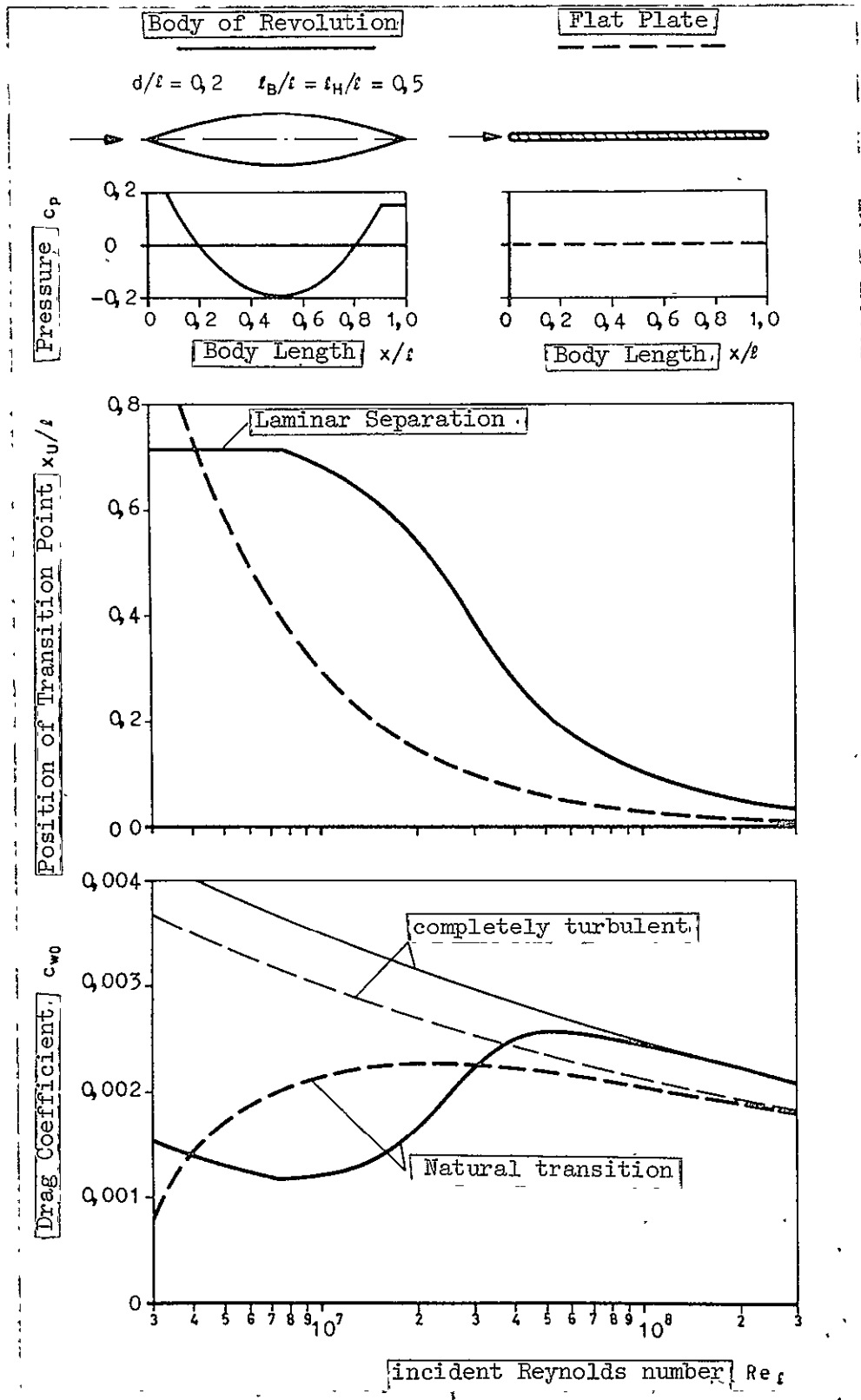

Figure 31: Body of Revolution - Flat Plate. Transition Points with Drag Coefficient as a Function of Incident Reynolds number.

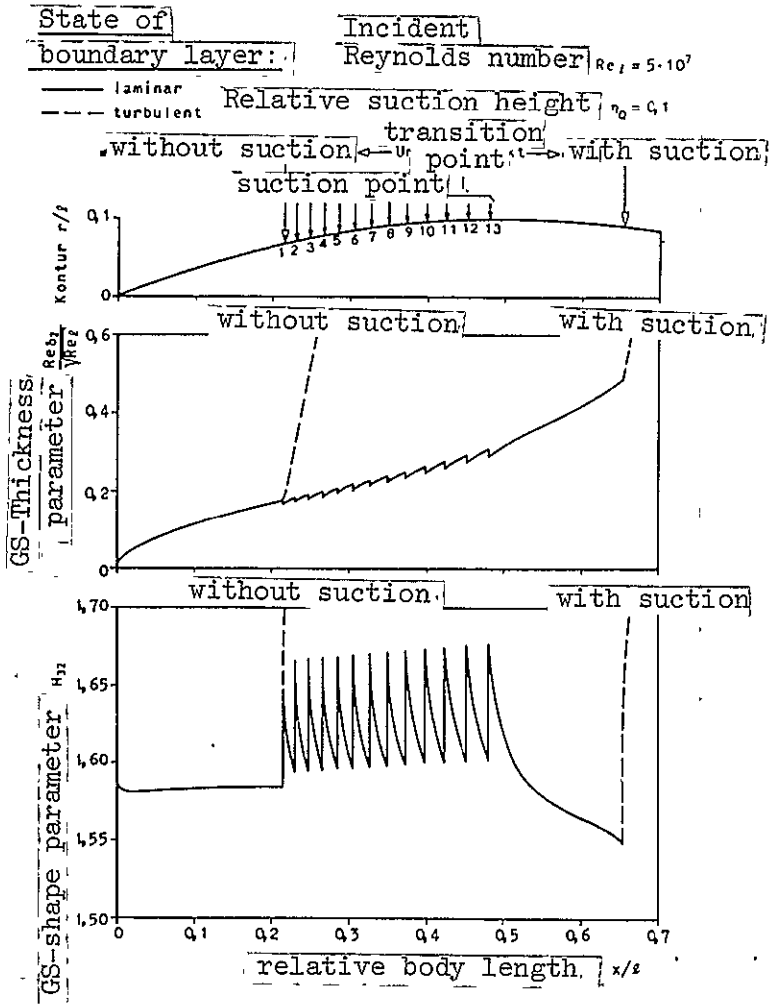

Figure 32: Boundary Layer

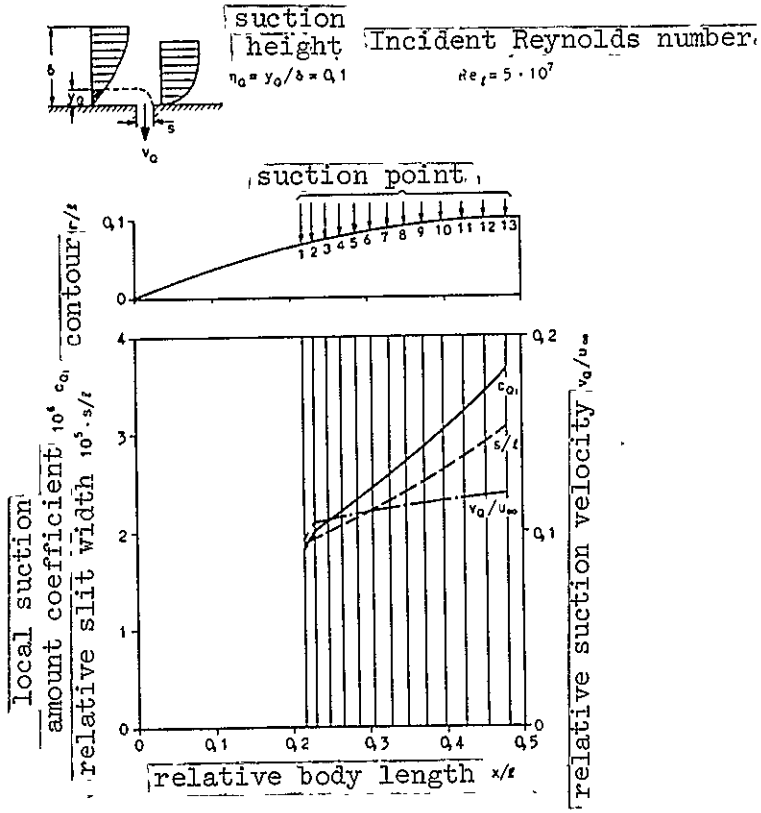

Figure 33: Local Suction Variables

Figures 32-33: Bodies of Revolution with Slit Suction.

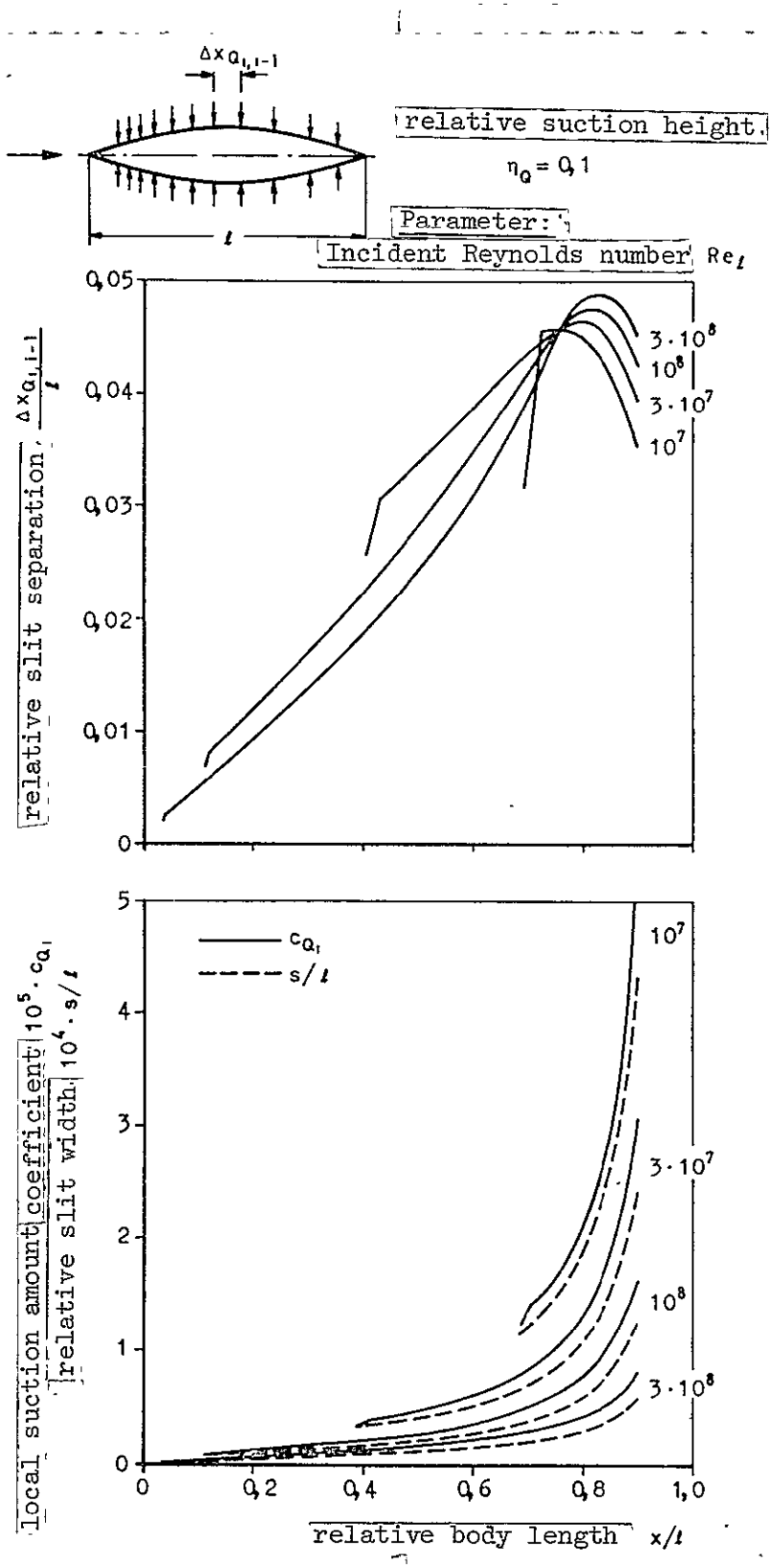

Figure 34: Body of Revolution with Slit Suction. Slit Separation, Slit Width. Local Suction Amount Coefficient.

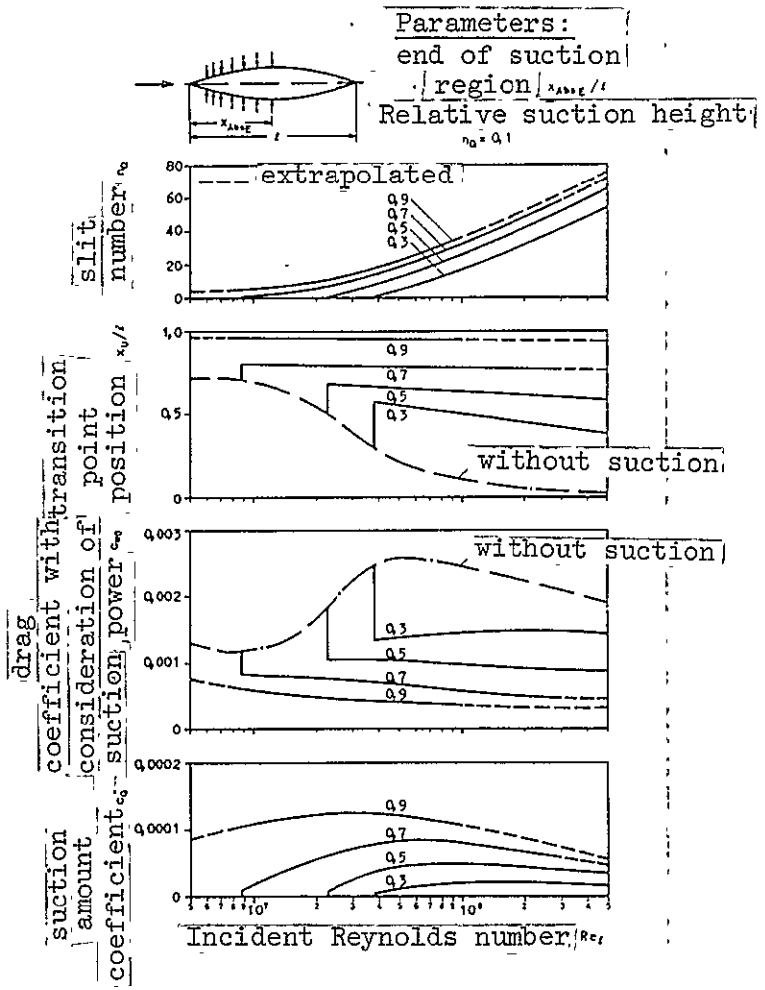

Figure 35: n_Q, x_U/l, c_{w0}, $c_Q = f(Re_l)$, Parameter x_{AbsE}/l

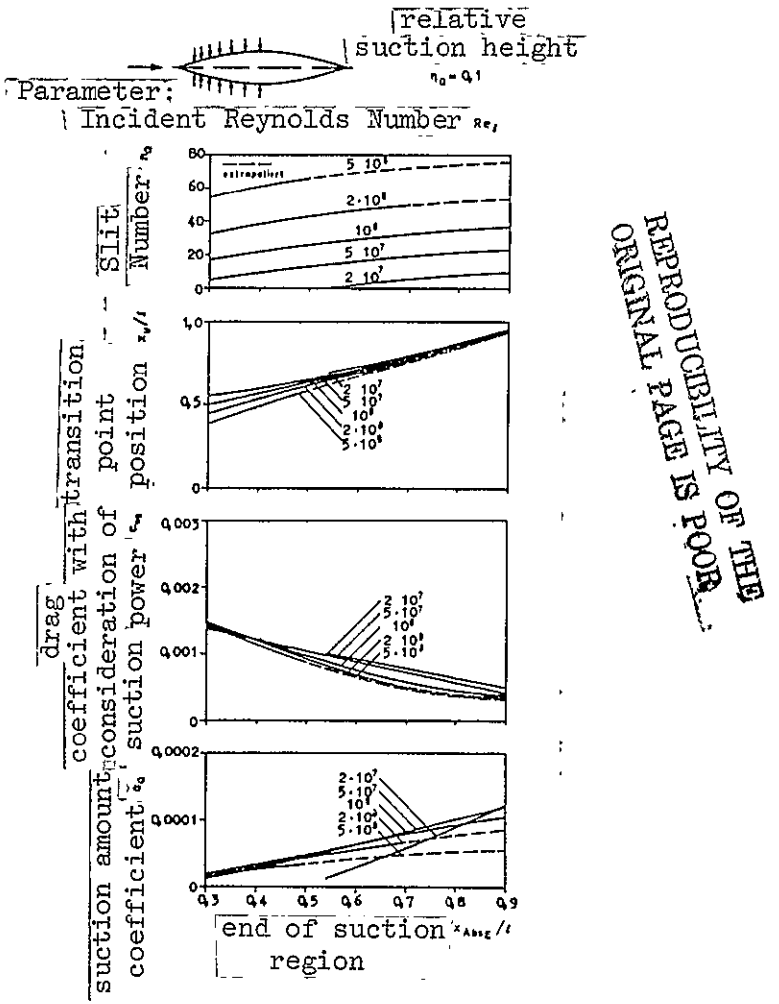

Figure 36: n_Q, x_U/l, c_{w0}, $c_Q = f(x_{AbsE}/l)$, Parameter Re_l

Figures 35-36: Bodies of Revolution with Slit Suction. Slit Number, Transition Point Position, Drag Coefficient, Suction Amount Coefficient.

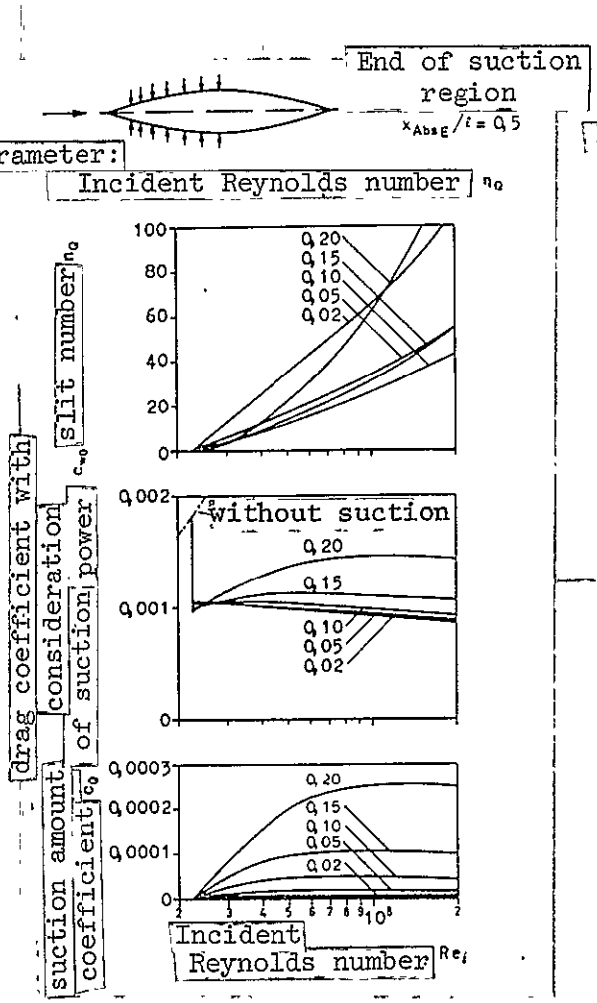

Figure 37 η_Q, c_{w_0}, $c_Q = f(Re_l)$, Parameter η_Q

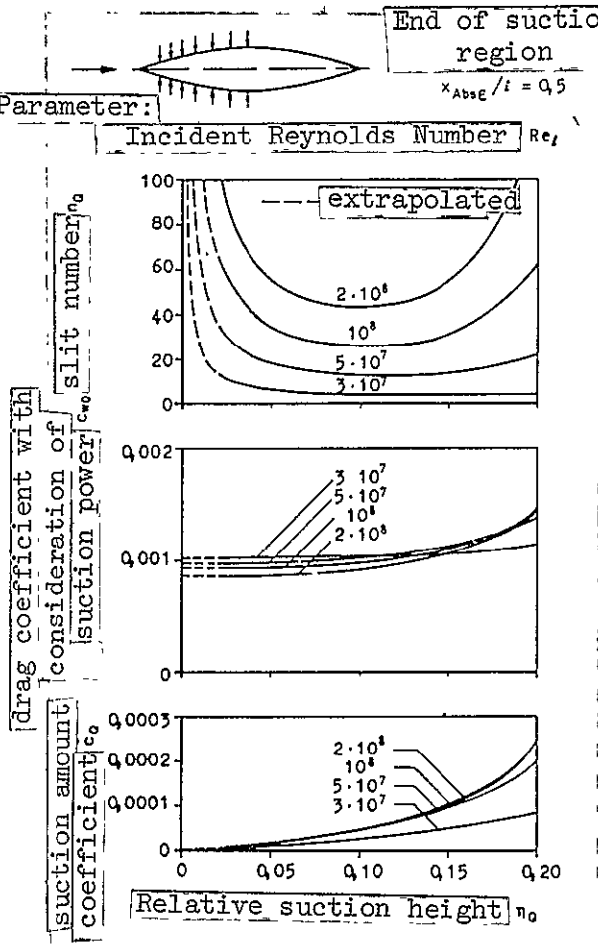

Figure 38 η_Q, c_{w_0}, $c_Q = f(\eta_Q)$, Parameter Re_l

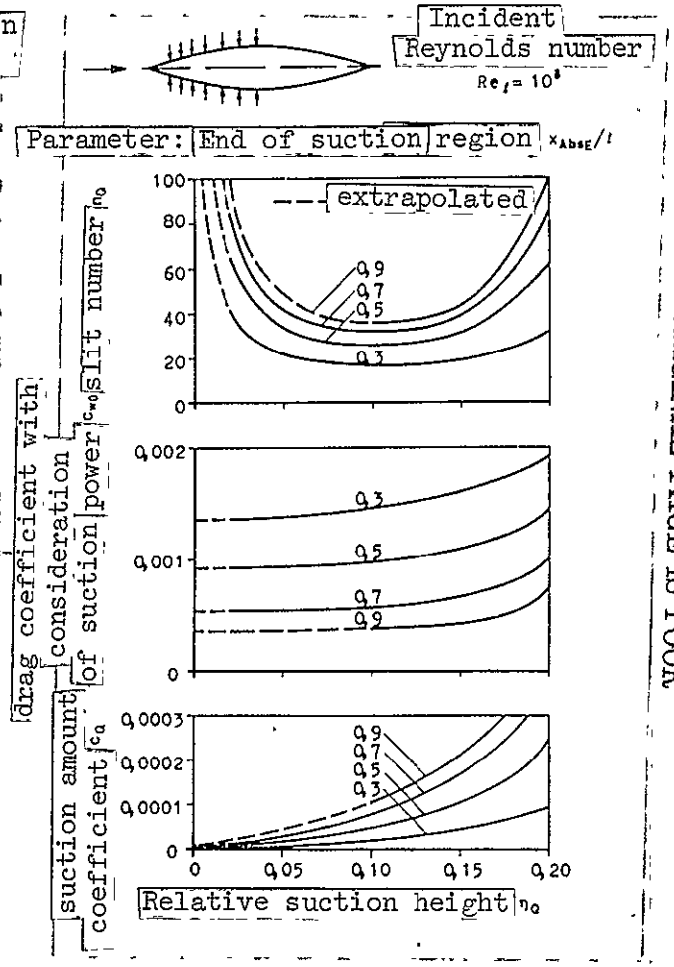

Figure 39 η_Q, c_{w_0}, $c_Q = f(\eta_Q)$, Parameter x_{AbsE}/l

Figures 37-39: Bodies of Revolution with Slit Suction. Slit number, drag coefficient, suction amount coefficient.

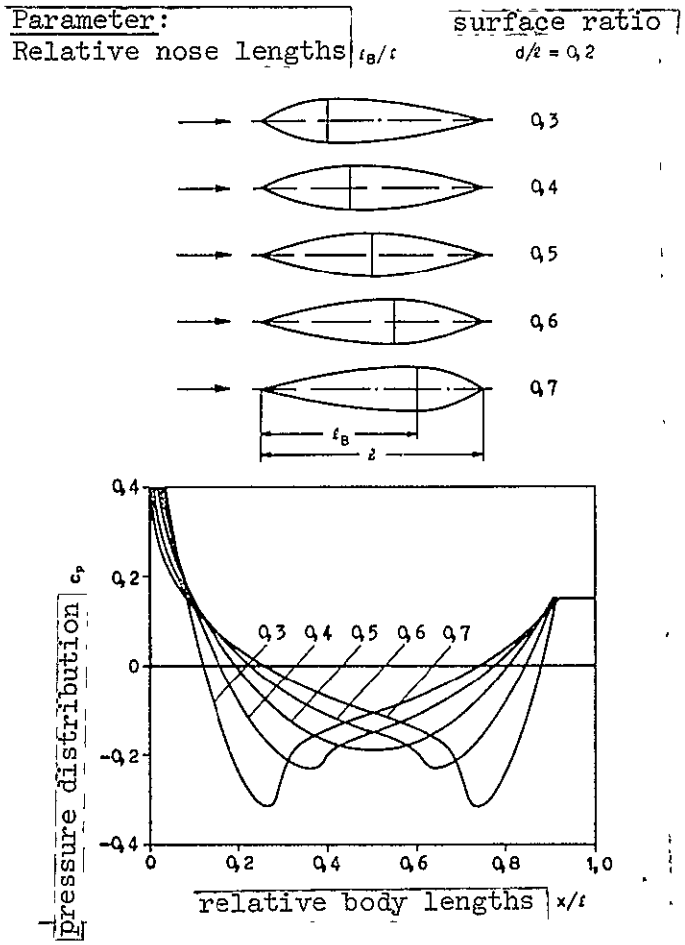

Figure 40: Contour and Pressure Distribution

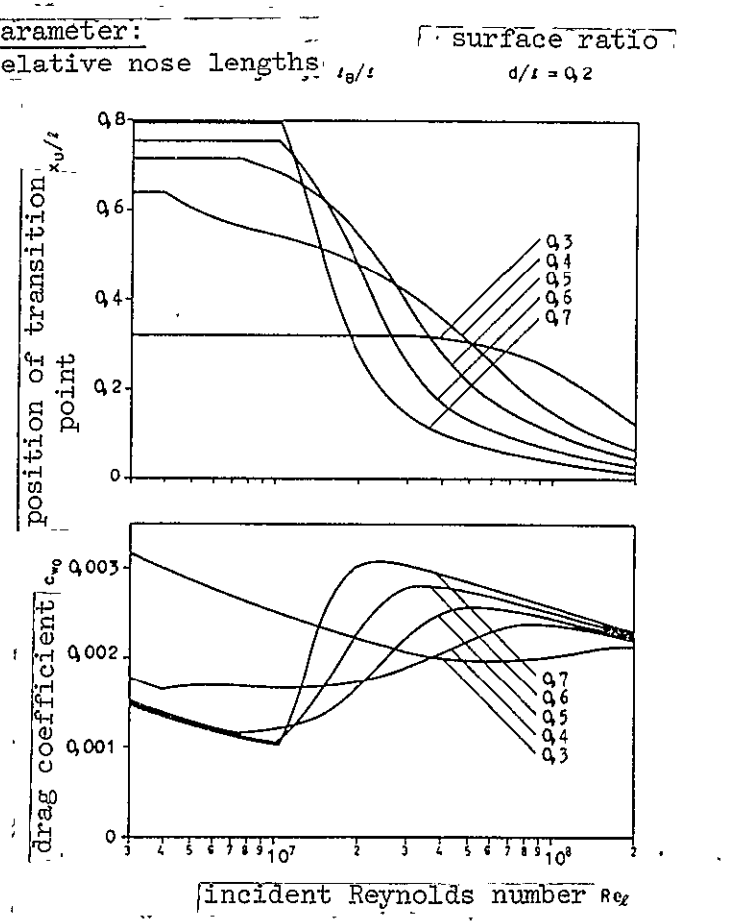

Figure 41: Transition point position and drag coefficient.

Figures 40-41: Bodies of revolution with various thickness setbacks.

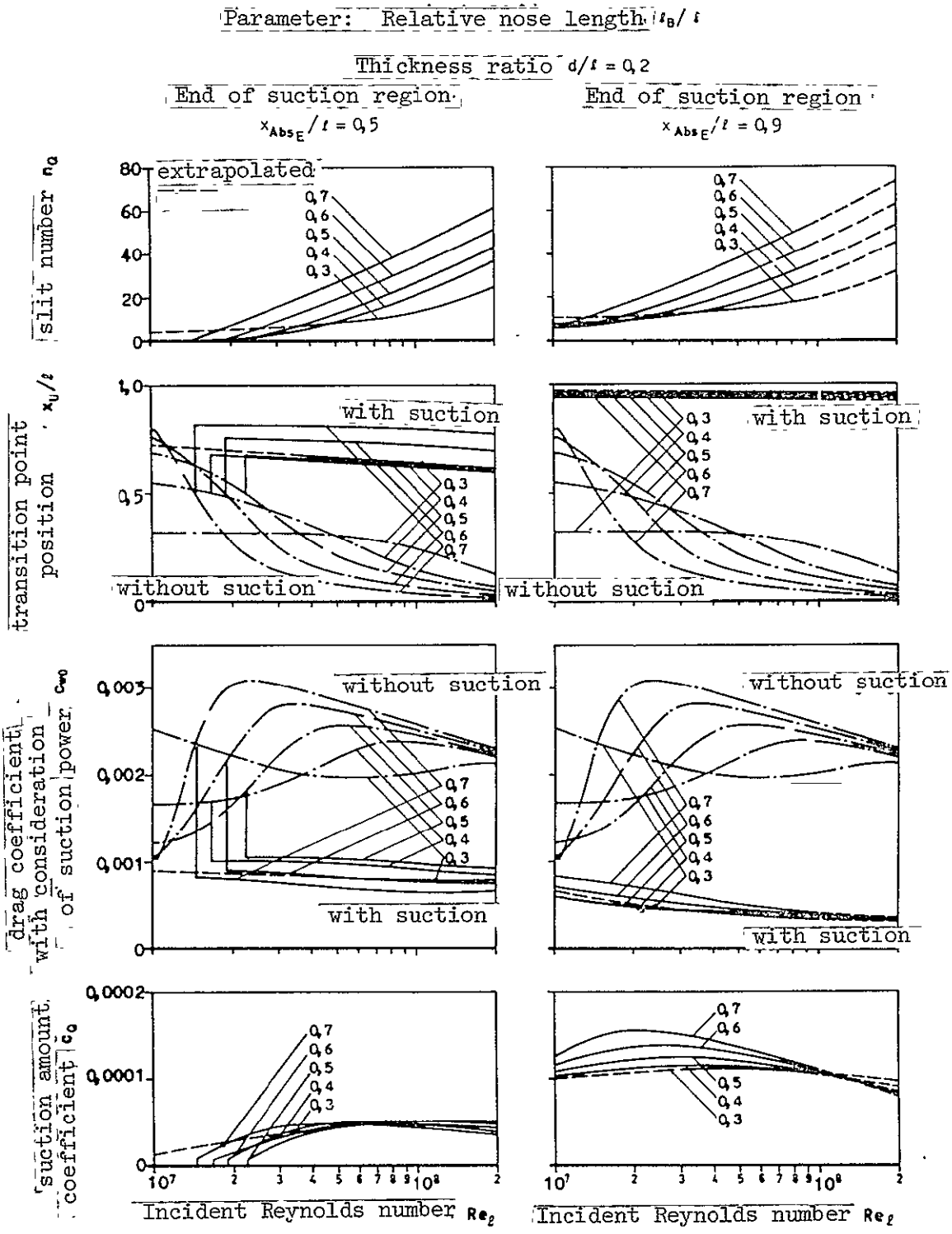

Figure 42: Body of revolution with various thickness setbacks with slit suction.

n_Q, x_U/ℓ, c_{w0}, $c_Q = f(Re_\ell)$, Parameter ℓ_B/ℓ, x_{AbsE}/ℓ.

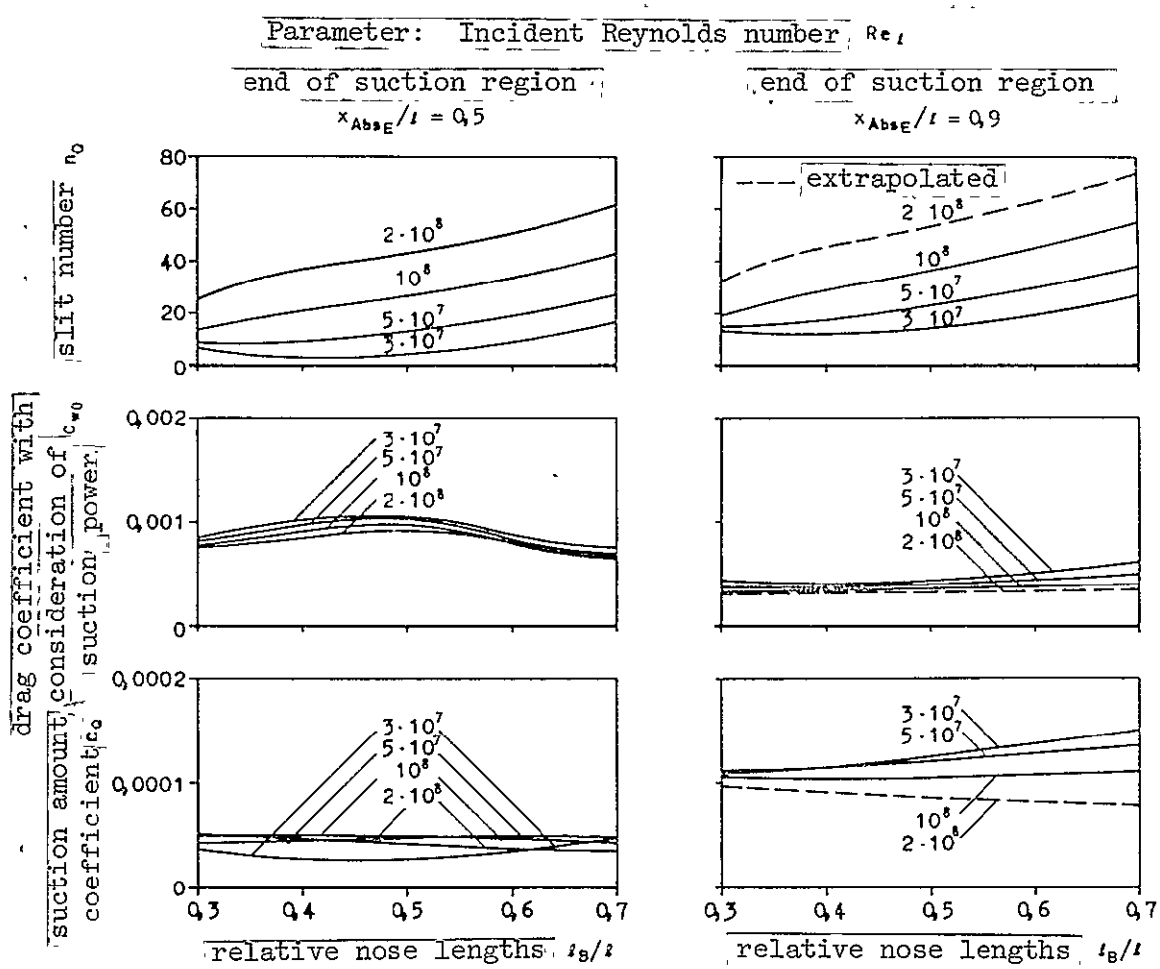

Figure 43: Bodies of Revolution of Various Thickness Setbacks with Slit Suction. Thickness ratio d/l = 0.2.

n_Q, c_{w_0}, $c_Q = f(l_B/l)$, Parameter Re_l, $x_{Abs,E}/l$.

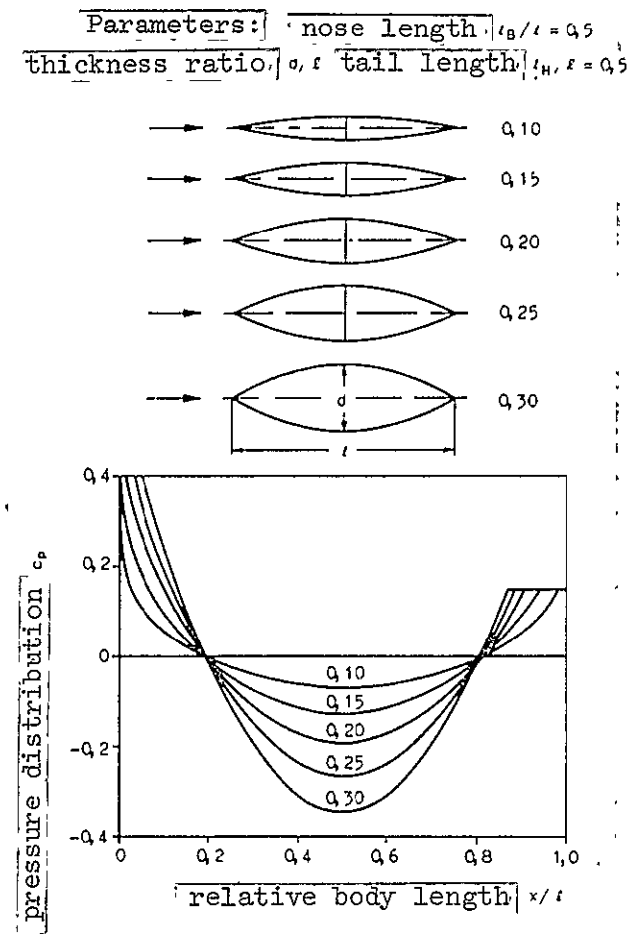

Figure 44: Contour and pressure distribution

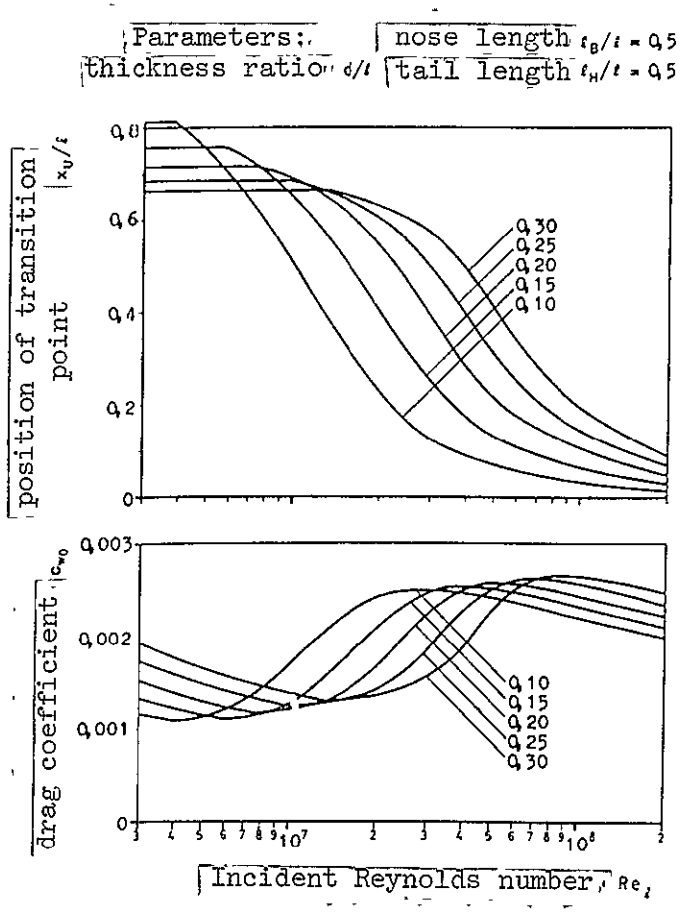

Figure 45: Transition point position and drag point coefficient.

Figures 44-45: Bodies of Revolution of Various Thicknesses

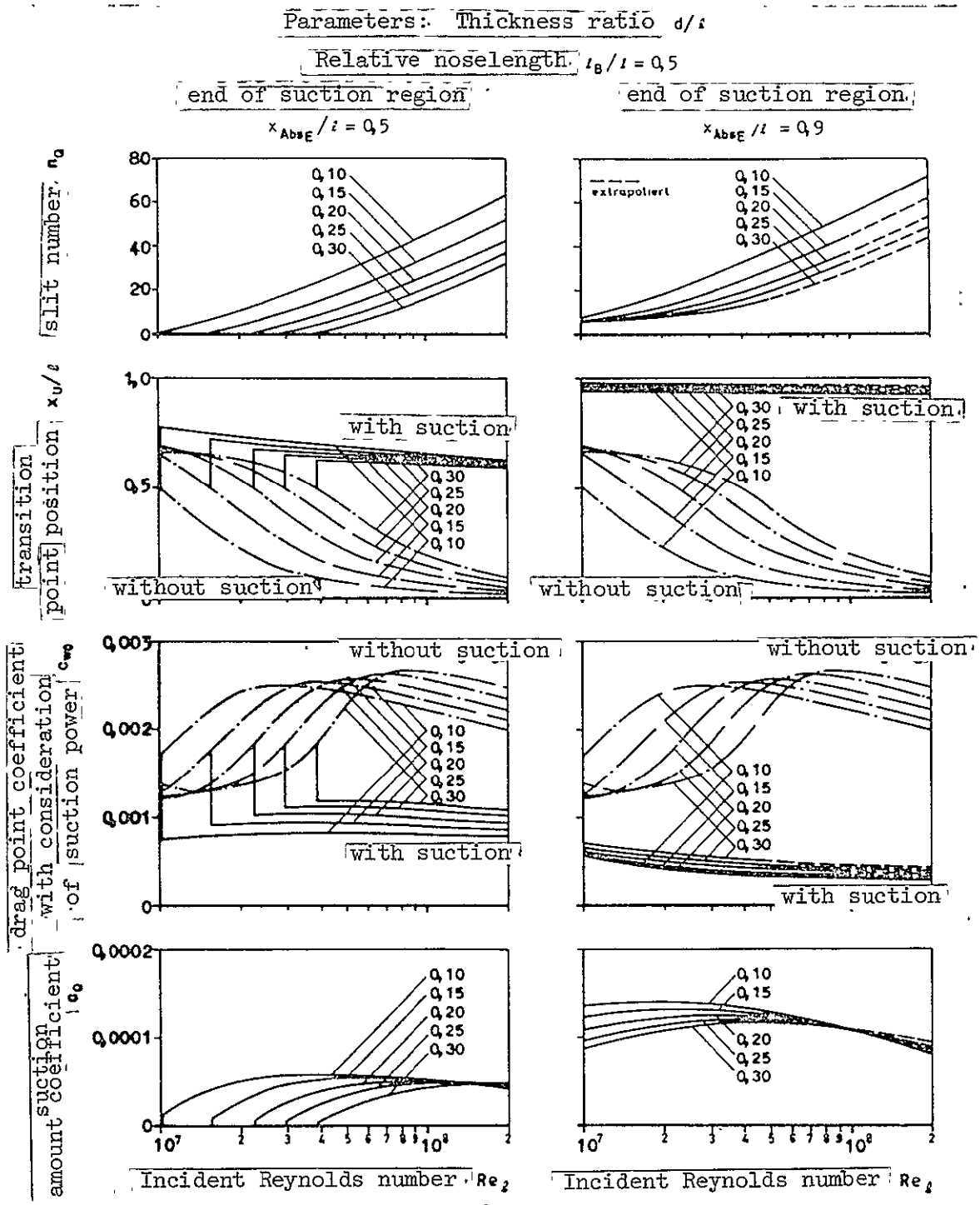

Figure 46: Bodies of Revolution of Various Thicknesses with slit suction.

n_Q, x_U / ℓ, c_{wQ}, $c_Q = f(Re_\ell)$, Parameter d/ℓ, x_{AbsE} / ℓ.

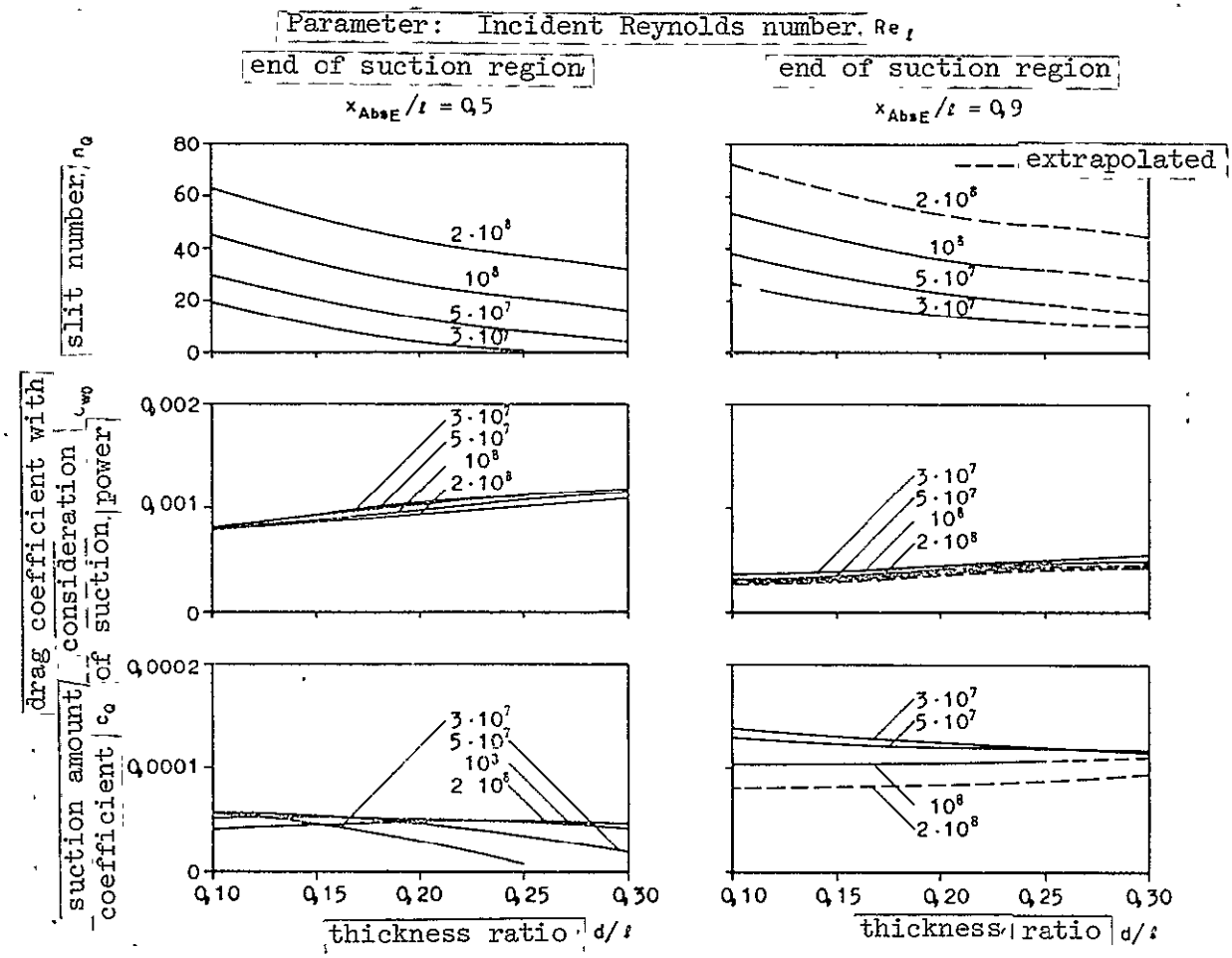

Figure 47: Bodies of Revolution of Various Thicknesses with Slit Suction. Relative nose length $l_B/l = 0.5$.

n_Q, c_{w0}, $c_Q = f(d/\ell)$, Parameter Re_ℓ, x_{AbsE}/ℓ.

13. Appendix

/110

Calculation of Integral Expressions used in Chapter 7.3.1

The integral expressions (7.18) and (7.23)

$$I_{1_I} = \int_0^1 (1-\eta)^c \; (1 + a_1\eta + a_2\eta^2 + a_3\eta^3)\, d\eta$$

$$I_{2_I} = \int_0^1 (1-\eta)^{2c} \; (1 + a_1\eta + a_2\eta^2 + a_3\eta^3)^2 d\eta$$

$$I_{3_I} = \int_0^1 (1-\eta)^{3c} \; (1 + a_1\eta + a_2\eta^2 + a_3\eta^3)^3 d\eta$$

$$I_{1_{II}} = \int_{\eta_a^e}^1 (1-\eta)^c \; (1 + a_1\eta + a_2\eta^2 + a_3\eta^3)\, d\eta$$

$$I_{2_{II}} = \int_{\eta_a^e}^1 (1-\eta)^{2c} \; (1 + a_1\eta + a_2\eta^2 + a_3\eta^3)^2 d\eta$$

$$I_{3_{II}} = \int_{\eta_a^e}^1 (1-\eta)^{3c} \; (1 + a_1\eta + a_2\eta^2 + a_3\eta^3)^3 d\eta$$

are calculated by introducing the following coefficients

$$\left.\begin{matrix} a_1 \\ a_2 \\ a_3 \end{matrix}\right\} \quad \text{(see (7.12)}$$

$$b_1 = a_1$$
$$b_2 = a_1^2 + 2a_2$$
$$b_3 = a_1 a_2 + a_3$$
$$b_4 = a_2^2 + 2a_1 a_3$$
$$b_5 = a_2 a_3$$
$$b_6 = a_3^2$$

$$c_1 = a_1$$
$$c_2 = a_1^2 + a_2$$
$$c_3 = a_1^3 + 6a_1 a_2 + 3a_3$$
$$c_4 = a_1^2 a_2 + 2a_1 a_3 + a_2^2$$
$$c_5 = a_1 a_2^2 + 2a_2 a_3 + a_1^2 a_3$$
$$c_6 = a_2^3 + 6a_1 a_2 a_3 + 3a_3^2$$
$$c_7 = a_1 a_3^2 + a_2^2 a_3$$
$$c_8 = a_2 a_3^2$$
$$c_9 = a_3^3$$

$$\bar{a}_0 = a_3\eta_{QG}^3 + a_2\eta_{QG}^2 + a_1\eta_{QG} + 1$$

$$\bar{a}_1 = 3a_3\eta_{QG}^2 + 2a_2\eta_{QG} + a_1$$

$$\bar{a}_2 = 6a_3\eta_{QG} + 2a_2$$

$$\bar{a}_3 = 6a_3$$

$$\bar{b}_0 = b_6\eta_{QG}^6 + 2b_5\eta_{QG}^5 + b_4\eta_{QG}^4 + 2b_3\eta_{QG}^3 + b_2\eta_{QG}^2 + 2b_1\eta_{QG} + 1$$

$$\bar{b}_1 = 3b_6\eta_{QG}^5 + 5b_5\eta_{QG}^4 + 2b_4\eta_{QG}^3 + 3b_3\eta_{QG}^2 + b_2\eta_{QG} + b_1$$

$$\bar{b}_2 = 15b_6\eta_{QG}^4 + 20b_5\eta_{QG}^3 + 6b_4\eta_{QG}^2 + 6b_3\eta_{QG} + b_2$$

$$\bar{b}_3 = 30b_6\eta_{QG}^3 + 30b_5\eta_{QG}^2 + 6b_4\eta_{QG} + 3b_3$$

$$\bar{b}_4 = 90b_6\eta_{QG}^2 + 60b_5\eta_{QG} + 6b_4$$

$$\bar{b}_5 = 90b_6\eta_{QG} + 30b_5$$

$$\bar{b}_6 = 90b_6$$

$$\bar{c}_0 = c_9\eta_{QG}^9 + 3c_8\eta_{QG}^8 + 3c_7\eta_{QG}^7 + c_6\eta_{QG}^6 + 3c_5\eta_{QG}^5 + 3c_4\eta_{QG}^4 + c_3\eta_{QG}^3 + 3c_2\eta_{QG}^2 + 3c_1\eta_{QG} +$$

$$\bar{c}_1 = 9c_9\eta_{QG}^8 + 24c_8\eta_{QG}^7 + 21c_7\eta_{QG}^6 + 6c_6\eta_{QG}^5 + 15c_5\eta_{QG}^4 + 12c_4\eta_{QG}^3 + 3c_3\eta_{QG}^2 + 6c_2\eta_{QG} + 3c_1$$

$$\bar{c}_2 = 24c_9\eta_{QG}^7 + 56c_8\eta_{QG}^6 + 42c_7\eta_{QG}^5 + 10c_6\eta_{QG}^4 + 20c_5\eta_{QG}^3 + 12c_4\eta_{QG}^2 + 2c_3\eta_{QG} + 2c_2$$

$$\bar{c}_3 = 168c_9\eta_{QG}^6 + 336c_8\eta_{QG}^5 + 210c_7\eta_{QG}^4 + 40c_6\eta_{QG}^3 + 60c_5\eta_{QG}^2 + 24c_4\eta_{QG} + 2c_3$$

$$\bar{c}_4 = 1008c_9\eta_{QG}^5 + 1680c_8\eta_{QG}^4 + 840c_7\eta_{QG}^3 + 120c_6\eta_{QG}^2 + 120c_5\eta_{QG} + 24c_4$$

$$\bar{c}_5 = 1680c_9\eta_{QG}^4 + 2240c_8\eta_{QG}^3 + 840c_7\eta_{QG}^2 + 80c_6\eta_{QG} + 40c_5$$

$$\bar{c}_6 = 6720c_9\eta_{QG}^3 + 6720c_8\eta_{QG}^2 + 1680c_7\eta_{QG} + 80c_6$$

$$\bar{c}_7 = 20160c_9\eta_{QG}^2 + 13440c_8\eta_{QG} + 1680c_7$$

$$\bar{c}_8 = 13440c_9\eta_{QG} + 4480c_8$$

$$\bar{c}_9 = 13440c_9$$

$$I_{1_I} = \frac{1}{(c+4)(c+3)(c+2)(c+1)} \cdot$$

$$\cdot[(c+4)(c+3)(c+2) +$$

$$+ \quad a_1 (c+4)(c+3) +$$

$$+ \quad 2a_2 (c+4) +$$

$$+ \quad 6a_3]$$

$$I_{2_I} = \frac{1}{(2c+7)(c+3)(2c+5)(c+2)(2c+3)(c+1)(2c+1)} \cdot$$

$$\cdot[(2c+7)(c+3)(2c+5)(c+2)(2c+3)(c+1) +$$

$$+ \quad b_1 (2c+7)(c+3)(2c+5)(c+2)(2c+3) +$$

$$+ \quad b_2 (2c+7)(c+3)(2c+5)(c+2) +$$

$$+ \quad 3b_3 (2c+7)(c+3)(2c+5) +$$

$$+ \quad 6b_4 (2c+7)(c+3) +$$

$$+ \quad 30b_5 (2c+7) +$$

$$+ \quad 90b_6]$$

$$I_{3_I} = \frac{1}{(3c+10)(c+3)(3c+8)(3c+7)(c+2)(3c+5)(3c+4)(c+1)(3c+2)(3c+1)} \cdot$$

$$\cdot[(3c+10)(c+3)(3c+8)(3c+7)(c+2)(3c+5)(3c+4)(c+1)(3c+2) +$$

$$+ \quad 3c_1 (3c+10)(c+3)(3c+8)(3c+7)(c+2)(3c+5)(3c+4)(c+1) +$$

$$+ \quad 2c_2 (3c+10)(c+3)(3c+8)(3c+7)(c+2)(3c+5)(3c+4) +$$

$$+ \quad 2c_3 (3c+10)(c+3)(3c+8)(3c+7)(c+2)(3c+5) +$$

$$+ \quad 24c_4 (3c+10)(c+3)(3c+8)(3c+7)(c+2) +$$

$$+ \quad 40c_5 (3c+10)(c+3)(3c+8)(3c+7) +$$

$$+ \quad 80c_6 (3c+10)(c+3)(3c+8) +$$

$$+ \quad 1680c_7 (3c+10)(c+3) +$$

$$+ \quad 4480c_8 (3c+10) +$$

$$+ \quad 13440c_9]$$

$$I_{1_{II}} = \frac{1}{(c+4)(c+3)(c+2)(c+1)} \cdot$$
$$\cdot[\bar{a}_0\ (1-\eta_Q^G)^{c+1}\ (c+4)(c+3)(c+2) +$$
$$+\ \bar{a}_1\ (1-\eta_Q^G)^{c+2}\ (c+4)(c+3) +$$
$$+\ \bar{a}_2\ (1-\eta_Q^G)^{c+3}\ (c+4) +$$
$$+\ \bar{a}_3\ (1-\eta_Q^G)^{c+4}\ ]$$

$$I_{2_{II}} = \frac{1}{(2c+7)(c+3)(2c+5)(c+2)(2c+3)(c+1)(2c+1)} \cdot$$
$$\cdot[\bar{b}_0\ (1-\eta_Q^G)^{2c+1}\ (2c+7)(c+3)(2c+5)(c+2)(2c+3)(c+1) +$$
$$+\ \bar{b}_1\ (1-\eta_Q^G)^{2c+2}\ (2c+7)(c+3)(2c+5)(c+2)(2c+3) +$$
$$+\ \bar{b}_2\ (1-\eta_Q^G)^{2c+3}\ (2c+7)(c+3)(2c+5)(c+2) +$$
$$+\ \bar{b}_3\ (1-\eta_Q^G)^{2c+4}\ (2c+7)(c+3)(2c+5) +$$
$$+\ \bar{b}_4\ (1-\eta_Q^G)^{2c+5}\ (2c+7)(c+3) +$$
$$+\ \bar{b}_5\ (1-\eta_Q^G)^{2c+6}\ (2c+7) +$$
$$+\ \bar{b}_6\ (1-\eta_Q^G)^{2c+7}\ ]$$

$$I_{3_{II}} = \frac{1}{(3c+10)(c+3)(3c+8)(3c+7)(c+2)(3c+5)(3c+4)(c+1)(3c+2)(3c+1)} \cdot$$
$$\cdot[\bar{c}_0(1-\eta_Q^G)^{3c+1}(3c+10)(c+3)(3c+8)(3c+7)(c+2)(3c+5)(3c+4)(c+1)(3c+2) +$$
$$+\ \bar{c}_1(1-\eta_Q^G)^{3c+2}(3c+10)(c+3)(3c+8)(3c+7)(c+2)(3c+5)(3c+4)(c+1) +$$
$$+\ \bar{c}_2(1-\eta_Q^G)^{3c+3}(3c+10)(c+3)(3c+8)(3c+7)(c+2)(3c+5)(3c+4) +$$
$$+\ \bar{c}_3(1-\eta_Q^G)^{3c+4}(3c+10)(c+3)(3c+8)(3c+7)(c+2)(3c+5) +$$
$$+\ \bar{c}_4(1-\eta_Q^G)^{3c+5}(3c+10)(c+3)(3c+8)(3c+7)(c+2) +$$
$$+\ \bar{c}_5(1-\eta_Q^G)^{3c+6}(3c+10)(c+3)(3c+8)(3c+7) +$$
$$+\ \bar{c}_6(1-\eta_Q^G)^{3c+7}(3c+10)(c+3)(3c+8) +$$
$$+\ \bar{c}_7(1-\eta_Q^G)^{3c+8}(3c+10)(c+3) +$$
$$+\ \bar{c}_8(1-\eta_Q^G)^{3c+9}(3c+10) +$$
$$+\ \bar{c}_9(1-\eta_Q^G)^{3c+10}]$$

The integral expressions in condensed notation are:

$$I_{1_I} = \frac{6a_3 + (c+4)\left[2a_2 + (c+3)\left[a_1 + (c+2)\right]\right]}{(c+4)(c+3)(c+2)(c+1)}$$

$$I_{2_I} = \frac{90b_6 + (2c+7)\left[30b_5 + (c+3)\left[6b_4 + (2c+5)\left[3b_3 + (c+2)\left[b_2 + (2c+3)\left[b_1 + (c+1)\right]\right]\right]\right]\right]}{(2c+7)(c+3)(2c+5)(c+2)(2c+3)(c+1)(2c+1)}$$

$$I_{3_I} = \frac{13440c_9 + (3c+10)\left[4480c_8 + (c+3)\left[1680c_7 + (3c+8)\left[80c_6 + (3c+7)\left[40c_5 + \right.\right.\right.\right.}{(3c+10)(c+3)(3c+8)(3c+7)(c+2)(3c+5)(3c+4)(c+1)(3c+2)(3c+1)}$$

$$\left.\left.\left.\left. + (c+2)\left[24c_4 + (3c+5)\left[2c_3 + (3c+4)\left[2c_2 + (c+1)\left[3c_1 + (3c+2)\right]\right]\right]\right]\right]\right]$$

and

$$I_{1_{II}} = \frac{(1-\eta_{QG})^{c+4}\left[\bar{a}_3 + \frac{c+4}{1-\eta_{QG}}\left[\bar{a}_2 + \frac{c+3}{1-\eta_{QG}}\left[\bar{a}_1 + \frac{c+2}{1-\eta_{QG}}\,\bar{a}_0\right]\right]\right]}{(c+4)(c+3)(c+2)(c+1)}$$

$$I_{2_{II}} = \frac{(1-\eta_{QG})^{2c+7}\left[\bar{b}_6 + \frac{2c+7}{1-\eta_{QG}}\left[\bar{b}_5 + \frac{c+3}{1-\eta_{QG}}\left[\bar{b}_4 + \frac{2c+5}{1-\eta_{QG}}\left[\bar{b}_3 + \frac{c+2}{1-\eta_{QG}}\left[\bar{b}_2 + \frac{2c+3}{1-\eta_{QG}}\left[\bar{b}_1 + \frac{c+1}{1-\eta_{QG}}\,\bar{b}_0\right]\right]\right]\right]\right]\right]}{(2c+7)(c+3)(2c+5)(c+2)(2c+3)(c+1)(2c+1)}$$

$$I_{3_{II}} = \frac{(1-\eta_{QG})^{3c+10}\left[\bar{c}_9 + \frac{3c+10}{1-\eta_{QG}}\left[\bar{c}_8 + \frac{c+3}{1-\eta_{QG}}\left[\bar{c}_7 + \frac{3c+8}{1-\eta_{QG}}\left[\bar{c}_6 + \frac{3c+7}{1-\eta_{QG}}\left[\bar{c}_5 + \frac{c+2}{1-\eta_{QG}}\left[\bar{c}_4 + \right.\right.\right.\right.\right.\right.}{(3c+10)(c+3)(3c+8)(3c+7)(c+2)(3c+5)(3c+4)(c+1)(3c+2)(3c+1)}$$

$$\left.\left.\left.\left.\left.\left. + \frac{3c+5}{1-\eta_{QG}}\left[\bar{c}_3 + \frac{3c+4}{1-\eta_{QG}}\left[\bar{c}_2 + \frac{c+1}{1-\eta_{QG}}\left[\bar{c}_1 + \frac{3c+2}{1-\eta_{QG}}\,\bar{c}_0\right]\right]\right]\right]\right]\right]\right]$$